The effect of modifications to a groyne area in the Nieuwe Waterweg

–

Project De Groene Poort
May 3, 2023

by

Tors Kouwenhoven

The effect of modifications to a groyne area in the Nieuwe Waterweg

–

Project De Groene Poort

May 3, 2023

by

Tors Kouwenhoven

to obtain the degree of Master of Science
at the Delft University of Technology,
to be defended publicly on May 11, 2023.

Student number:	4382420	
Thesis committee:	Dr. ir. B. C. van Prooijen,	TU Delft, supervisor
	Dr. ir. E. Mosselman,	Deltares/TU Delft
	Dr. ir. C. J. Sloff,	Deltares/TU Delft

TU Delft

Preface

It has been a long journey from the moment Kees presented this pilot to me, to the moment that I have finished this research. I looked for a research that contained more than only literature studies and data obtained from other researchers because I wanted to experience planning and to lead a measurement campaign and that goal has been achieved for sure. To work with the data obtained from the equipment, you programmed and placed yourself gives an extra excitement to an already exciting research. It was amazing to have been given the freedom and responsibilities to plan the campaigns my way and I learned a lot from that. I want to thank Pieter, Chantall, Arie and Arno from the hydraulics lab for helping in the planning stages and during the measurement campaigns. For processing the obtained data I have to thank Jianwei Sun for helping me building the codes and always quickly answering my questions through the mail. Finally, I want to give a special thanks to Steven with whom I worked together learning about the different equipment and lending me a hand during the actual measuring campaigns.

Project De Groene Poort is an exciting project, which I believe has a lot of potential when used on larger scales. During the meetings with the project team, I learned how such a project works in practice, so I want to thank all the members of the project team for that.

It took me a long time to design and build a good research and even one of the field campaigns failed. Luckily the members of my committee were always patient with me and helped me with everything, so I want to thank them for that. I want to thank Bram and Kees as well for their help out in the field during measurement campaigns, which were not always during the warmest weather conditions.

Finally, I want to thank all the people around me for their mental support and my dad, both Sanders and Leoni for checking my paper.

During the difficult moments of this research there the one quote that keeps repeating in my mind is from the first moon mission: *"We choose to go to the moon in this decade and do the other things, not because they are easy, but because they are hard because that goal will serve to organize and measure the best of our energies and skills, because that challenge is one that we are willing to accept, one we are unwilling to postpone, and one which we intend to win." - John F. Kennedy*

Tors Kouwenhoven
Delft, May 2023

Summary

Natural areas have had to make room for shipping and have mainly disappeared from the areas surrounding the Port of Rotterdam. In the Nieuwe Waterweg, the idea is to create new intertidal areas by modifying the existing groyne areas in the river. The future function of these created intertidal areas is to accommodate flora and fauna and by doing so to let nature reclaim this area. The first pilot has been done in groyne area number 9. In this groyne area a dam has been constructed between the two groynes containing a gap in the middle. These groynes have been partially heightened. Both groynes contain an entrance that allows water to enter the groyne area during lower water levels. The first of the two nourishments created an elevated island in the groyne area. The heightened groynes are completely submerged during the peak of the tide, while the dam in front of the groyne area is always emerged.

The ecological value of the groyne area can change due to changes in the hydrodynamic forcing and the behavior of the sediment. This will impact the potential habitat that can be created, therefore insights into these forcing conditions are required. The objective of this research is to obtain a better understanding of the flow inside the modified groyne area and the abiotic conditions which influence this behavior.

Two field campaigns have been carried out to obtain data from inside the groyne area. In the first field campaign, three weeks of pressure and velocity data were obtained for six locations in the groyne area using ADVs. During this campaign, also sediment samples have been taken for every location. In the second campaign, the velocity profiles of five cross sections in the groyne area have been obtained from a floating ADCP. These measurements have been done during the different stages of one tide.

Multiple processes influence the flow of the river and the groyne area. From these processes is tide the most dominant force on the flow. The velocity signal follows the shape of the tide precisely and is influenced by the height of the tide. Changes in the discharge didn't directly result in increased or decreased velocities in the groyne area. Regulation of the river discharge with the Haringvlietdam limits its effect on the groyne area. From the effects of winds and local storms as well as storms at sea, it was found that the local winds created small continuous oscillations in the water surface. These oscillations were negligible compared to the effect of ships and did not have noticeable effects on the flow velocities, therefore these effects have not been considered further. No clear relations could be found between the flow velocities and the storms at sea.

The sediment samples have been analyzed using laser diffraction. Sediment from the bed in the surrounding area of the first nourishment has a comparable size to the nourished material. The sediment size decreases in the groyne area in the locations further away from the nourished island. Locations in front of the gap between the dam and the entrance in the groyne area which are located at the other side of the nourishment, contain coarser sediment than nearby locations. Samples with smaller sediment sizes were observed to contain a higher percentage of clay and silt particles.

With the velocity and pressure data, there is a clear distinction between the flood flow and the ebb flow through the groyne area. The flow in the groyne area depends during the rising stage of the tide on the water level. The amount of water that flows through the groyne area and its flow velocity increases with the water level. This behavior is reinforced from neap to spring tide. A number of the locations have a threshold water level that has to be reached during flood until water starts flowing through that location. The ebb flow is significantly less dependent on the water level of the tide. During the ebb tide, the maximum velocities are reached in the middle of the falling stage, giving a more classic parabola shape between the velocities and the water levels.

Ships have a significant impact on the flow velocities in the groyne area. The waves created by the passing ships enter the groyne area first through the entrances in the groynes and later through the gap in the dam. These waves propagating through the area interfere with the waves from the same

ship that enters through the gap in the middle of the dam. The largest secondary ship waves have been analyzed from ships that pass with a time of 10 minutes between them. Different data has been compared to the velocity increase caused by these waves. Correlations between the velocity increase caused by waves to both the wave height and the ratio of water depth to wave height have been found. No direct correlation has been found to tidal velocity.

From the sediment characteristics, the critical velocities at the different locations in the groyne area have been found. In the majority of the locations is the threshold of motion exceeded during both ebb and flood however, this is not the case at all locations. This threshold of motion is primarily exceeded during ebb at the gap in the middle of the dam. In the upstream corner of the groyne area, where the dam meets the groyne, the threshold only gets exceeded during ebb flows.

During normal conditions, the dominant transport direction for sediment is in the flood direction. From spring to neap tide the flood transports decrease, while the ebb transport stays consistent changing the dominant direction from flood to ebb. During the passage of a wave, the dominant direction is in the propagation direction of the wave. The tide can change this direction if its velocity can counter the velocity increase of the wave.

The results of this research give a better understanding of the impact of the groyne field modifications. From the data, has been seen that the flow, as well as the sediment, is impacted by both the modifications to the dam and groynes and also to the first nourishment. Typical behavior for both emerged and submerged groyne area's during a tide or ship's passage is unrecognizable. The direct influence of ships on the groyne area is reduced by the sheltering from the dam and limiting the exchange of water between the main channel and the groyne area. However, ship waves still have a significant impact on the groyne area. This knowledge is essential for future modifications to this groyne and determining the success of the pilot. It can help with the design of the modifications of other groyne areas as well.

This research is limited to the flow and sediment behavior inside the groyne area itself. It is recommended to expand this research out of the boundaries of this particular groyne area and look at different setups for a modified area or the effect of multiple adjacent modified groyne areas. A computer model and the other data can be used to look at other conditions and influences to the groyne area as well.

Contents

1 Introduction

Rivers form an essential part of the import and export of goods due to their growing demands. Past projects have aimed to improve navigation and flood safety in rivers. The Nieuwe Waterweg is a part of this system as it helps ships navigate from and to the constantly expanding port of Rotterdam. Groynes help reduce the amount of maintenance dredging needed in this river for its navigability. Nature and its ecosystems did not play an important part in these past designs, but the tide has turned with nature-based solutions gaining a more and more critical role. According to the PBL Netherlands Environmental Assessment Agency: "Nature-based Solutions (NbS) are actions that enable the protection, sustainable management and restoration of natural and managed ecosystems, that can simultaneously provide human well-being and biodiversity benefits". Project De Groene Poort is a project in which these Nature-based Solutions are incorporated into the groyne field of the Nieuwe Waterweg with the goal to restore the intertidal areas and bring back some of the plant and wildlife to the area.

1.1. Background

1.1.1. Project "De Groene Poort" and "Proeftuin Sediment Rijnmond"

For the KRW (Europese Kaderrichtlijn Water) new sustainable and eco-friendly projects must be realized. For this reason, Rijkswaterstaat, Port of Rotterdam and the city of Rotterdam have initiated "Proeftuin sediment Rijnmond". Proeftuin Sediment Rijnmond has multiple projects in which dredged material is reused. This dredged material is used for the creation of intertidal areas, small-scale sand engines and addressing the problems with scour holes. These different projects are all located in separate parts of the Rhine estuary. One of The projects in this is "De Groene Poort". In this project, new intertidal areas will be created, which will eventually be claimed by nature. Near the town of Rozenburg in the Nieuwe Waterweg at groyne area number 9 a pilot has started for this project. Figure 1.1 shows the location of this project on the map of the Port of Rotterdam.

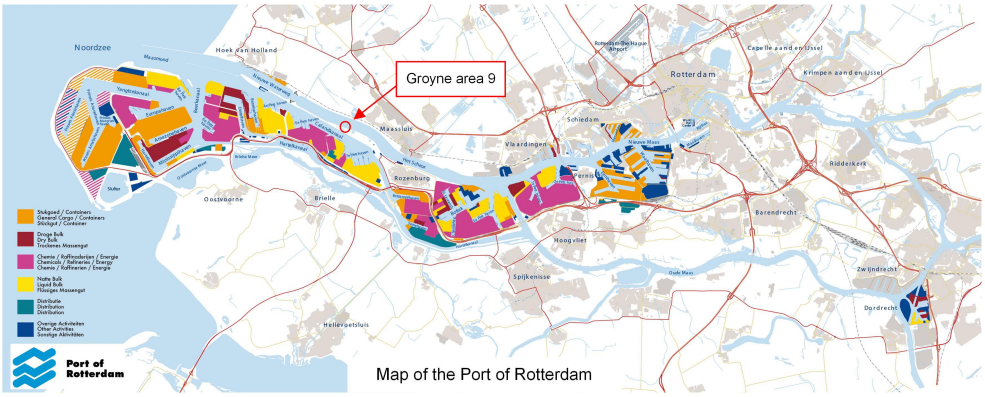

Figure 1.1: The location of the pilot on the map of the Port of Rotterdam.

In order to create such an intertidal area, new dams will be placed at the groyne areas to shelter the sediment from the waves created by storms and ships. In these sheltered areas, sediment will be deposited from either the dredging operations in the Port of Rotterdam or building projects across the city. This approach aligns with the building with nature philosophy in which as much material is recycled and reused as possible. The reused sediment is a silt sandy material, but the full characteristics depend on the original location of the obtained/dredged sediment. This obtained sediment will be placed into the modified groyne areas. The height of the deposited sediment is lower than the high tide, so these areas can be flooded at high tide and fall dry at lower tides. The importance of this partial flooding is further explained in Section 1.1.3.

Figure 1.2: Artist impression of the project (Helmer, 2013).

1.1.2. Layout of the area

The two groynes surrounding the area of the pilot have been partly heightened and a dam to shelter this area from the canal has been constructed. The material that is used to construct and heighten the groyne area is rock, but there are ideas to change this in the future to old sewer pipes. For the sewer pipe dams the first pilot has been started in the groyne area downstream of the researched groyne area and three more have been planned for in the future. In the dam, there are three gaps: two of the gaps are positioned at the place where the dam and the groynes meet, and the other one is located in the middle of the dam. The gaps at the sides are an unintentional cause of the poor fit between the dam and the groynes which are perpendicular to each other. The layout and a photo of this groyne area can be seen in Figure 1.3. For the pilot, the nourishment will be placed in the groyne area in two parts. The first nourishment was deposited in the downstream section in 2016 and during the end stages of this research the second nourishment was done in December 2022. This second nourishment was completed after the data for this research was obtained.

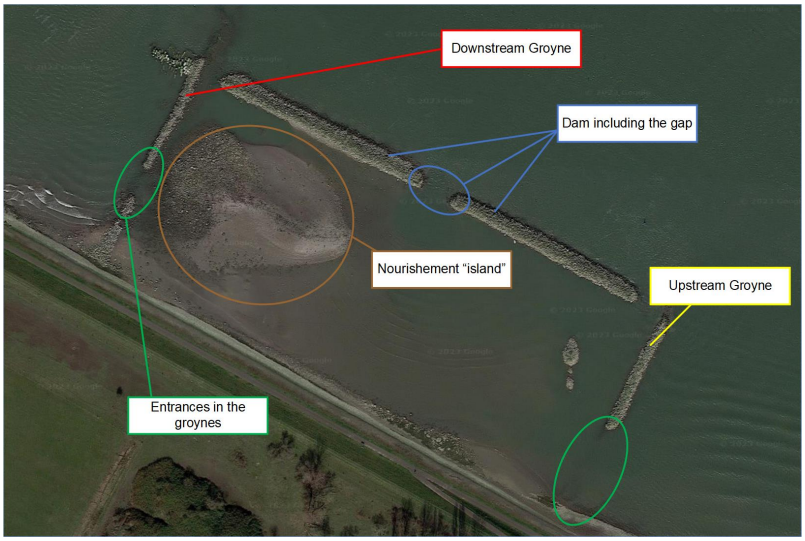

(a)

(b)

Figure 1.3: Both images show the modified groyne area during a low tide. (a) Overview of the modified groyne area, with the most important features marked. (b) Photo taken by Kees Sloff of the groyne area.

1.1.3. Ecological value

The future function of the intertidal area is to accommodate flora and fauna and let nature reclaim the area. The Atlantic Sturgeon is a part of the fauna that benefits from the newly created intertidal area. These fish are threatened by extinction, so measures like these will help the population. Different fauna including the Atlantic Sturgeon come from the sea or go the opposite direction for breeding. These areas will be used as a resting place during the trip, so they can get used to differences in salinity (Kranenbarg et al., 2017). Another way for nature to benefit from this area is through plant seeds. These seeds can be carried by birds or the river and come to the intertidal area within the groyne field. Plant life can emerge and flourish in this unique habitat with the right conditions. Such a similar intertidal habitat can be found upstream of the river in the gors Rozenburg (Stolk et al., 2015). This is this area's last natural intertidal habitat and a model for future projects. Its low gradient towards the water makes such an intertidal area special. It creates different flood durations for the different heights as shown in figure 1.4b, where 'piekoverstroming' means peak flooding, 'periodieke overstroming' means periodic flooding and 'dagelijkse overstroming' means daily flooding. Which will attract different types of vegetation improving the biodiversity of such an area.

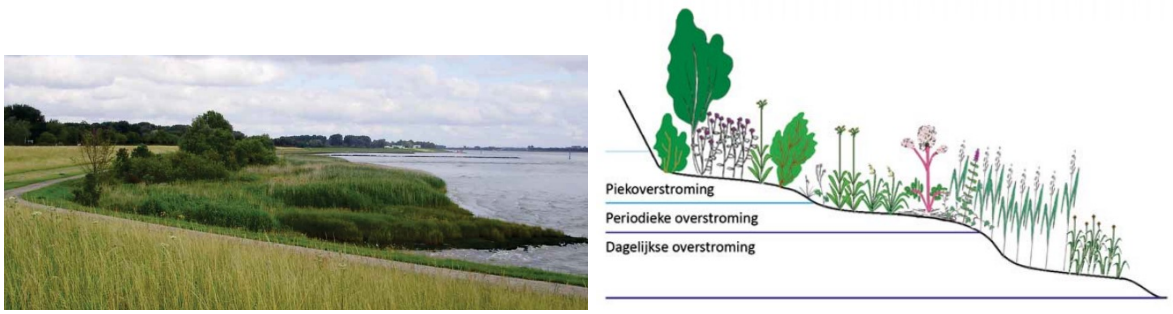

(a) (b)

Figure 1.4: The natural vegetation of an intertidal area. (a) The photo shows the Gors at Rozenburg (Stolk et al., 2015). (b) A sketch of the intersection of an intertidal area.

The changes that have been made to the groyne area will influence the flow and morphology of this area. This will have consequences for the ecological value of this project. The project's primary focus will be on creating a more considerable ecological value for this area, this means that the success of the project depends on creating this ecological value. Ecological value can be defined in different ways, which can range from extremely small species and insects that live in the sediment to larger fauna like fish and birds. The large amount of birds that visit the groyne area after the first nourishment is already visible, but there are no signs of vegetation yet.

1.1.4. The Nieuwe Waterweg

The Nieuwe Waterweg is a channel connecting the Rotterdam port with the North sea. The construction of this channel started at the 31^{st} of Oktober 1863, while the first ship sailed through on March 9^{th} 1872. The channel has been constructed in order to accommodate the demand of expansion from the port and city of Rotterdam ("De aanleg van de Nieuwe Waterweg", n.d.).

Over the years the Nieuwe Waterweg has been deepened by dredgers in order to keep up with the increasing size and depth of the vessels that come to the port. The most recent extensive dredging activities in this channel are from 2018 when 5 million Cubic meters of sand and sludge have been dredged in order to deepen the channel by $1.5\,\mathrm{m}$ meters. This deepening allows vessels with a draft up to $15\,\mathrm{m}$ meter to sail through the channel (Coomans, 2018). Figure 1.5 shows dredging activities in the Nieuwe Waterweg upstream of groyne area number 9.

The effect of the groynes in the channel is to narrow the river's flow artificially. By doing this the Flow velocities will naturally increase and as a reaction to this, also the erosion of the bed will increase. This means that the equilibrium depth of the river will increase and the bed will lower in order to balance the sediment going in and out of the river. The sediment is in perfect balance when the amount of sediment that comes into the river equals the amount of sediment that leaves the river. In reality, this perfect balance is never the case, so continuous dredging works are needed to ensure the depth of the channel.

Figure 1.5: Dredging in the Nieuwe Waterweg. Other modified groyne areas with different configurations can be observed as well. Photo obtained from "Boskalis en Van der Kamp baggeren Nieuwe Waterweg: nu geschikt voor grootste mammoetschepen" (2018).

1.2. Problem definition

In the pilot of groyne area number 9 there are a lot of uncertainties about its behavior in the future and its ability to fulfill the needs of the project. The ecological side of the project has big uncertainties over how nature will reclaim the tidal flat. The problem with measuring and predicting how the ecology will develop in this area is the large uncertainty and differences of opinions between ecologists. Different theories and approaches exist about how and where the flora and fauna should and will develop in that area. In order for ecologists to make a proper prediction the conditions of the intertidal area have to be known. Important aspects of these conditions are the movement of the sediment and the flow in the groyne area under different circumstances, which will be heavily influenced by modifications made to the groyne area. This is important for the second big deposition of sediment in the groyne area, which is done in December 2022. This research will be used to give an overview of the conditions in this groyne area after the first nourishment.

Previous researches have been conducted to the groyne areas in this region. One of these Previous researches has been conducted based on computer models and calculations. In the research of Nijhuis (2021), a depth average model was build in Delft3D of a tidal park. From that model the behavior of the sediment and flow as a reaction to different parameters has been tested. That research has been done for different types of groyne fields along the Nieuwe Waterweg. This research will focus entirely on the groyne area number 9 which has a specific layout that is not found in any other groyne area along the Nieuwe Waterweg. Fieldwork experiments in this groyne area and the data that is obtained from these experiments will give a new and additional perspective to the influence of these modifications on the flow inside such a groyne area.

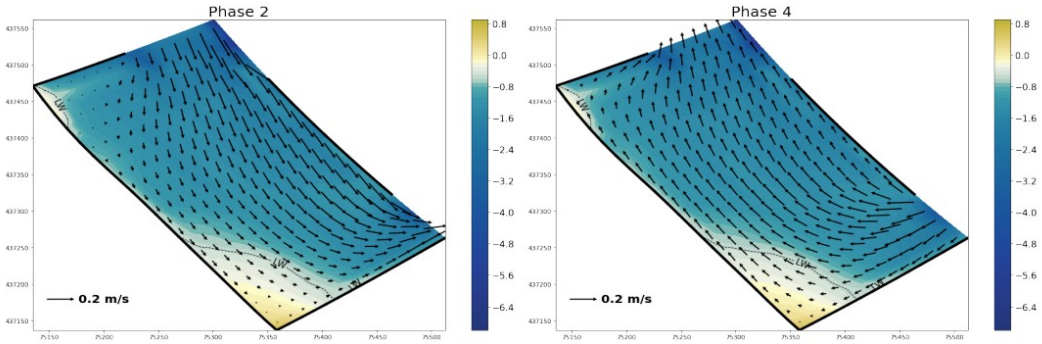

Figure 1.6: Ebb and flood flow modeled by Nijhuis (2021), this model has been made with a modified groyne area which has a different layout than groyne area 9. Phase 2 is during flood and Phase 4 is during ebb.

1.2.1. Objective

The objective of this research is to obtain more knowledge on how the flow and sediment behavior has changed due to the modifications to the groyne area, under the influence of natural phenomena and the passing of ships. This research will focus on the abiotic conditions contributing to ecological values. The selected area of focus is the groyne area number 9, because this is the chosen area for the pilot of the project "Proeftuin Sediment Rijnmond".

1.2.2. Research question and sub-questions

To achieve this objective an answer has to be given to the research question: *What is the influence of the groyne area modifications to the flow characteristics inside this area?*

Additional sub research questions have been defined to answer the research question stated above:

1. *What is the effect of physical processes on the flow inside the groyne area?*
2. *What is the effect of passing ships on the flow inside the groyne area?*
3. *What are the effects of the hydrodynamic conditions on the behavior of the sediment?*

1.3. Research method and structure

Before the research is done a baseline of understanding is needed. This is done in the first section, where the information is displayed and dissected. The scale of this information ranges from large-scale processes such as tides and river systems to small-scale processes like the forces on a sand grain. The structure that will be followed in that section starts with the large-scale processes and advances to smaller scales, so it will eventually end with the smallest scales. In this section, only the basic information is provided. During the analysis of the results, extra information will be covered which is essential to that particular section.

The knowledge for answering the research question will be obtained by measuring in the field and analyzing the data that has been obtained. The analyzed data will give an insight into the flow of the water through the groyne area and the shipping and natural influence on this flow. Because this is the field research in this groyne area, the measurements can also be regarded as a baseline measurement of the area. This baseline measurement is important to give an impression of the present activities in this pilot and predict the behavior after future nourishments and modifications.

The data for this research will be collected with measurement campaigns in the project area. For these measurement campaigns, choices have been made regarding the type of equipment, placement of this equipment, duration of the data collection and the settings of this equipment. All these choices influence the data that is obtained during these campaigns. For understanding these choices a certain degree of technical knowledge about the measuring equipment is provided. As well as the technical knowledge, information has been given about some practical problems that emerge during a measurement campaign. All these practical and technical choices and limitations will give a good layout of the measurement campaigns which have been carried out. After the campaigns, quality assurance has been carried out.

In total there have been two measurement campaigns. The first measurement campaign was intended to obtain data over an extended period. From this campaign point data about the flow velocities, direction and pressure have been obtained for three weeks. This point data was obtained from six locations inside the groyne area. The second measurement campaign was intended to obtain more detailed flow data from one tide. With line measurements at different intervals in the groyne area changes in the flow over space during one tide have been measured.

The obtained data has been filtered to make it usable for further analysis. The data contains point measurements of the water velocity and pressure for the six locations. From this velocity data, the directions and magnitude of the flow over time are obtained. Also, velocity data over the depth has been obtained for only one tide. This will be combined with the point data to fill the needed gaps. In this data, a distinction will be made between small-scale events within several seconds to large-scale events ranging from hours to days. Distinctions in time like this present the different influences on the flow in groyne area and help to explain and dissect the point data. This is necessary to answer the questions about the flow in the groyne area.

The sediment compositions for all locations have also been obtained. Combining the characteristics of the sediment gives information about the movement of this sediment by the different influences on the flow.

2 | Background

In this chapter the knowledge needed for the research will be explained. To understand the changes in the system, the behavior of the original system must be known. This original system consisted of a typical open groyne area connected to the Nieuwe Waterweg. The scales of the different systems will differ from large-scale river systems to small-scale behavior of sediment grains. This literature overview will be structured in this chapter from large-scale to small-scale processes to get an overview of the complete system.

2.1. The main channel

Multiple physical influences control the flow in the river's main channel. These influences can come from artificial structures and interventions in the river. In addition, natural processes like local winds and river discharges cause other processes that influence the river. All these processes determine the flow and the behavior of the water.

The Nieuwe Waterweg is the connection between the Port of Rotterdam and the sea. The Oude Maas and the Nieuwe Maas are branches of the Rhine river and flow into the Nieuwe Waterweg, which can be seen in Figure 2.1. This flow through the channel of the Nieuwe Waterweg is influenced by the sea and these two branches of the Rhine. The Oude Maas also branches into the Haringvliet, which is disconnected from the sea by the Haringvliet dam. This dam controls the discharge from Haringvliet into the sea, and by doing so it also controls the distribution of the water that comes from the Oude Maas.

Figure 2.1: River map of the Netherlands. The rivers close to the Nieuwe waterweg are highlighted

The other driving force of the main channel comes from the tide of the sea. Because of the semi-diurnal tide, there are two high and low waters a day in the main channel. This tide also brings in saline water, which is a problem for agriculture, industry and drinking water. To control the saline water intrusion, it is necessary to maintain a minimum discharge in the channel. Still, increasing water levels at sea and decreasing river discharges reduce this effect, causing saline water to penetrate further inland (Klijn et al., 2012). Above is described how the discharge in the Nieuwe Waterweg is controlled by the dam and this mechanism is also used to maintain a minimum discharge in the main channel.

Ships also have and significant impact on the main channel. From the AIS data, it has been seen that the average amount of ships that pass through the channel is 151 ships a day, with a maximum draught of $25\,\mathrm{m}$ and an average velocity of $6\,\mathrm{m\,s^{-1}}$. The waves created by these ships cause a significant load on the river banks and groynes.

2.2. Ecology

Ecology is a widely used term for all life in the area. This research will only focus on the most essential parts of the ecology in this area. The Dutch government categorizes the ecological goals for the different areas. The Nieuwe Waterweg falls under category O2b (Altenburg et al., 2021). Category O2b is "an estuary with moderate tidal range and with shipping and/or no tidal current". For the fish population in this area, the Nieuwe waterweg scores unsatisfactory to moderate for the amount of fish. Certain fish species use the intertidal areas as a resting place to acclimate salt and fresh water. It is crucial for these intertidal areas to have creeks that do not get cut off from the channel during low water. If fish get cut off from the channel they become an easy prey for birds and other predators (Altenburg et al., 2021).

The aim of the project is to create an intertidal area, which is an ecosystem with a particular behavior. Conditions that such an ecosystem needs to thrive can be divided into abiotic and biotic conditions. Abiotic conditions are non-living physical and chemical conditions that influence the ecosystem like the tidal elevation (Wolters et al., 2005). In contrast, biotic conditions are the living conditions for example: the predators, grazers and seed dispersion.

For this research, the biotic conditions will be neglected. These biotic conditions don't influence the flow and sediment inside the groyne area, because of this a deeper understanding of the biotic conditions is unnecessary to answer the research question. The two essential conditions for such a system are a fluctuating water level and a gradually sloping bed. The fluctuating water level is caused by the tide and floods the vegetation for a part of the day. Another effect of the tide is a fluctuation in salinity. In a high tide, the water flowing in from the sea causes a higher salt concentration in the water than during a low tide when the water flows in from the river. Because of the sloping bed, the amount of time that the different areas are flooded differs due to the difference in elevation. Vegetation types that need more water and can endure longer flooded periods will develop on the lower parts. In contrast, plants with a lower tolerance to flooding will develop on the higher parts.

Z. Zhu et al. (2021)) has done an experiment to research the resilience of seeds to hydrodynamic conditions. This has been done by placing a mixture of natural seeds, mimic seeds and tracer particles in the ground at several different locations at the eastern and western Scheldt. These have been placed in both regular and defaunated soil. The sediment disturbance, water pressure and velocity were measured during the period. After eight weeks the seeds were dug up or relocated and the persistence of the seeds was calculated as the recovered amount of seeds divided by the total amount. Both Scheldts have similar conditions compared with the Nieuwe Waterweg. The Western Scheldt is similar to the Nieuwe Waterweg a busy shipping route that is openly connected to the sea, meaning that waves and the tide are both necessary hydrodynamic conditions. In Figure 2.2 can be seen that waves and sediment disturbance significantly impact seeds persistence.

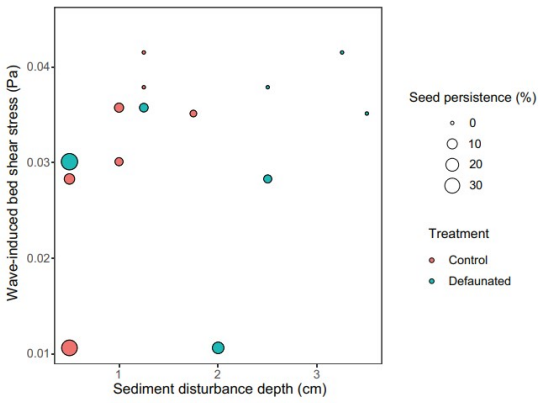

Figure 2.2: The combined data from the defaudated treatment and the control showed that the persistence of seeds on the surface decreased with increased wave disturbance and sediment disturbance (Z. Zhu et al., 2021).

2.3. Flow inside groyne areas

Multiple types of research have been done on the flow within a typical groyne area. These researches show that eddies dominate the flow inside typical groynes. However, the groyne area in this research has been modified, which will alter this behavior. As a result, the groynes from the pilot will vary between being emerged and submerged, and the dam will change the flow exchange between the river and the groyne area.

2.3.1. Typical emerged groyne areas

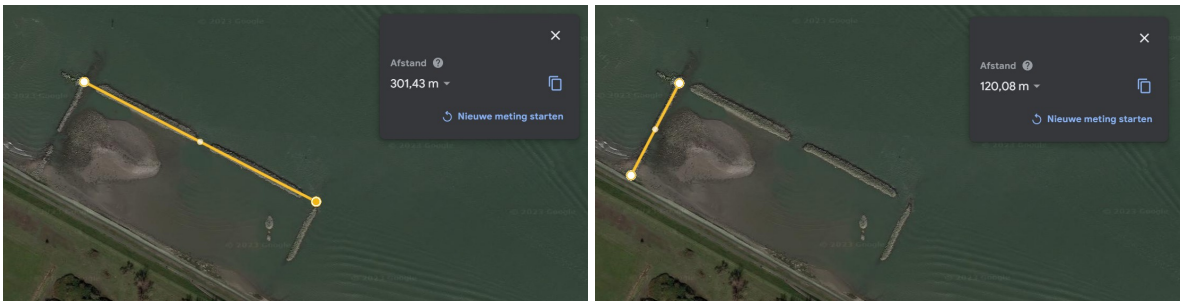

(a) (b)

Figure 2.3: The measured lengths of the dam and the groynes using Google Earth.

In the original situation with the groynes in the Nieuwe Waterweg the height of the groynes is approximate $-1\,\mathrm{m}$ from NAP. For specifically groyne area number 9 the length of the groynes is around $120\,\mathrm{m}$ and the distance between the groynes is around $300\,\mathrm{m}$, but this should not differ too much from the other groyne areas as can be seen in Figure 2.3.

In general groynes have multiple functions in the channel:

- Groynes are an efficient way to narrow a channel or river. When the channel gets narrowed, the velocities in the main channel will increase. This increase in velocity will increase the amount of suspended material that can be carried by the flow, resulting in an erosion of the bed. Eventually, this will lead to a morphological equilibrium with increased water depth and a lowering of the bed.
- Groynes protect the shores of the channel against erosion. In between the groynes eddies are formed from the flow. The size and number of eddies depend on the configuration of the groynes with respect to each other and the river. These eddies dissipate the energy from the flow and this causes lower velocities at the banks of the river.

- The groynes also help as a protection against flooding. In a flood event, the discharge through the channel increases significantly and automatically increases the water depth. The groynes narrow the flow in the channel but do not physically narrow the river. When the water depth increases above the level of the groynes the flow width of that part of the channel increases to the physical width of the channel. This means that because of the significant increase in the river's width, the depth increase will slow down and the discharge increases.

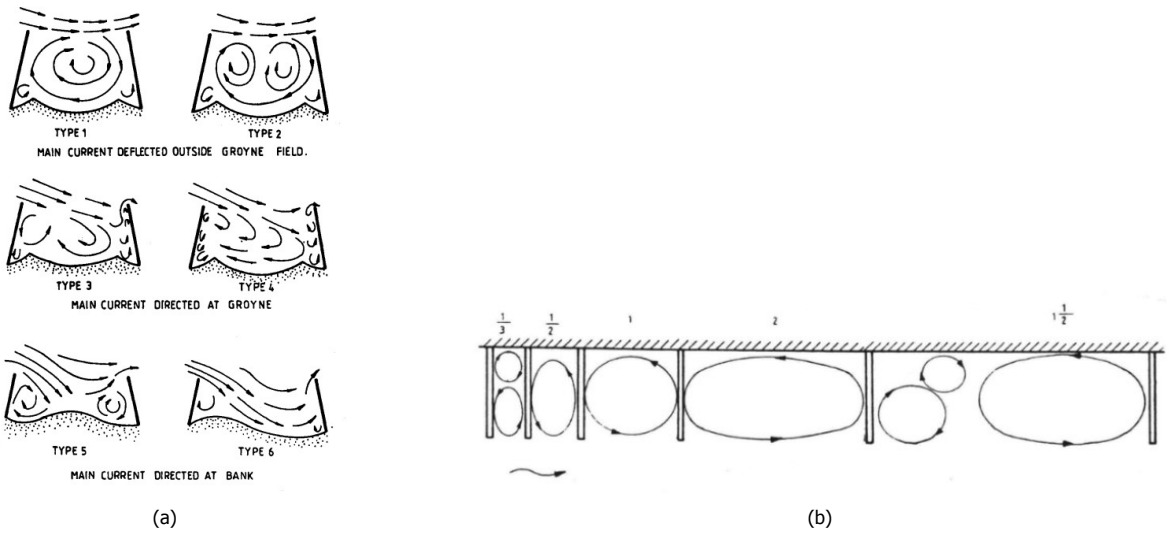

Figure 2.4: The different types of eddy formation in an emerged groyne area. (a) 6 different types of eddy formation (Przedwojski et al., 1995). (b) Eddy formation due to the length of the groyne area (Bouwmeester, 1987).

According to Przedwojski et al. (1995), six types of different eddy formations are possible in a groyne area. The groynes in the Nieuwe waterweg are perpendicular to the channel. From Figure 2.4b it can be seen that with the length and width which are mentioned above more than one eddy will form between the groynes. When two eddies are present in the groyne area from Figure 2.4a a type 2 situation would exist. Such flow patterns have also been measured in a groyne area in the Waal. In Figure 2.5 are measured flow velocities and directions with 4 ADVs. These directions indicate the flow same flow pattern as in Figure 2.4.

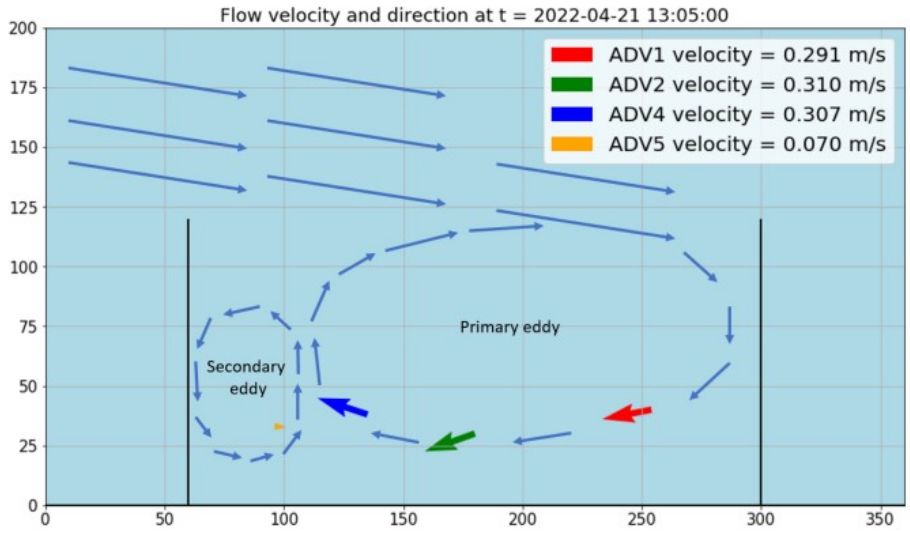

Figure 2.5: Flow observed in a groyne area in the Waal (Brouwers, 2022).

In Brouwers (2022) the effect of ships on a groyne area has been researched. In this research, the flow velocities have been measured in a groyne area in De Waal. A total of four ADVs have been placed

in this groyne area and measured the pressure and the flow velocities at different locations. In that location is no tidal influence on the river, so the groyne area is only affected by the river discharge and shipping. It was found that for a flow without the influence of ships, the flow consisted of 2 eddies. The measured flow in the open groyne area corresponds to the flow from Figure2.4a.

2.3.2. Submerged and modified groyne areas

The groynes from the project area are designed to be submerged by high tide and emerged by low tide. This means that in low tides the flow can only flow in and out through the openings in the dam and the groynes, while in high water this flow completely changes. The submerging of the groynes causes the flow to flow in and out of the area over the groynes while still favouring the areas with the openings. These openings give the least resistance to the flow but can only handle a limited discharge. When the water flows over the groynes, the vertical flow can be compared to the flow over a weir. Because weirs have different shapes and characteristics, this comparison still has complications.

The conservation of energy and momentum governs the flow over a weir. Upstream of the weir, the flow gets contracted while downstream the flow expands. In the passing of the weir the flow experiences a loss of energy which can be seen in Figure 2.6 as ΔH. The acceleration zone is the area indicated between 0 and 1 which is governed by the conservation of energy.

The equation for the conservation of energy, where H is the energy head, d is the water depth, U the velocity and both α's are correction coefficients.

$$H_0 = H1 \rightarrow d_0 + \alpha_0 \frac{U_0^2}{2g} = d_1 + \alpha_1 \frac{U_1^2}{2g} \tag{2.3.1}$$

The deceleration zone, which is located between 1 and 2 is governed by the conservation of energy, because of the lost of energy. When the flow leaves the weir, it has to reattach to the bed. This reattachment causes an eddy that recirculates the water in the zone behind the weir. The shape and size of this re-circulation zone depend on the flow conditions of the water and the shape of the weir itself, the type of flow regime, the difference in water depth and the backwards facing step depend on these conditions.

The equation for the conservation of momentum, where h_g is the height of the weir and q the discharge.

$$\frac{1}{2} g \left(d_1 + h_g\right)^2 + q_1 u_1 = \frac{1}{2} g d_2^2 + q_2 u_2 \tag{2.3.2}$$

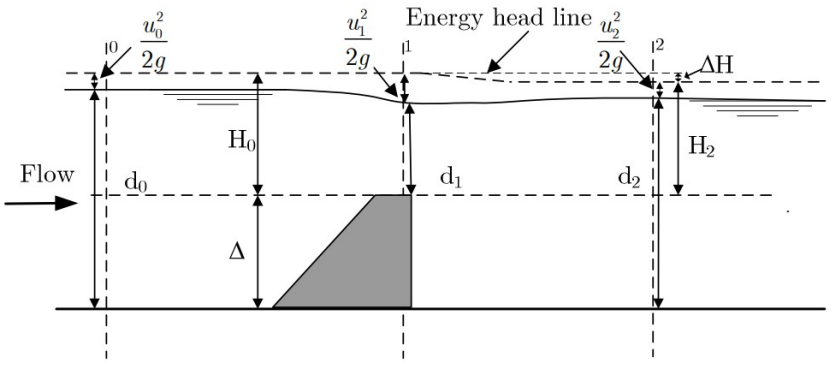

Figure 2.6: Schematic overview of the flow over a weir (Ali, 2013).

When a groyne area changes from emerged to submerged the flow changes. The flow that is governed by the eddies is replaced by a flow that resembles the flow over a weir. In Ambagts (2019) the flow over and around submerged groynes is analyzed using a numerical model. Figure 2.7 shows a sketch of the flow over such a groyne field. Only a section of the discharge will pass over the groyne field and the majority will flow through the main channel.

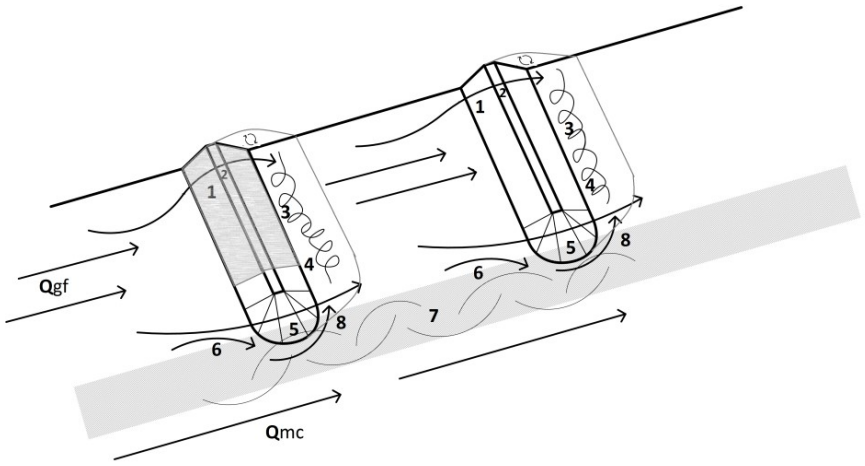

Figure 2.7: A sketch from Ambagts (2019) showing the flow over and around a submerged groyne field.

From 1 to 3, a section of the flow approaches the submerged groyne and accelerates over the slope. The flow separates from the top and a re-circulation zone forms showing the same behavior as discussed from the weir. Over the length of the groyne the thickness of the re-circulation zone is constant until 4 where its decreases and vanishes at the edge of the groyne. At 7 a mixing layer forms between the main channel and the groynes, which increases in thickness with increasing water levels. The flow near the bottom is directed into groyne field, while the flow at the top is in the opposite direction. This flow hits the groyne and is deflected away from the main channel except for the flow at a small portion of the tip, which is reflected in the opposite direction.

Nijhuis (2021) researched how modifying a groyne area affects the flow within that area. This was done by simulating the flow through a groyne area with an opening at the end of the downstream groyne and a dam sheltering the groyne area. Only the effects of the tide on the groyne area have been included in this study. The velocity graphs obtained from the different simulations can be seen in Figure 2.8.

Various boundary conditions have been used to obtain an overview of the effects on the groyne area. Changing the hydrodynamic forcing was found to have a limited impact on the flow velocities during spring tide conditions. Changing the bed level in the groyne area does have a significant effect on the velocities. Increasing the bed level decreases the flow velocities in the groyne area. Decreasing the length of the dam increases the ebb velocities. Changing the height and size of the groynes affects both the ebb and flood velocities. The velocities increase with a decreasing groyne height, while the decrease in the length of the groynes only has an impact on the flow velocities when the size is decreased at both upstream and downstream groynes.

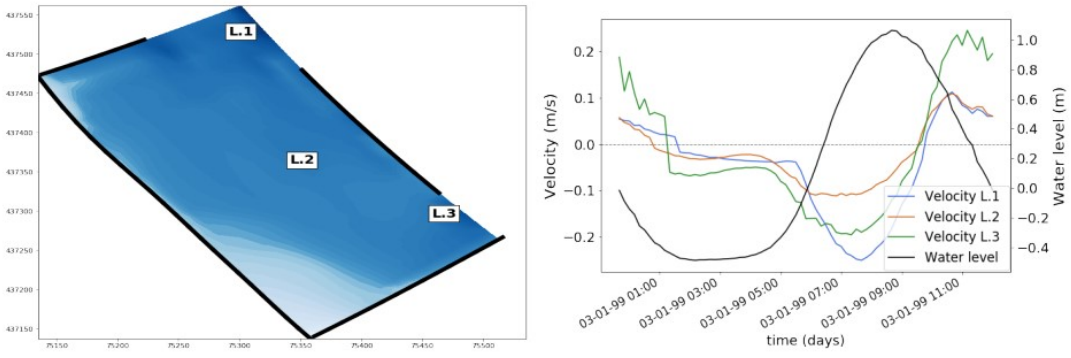

(a)

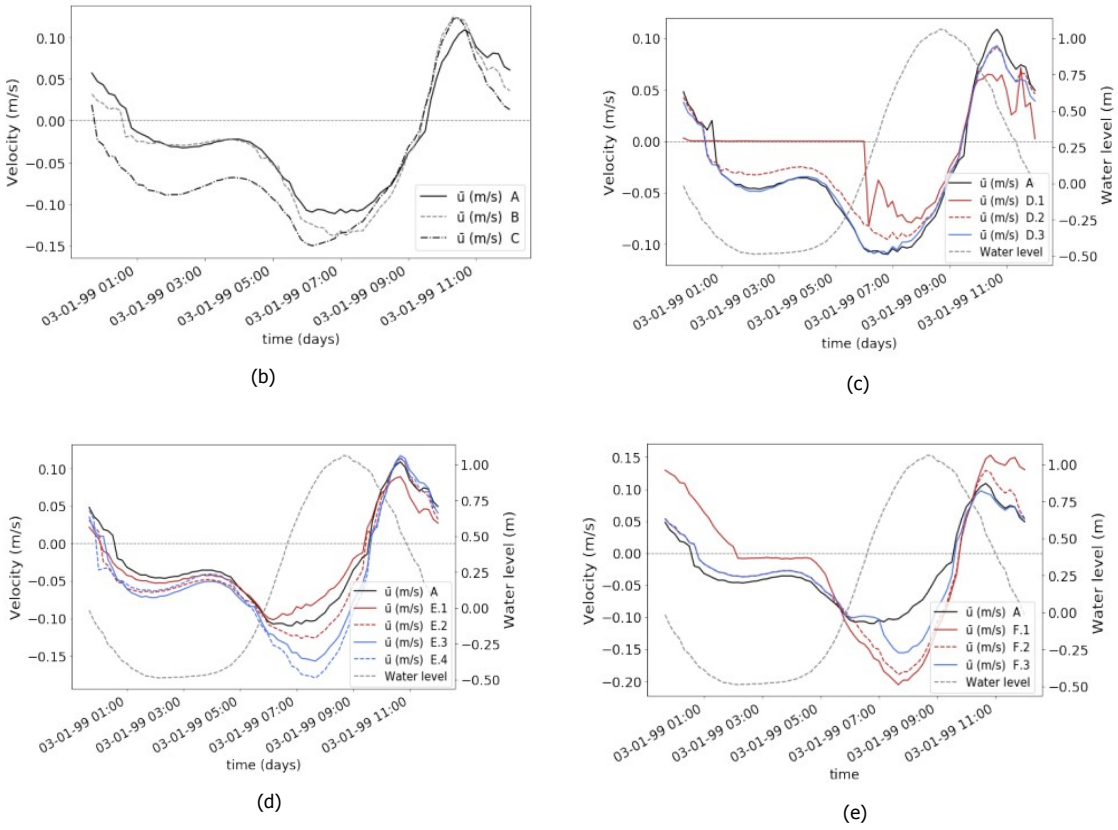

Figure 2.8: The simulations with different parameters (Nijhuis, 2021). (a) The base case for the model. (b) A is a normal tide, B is a spring tide and C is a spring tide in combination with a surge of one meter. (c) From D1 to 3 the bed is lowered. (d) From E1 to E3 the dam is shortened and at E4 the dam is removed completely. (e) From F1 to F3 the groynes are heightened.

2.3.3. Ship and interactions with groyne areas

When a ship sails through the water it creates a flow alongside the ship itself. At the front of a ship a wave is created, which is called the primary wave. This wave is created by the water that collides with the ship. This causes the water level at the front of the ship to rise. At the sides of the ship, a drawback and water level depression develop. Secondary waves develop at the end of the ship. These waves are caused by the pressure pattern due to the discontinuities in the hull profile (Schiereck and Verhagen, 2012). The complete water behavior due to a sailing ship can be found in Figure 2.9a.

These different water motions from the ship have an impact on the groyne area. The primary and secondary waves travel at an angle from the ship itself. The impact of these waves does not differ from average wind or sea waves with similar wave characteristics. Between the primary and secondary waves at the ship the water level drops, this is called the drawback (Yossef, 2002). The drawback causes the water to be pulled to the ship, similar to the pullback of water that is experienced at a coast before a wave. From the Bernoulli and continuity equations it can be found that the depression of the water depends on the blockage and the relative velocity of the water according to the ship. The blockage is the relation between the underwater cross-section of the ship and the cross-section of the channel. The velocity of a typical ship is limited by the velocity at which the return flow is a critical flow. This is called the limiting velocity. Above this velocity, the energy used significantly exceeds the velocity that is gained. A ship's limiting velocity depends on the ship's length and the water depth. A ship typically sails with a velocity at 90% of its limiting velocity (Schiereck and Verhagen, 2012).

Brolsma et al. (1988) researched the effects of a ship passing a groyne area. The velocity of the ship itself and the drawback it causes, makes it difficult to precisely predict the behavior of the water in the groyne field. From this research with different ships, a 2D stigmatization has been made to indicate the

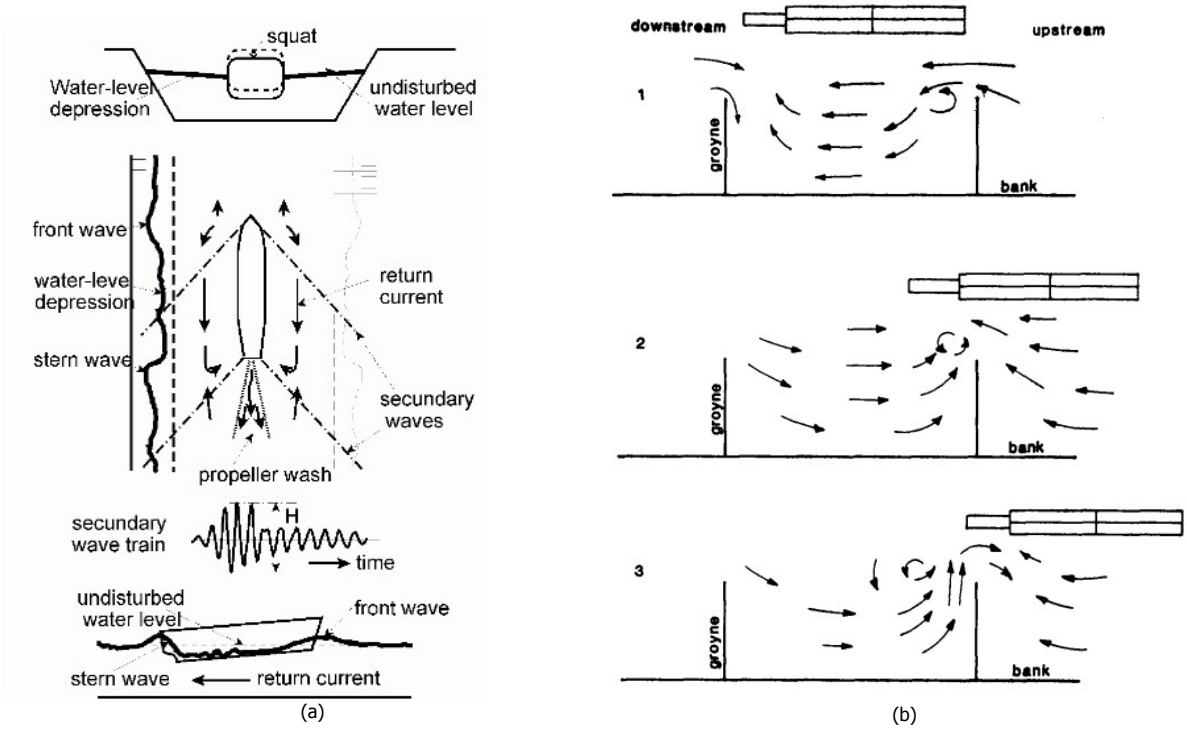

Figure 2.9: Influence of passing ships on the flow. (a) Water motions due to sailing ship (Schiereck and Verhagen, 2012). (b) Different stages of a ship passing a groyne area (Brolsma et al., 1988).

flow directions inside the groyne field which are shown in Figure 2.9b. This figure shows the pull effect of the ship on the water in the groyne area. The flow velocities increase with an increase in relative sailing velocity, a decrease in passing distance between the ship and the groyne field, or a decrease in the size of a groyne field (Yossef, 2002).

Brouwers (2022) researched the different effects of the different ship characteristics on wave influence in the groyne area. The influence of different ships that passed the groyne area was analyzed at four different locations inside the groyne area. Two different effects from the crossing ships were measured: the increase in water level and the increase in velocity. The ship's draught was found to have no influence on the water level or velocity increase at all locations. The effect of the width is questionable for the increase in velocity, while it has an apparent effect on the water level at all locations. For the other characteristics, the effects were apparent for some of the locations.

2.4. Behavior of the sediment

The sediment behavior is governed by the different forces that work on a sediment particle. The force balances determine if the sediment particle will be brought in motion or if it settles. The most important external force on such a grain is the water itself. Nothing happens when there is a balance between this force and the other forces. But, when the forces exerted from the water on the sediment particle increases relative to the other forces, the in balance of the forces initiates the motion of the particle.

2.4.1. Initial movement

There are different approaches that translate the forces on the soil to whether or not there is movement. The most common approach is from Shields (1936). The basis of Shields is that there is only sediment transport if the shear stress exerted on the bed, which is shown as τ is larger than the critical shear stress of the sediment particles. The shear stress on the sediment is caused by the flow of the water over the bed. This theorem doesn't look at the individual sediment particles but rather at the whole bed. In this approach, the shear stress is the active force on the bed and the resistance is the gravity force

on the bed. This is used in the relation between dimensionless shear stress and the particle Reynolds number (Schiereck and Verhagen, 2012). This critical dimensionless shear stress is also called the Shields parameter, which is shown as ψ_c. This can be seen in Equation 2.4.1, where u_{*c} is the critical shear velocity and D the characteristic grain size.

$$\psi_c = \frac{\text{load}}{\text{strength}} = \frac{\tau_c D^2}{(\rho_s - \rho_w)\, gD^3} = \frac{\tau_c}{(\rho_s - \rho_w)\, gD} = \frac{u_{*c}^2}{\Delta g D} = f\,(\mathrm{Re}) = f\left(\frac{u_* D}{\nu}\right) \tag{2.4.1}$$

van Rijn (1984) used the theory that delta has minimal variations and can be seen as a constant. Delta can be obtained with $(\rho_s - \rho)/\rho$, where ρ_s is the density of the particle and ρ the density of the fluid surrounding the particle in this case being water. With this, it is no longer necessary to iterate the formula to obtain the critical shear stress, which is needed in Shields's formula. Van Rijn uses the dimensionless particle diameter, which contains the particle diameter as the only variable.

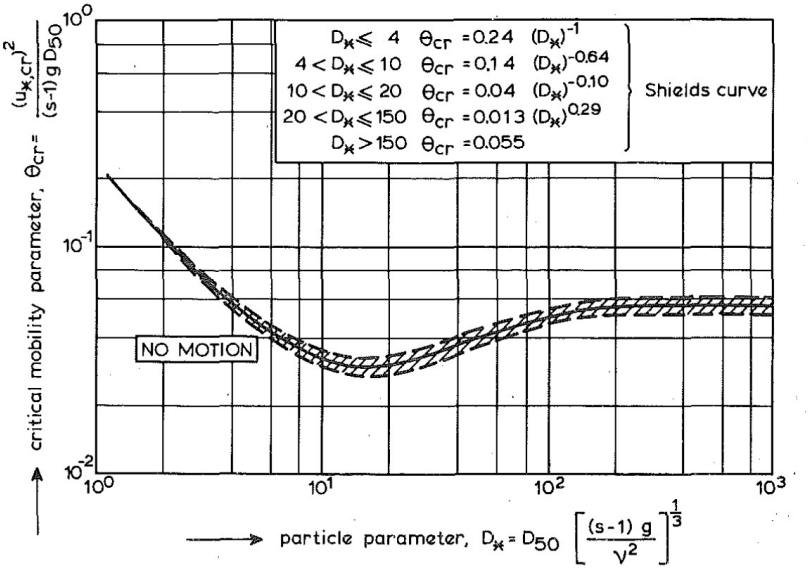

Figure 2.10: The Shields curve modified by van Rijn, 1984. The approach of van Rijn has been used in a uniform flow.

2.4.2. Bed friction and shear

When water flows over an object there is a difference in the water velocity and the velocity of the object itself. In most cases, the object consists of a bed that does not move, so the object itself has zero velocity. At this bed, the water particles get slowed until they eventually reach a velocity of zero when they are at their nearest point to the bed. The zone where the water gets decelerated by the bed is called the boundary layer. This force from the bed to decelerate the water flow is called the shear force or shear stress. When this boundary layer grows, it can change from a laminar boundary layer into a turbulent boundary layer. The turbulent boundary layer consists of 3 different layers (Elger et al., 2012): first the viscous sublayer, then the logarithmic region and at last the velocity defect region. The first layer is governed by laminar flow and has a minimal thickness. The thickness of this layer increases when the shear stress from the bed decreases. The next layer is governed by turbulence. The fluctuating velocities and eddies cause the deceleration of the flow in this layer. Eventually, the flow is too far away from the first layer that the rules from the second layer can't be applied anymore and that's when the last layer starts, although there is still a slight overlap between the second and third layers. A sketch of these different layers is shown in Figure 2.11.

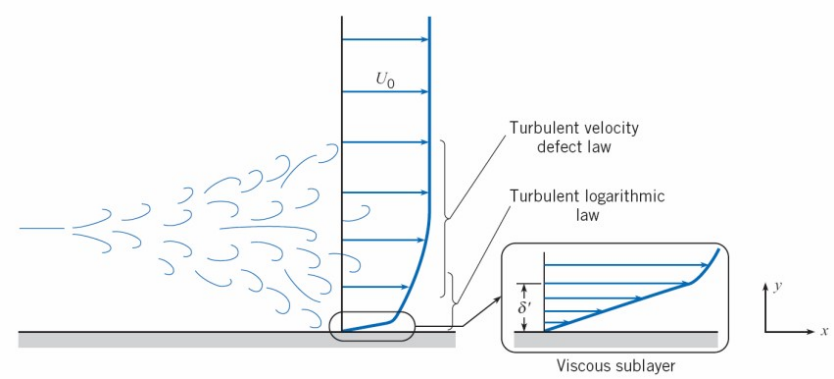

Figure 2.11: Sketch of the different zones in the turbulent boundary layer (Elger et al., 2012).

The shear stress is caused by the friction of the bed and this friction depends on the roughness height. This height can be either caused by the thickness of the viscous sub-layer or by the roughness of the bed itself. When the bed roughness exceeds the thickness of the viscous sub-layer the bed is called hydraulically rough and when this is not the case, it is called hydraulically smooth. The shear stress consists of a combination of skin friction and form drag. The sediment particles themselves cause skin friction while form drag is created by the bedforms in the sediment.

There are many different approaches to obtaining the values for the roughness height and the shear stress. Combining waves and the current increases the difficulty of obtaining these values. In Q. Zhu et al. (2016) different approaches were used to calculate the combined shear stresses from field data. In this research, it was found that it was difficult to calculate the current shear stress with winds and waves present using the different methods. This results in more significant differences when calculating the combined shear stress under more windy conditions. The combined bed shear stress doesn't increase linearly. In Soulsby and Clarke (2005) an overview is given for calculating the current, wave and combined shear stresses for smooth and rough beds.

2.4.3. Sediment erosion and deposition

There are different types of sediment. The most commonly found in rivers are gravel, sand, silt and clay. Gravel and stones are only found in the more upstream regions of the river, so these will not be found near a natural basin. This means that in the project area, only sand silt and clay are important. For the classification of the different types of sediments, the size of the particle will be used.

- Sand has a particle size larger than $63\,\mu m$
- Silt has a particle size between $2\,\mu m$ and $63\,\mu m$
- Clay has a particle size smaller than $2\,\mu m$

The classification of the different particles is essential because there is a difference in behavior. Sandy material has no cohesion, which means that its behavior can be accurately predicted by shields and other approaches. The behavior of silt particles is similar to that of sand. Silt is not a cohesive material itself, but it increases the cohesion of the mixture. Clay has the smallest particle size and has a very different behavior compared to sand and silt. Where sand and silt grains have shapes comparable to a sphere, clay particles are shapes that are more comparable to plates. This shape makes that clay particles have a large area relative to their mass. Clay particles are negatively charged and because of this, the particle is surrounded by a cloud of positive charged ions called the electric double layer. The electric double layer of a clay particle is attracted to the negatively charged particle itself, but at the same time repelled by the electric double layer of the other clay particle. The clay particles can bind together if the double layer is sufficiently small. This process of the binding of multiple clay particles is called flocculation.

The strength of the binding in a flocculated particle differs due to type of clay particle, the charge of the electronic double layer and the type of flocculation. The binding between the particles can fail if the forces on the particles are too large. Turbulence and high flow velocities cause these forces to

exceed the strength of the bonds, which results in the separation of flocs. Flocculation can occur to clay particles because of their large surface area compared to their mass. This is impossible for sand and silt particles due to their relatively large mass (Chassagne, 2021). According to S. AI Ani and Huntley (1991) salinity increases the bonding strength of a floc. This can have a significant impact on brackish areas where sea water and freshwater meet. In these areas, the salinity differs from flood to ebb.

3 | Methodology

To get a better understanding into the hydrodynamic processes in the groyne area data has been obtained from the area. This data has been acquired from two measurement campaigns in the groyne area. More details about the campaigns and the fieldwork can be found in appendix A. These details extend to day-to-day activities and the research team.

With specialized measuring equipment, the area has been monitored in different ways. The processes which have been monitored will consist of velocities, directions and water depths. Together with the obtained sediment compositions, this data is the basis for understanding the critical processes influencing the flow inside the groyne area. With this better understanding of the flow, movement patterns of the sediment can be predicted and their influence from the external factors can be found. This information on the flow can be used to predict the behavior after the planned second nourishment.

3.1. Existing data

After the first nourishment, the changes in the flow behavior in the groyne area have not been measured. The only measurements carried out in this groyne area before this research are scans of the bed level, done twice yearly. When these scans are put together, they reveal the bed level changes in the groyne area, as shown in Figure 3.1. These bed scans are also used to obtain the bed topography of the groyne area, which is shown in Figure 3.2. With a time of half a year between scans, the effects of smaller-scale influences, such as the tides or shipping, can't be seen.

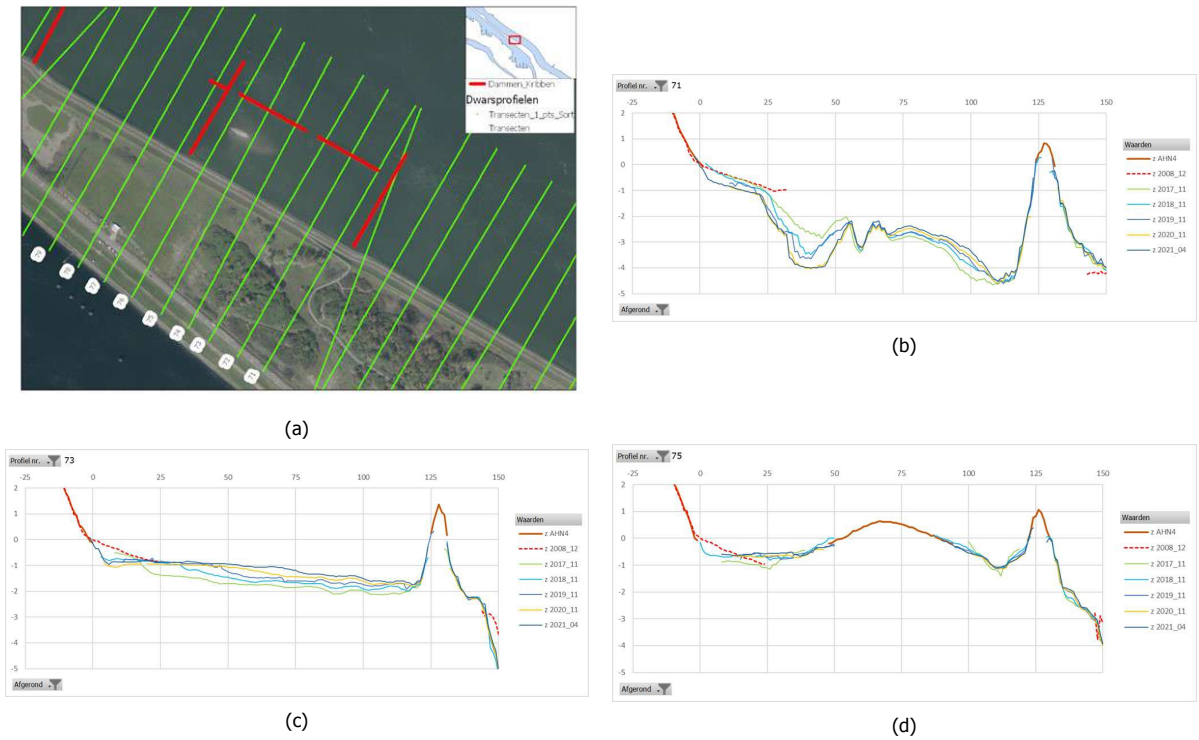

Figure 3.1: Changes in bed level observed by Rijkswaterstaat. (a) Overview of the locations of the cross sections. (b) Location 71. (c) Location 73. (d) Location 75.

These bed level changes from Rijkswaterstaat indicate erosion in some spots inside and outside the groyne area. Figures 3.1 and 3.2 show a significant difference in the erosion and deposition magnitude

of the different locations inside the groyne area. This gives a first indication of the effect of the nourishment and the modifications to the flow and sediment inside the groyne area. Many of these processes have a smaller time scale than half a year. This makes that the data of Rijkswaterstaat can only give an indication but can't give definitive answers to questions in this research.

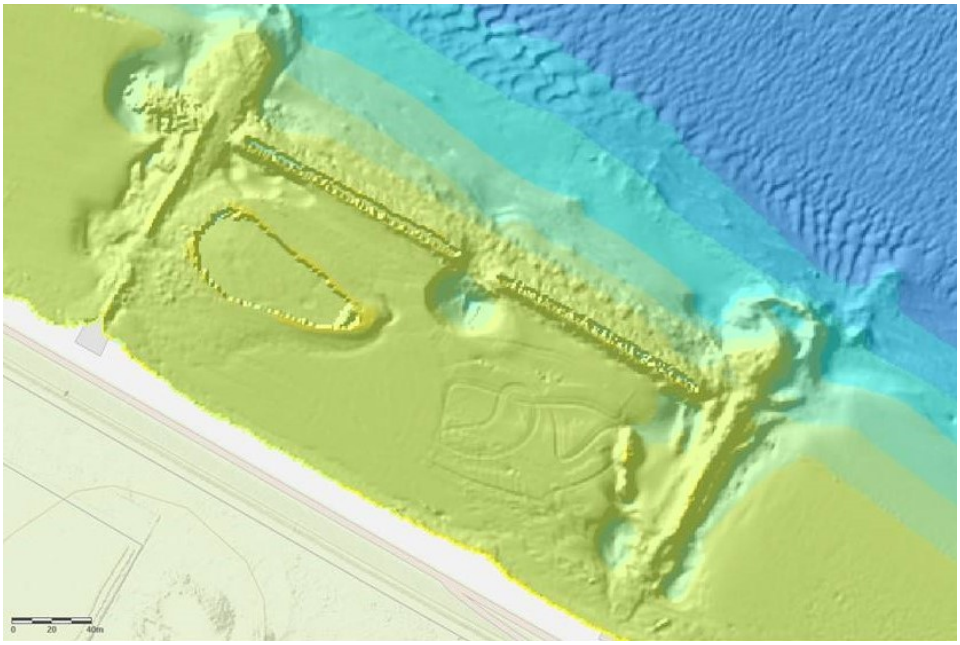

Figure 3.2: Topography of the bed in the groyne area. The deeper parts are colored in blue and the more shallow parts in green. This data has been acquired by Rijkswaterstaat.

To obtain data on the effects of the different physical processes that influence the flow within the groyne area, it is essential to use a time scale that is able to capture these different mechanisms. All research equipment is limited to a range of measuring frequencies depending on the type, brand or model. This means that the measuring frequencies of such equipment are a factor in selecting the materials used in the measuring campaigns.

3.2. First measurement campaign

The first measurement campaign aimed to obtain data for three weeks. During these three weeks, changes in the hydrodynamic conditions become apparent. These changes give insight into the flow difference between the different tides. Furthermore, with this data, the effects of ships with varying characteristics at changing moments in the tide can also be observed.

3.2.1. Equipment

Different instruments have been chosen for different measurements. Availability and practicality can differ significantly between the pieces of equipment that have been used.

The Nortek vector ADV has been selected for the flow measurements. The working principle of this instrument uses a physical phenomenon called the Doppler effect. This is the effect of a change in the frequency of sound waves when the transmitter and observer move in respect to each other. The ADV transmits sound waves that will be reflected back by the suspended matter organic and non-organic. Due to the Doppler effect, the reflected signal will be shifted by the movement of the suspended material. The extensions of the ADV head will detect this shifted signal, and this detected signal is used to calculate the velocity and the direction (*The Comprehensive Manual for Velocimeters*, 2019).

The Acoustic Doppler velocometer or in short ADV measures the flow velocity in three different directions as shown in Figure 3.3b. With these three measurements, the direction and the total amount of

the velocity can be obtained. This equipment also contains a pressure sensor that can measure the fluctuations in the water pressure, which can be used to detect and measure waves. The equipment has been set to measure with a frequency of 8Hz.

(a)

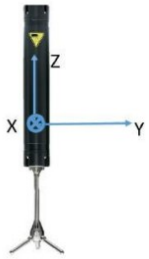

(b)

Figure 3.3: Photo of an ADV in the groyne area. (a) ADV with with battery canister mounted on a pole in the groyne area. (b) Coordinate system used by the ADV (*The Comprehensive Manual for Velocimeters*, 2019).

The CTD has been used to measure the salinity and temperature difference in the groyne area over time. These variables will differ between both the neap-spring and ebb-flood cycles. This instrument will also measure the pressure, but because of the lower frequency of 2Hz, this can't be used to obtain accurate wave data. The CTD will, however be used to measure the air pressure. The air pressure fluctuations are smaller than water pressure fluctuations due to waves. Because of this the air pressure measurements require a lower frequency for accurate measurements.

The RBR solo 3 is used to measure the water pressure with the same frequency as the ADV. The smaller size of this equipment gives it an advantage when placing it on more difficult accessible terrain. The pressure sensor on this device measures the same frequency as the pressure sensor on the ADV.

3.2.2. Positioning of the instruments

For positioning the instruments, there are specific areas and limitations on which the choice of the final locations is based. All the instruments were placed and picked up during low tide.

1. All the instruments are installed by hand. The water depth at the specific installation area is limited during these installations because the instruments have to be above or close enough to the surface to remain visible from the water. Underwater installation of the measuring setup is dangerous when this can't be done from above the water's surface. This condition was not met in the gully located in the upstream section of the dam and the scour zones shown in Figure 3.4.

2. The frames at which the instruments are attached have to be placed into the soil. This can't be done at places where there are larger stones present in the bed. These stones are mainly located at the opening of the downstream groyne and at the nourishment. These stones are not always visible from the surface as they are sometimes buried in the soil.

3. Because of the limited number of batteries available only four out of six ADVs could measure continuously for the whole period. Therefore, the other two instruments measured in burst intervals to use less energy. The instruments with a burst setting measure in intervals, meaning they do fewer measurements during the total measuring campaign than the other instruments.

From the data report shown in Figure 3.4 and supplied by Rijkswaterstaat, the zones with high sedimentation and erosion can be distinguished. These are the morphological and hydrodynamical interesting zones, because of the known activity. These zones are located at the openings of the groynes, the opening in the dam and the openings where the groynes and the dam are connected and downstream from the nourishment.

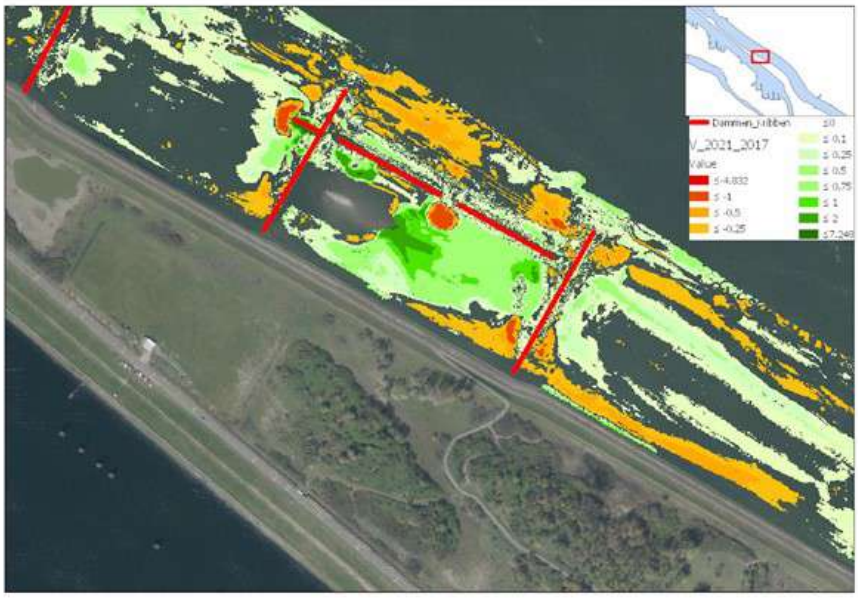

Figure 3.4: Scour and sedimentation zones. Erosion is indicated in red and sedimentation in green.

From inside the groyne area at low tide, it is visible that there are big differences in the depth of the gullies alongside the nourished island. The gully at the river bank is the first part of the groyne area that falls dry during ebb tide, while it takes longer for the gully at the dam if it falls dry at all.

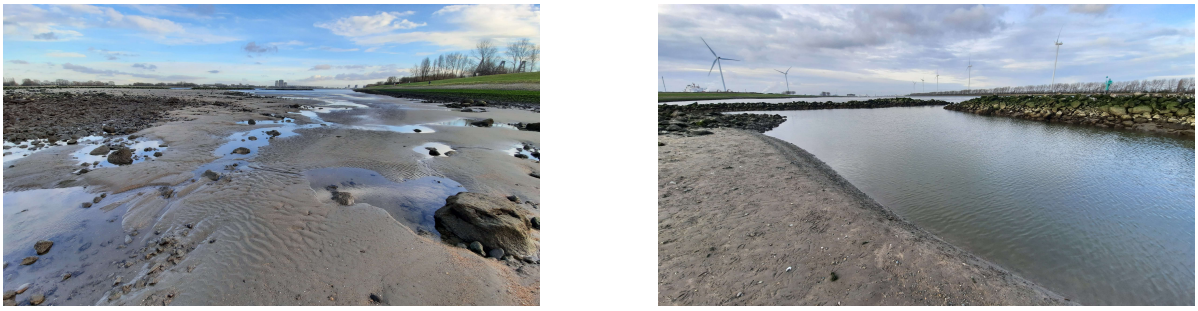

(a) (b)

Figure 3.5: Both the gullies alongside the nourished island, where (a) is located at the river bank and (b) at the dam.

The definitive positions of the ADVs are shown in Figure 3.6. The choice for these positions is based on accessibility and activity, as described above. The flexible heads of the ADVs are positioned horizontally, which means that the original X-direction of the ADV axis is pointing upwards. From the manufacturer's manual (*The Comprehensive Manual for Velocimeters*, 2019), it is stated that the accuracy of velocities that are perpendicular to the head are higher than velocities that are in line with the head. This means that the Y and Z velocities have the most significant accuracy.

Because of the limited amount of battery canisters that can store extra batteries for the ADVs, only some of the ADVs could measure continues. Two of the ADVs had to be chosen to measure in a burst. Burst measurement means that every ten minutes the ADV measures during the first six minutes. This amount of minutes it measures depends on the battery capacity and the total time they have to function. Two of the six ADVs have been chosen to measure in burst. Locations 4 and 5 have been chosen for this. Location 5 is not positioned close to any entrances or morphological active spots. Due to its high position, location 4 will be the first ADV to be above the water level also the groyne, the nourished island and the river bank will cause this location to be sheltered.

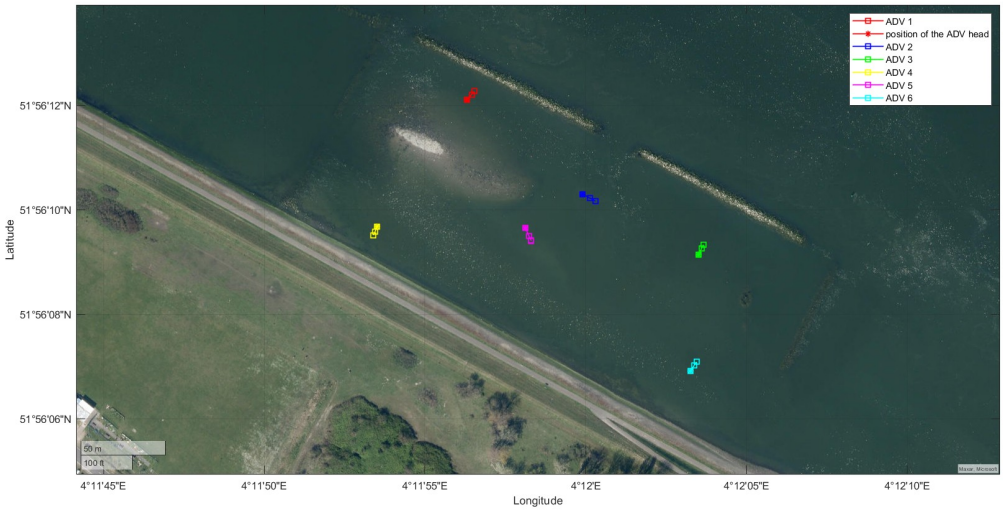

Figure 3.6: Final placement of the ADVs and the direction of the head.

Figure 3.7 shows the setup for the ADVs. Rotation of the ADVs in their setup is impossible because of the rubber strips between the ADVs and the clamps that connect them. The height of the ADVs was measured with GPS after the installation. These ADV heights were not specified before their installation. A brace has been placed to prevent the pole from rotating in the soil. The setup has been kept as slim as possible to minimalize its influence on the flow.

Figure 3.7: Setup of the ADV 1. The setup is made of scaffolding tubes and connector claps.

3.2.3. Handling of the data

The pressure sensor is located on the ADV. This pressure sensor is located at the bottom of the ADV in the setup used during the measurement campaign. Because the ADVs have been placed at different distances from the bed, the coordinates of the bed and the ADVs have been measured with GPS. The pressure measurements of the ADVs have been compensated with the measured heights from the bed in order to obtain the actual water depths at all six locations.

Table 3.1: Measured heights of the pressure sensor on the ADV and the height of the bed. The heights are measured from NAP.

ADV	height bed	height ADV	distance ADV from the bed (m)
1	-0.941	-0.576	0.365
2	-0.961	-0.589	0.372
3	-1.606	-1.273	0.333
4	-0.666	-0.394	0.272
5	-0.747	-0.452	0.295
6	-1.349	-0,918	0.431

The ADVs have been programmed to start measuring automatically on March 21^{st} at 15:40. This is the time of the first peak of the tide after the installation of the measuring setups in the field. The measurements have to be stopped manually. This was done at the university's lab to minimize the risk of damage to the hardware of the ADVs due to the saline water. The ADVs continued measuring during removal and transportation until they were manually stopped. These measurements still produced faulty data and has been removed after April 12^{th} at 7:10, meaning that the start and end dates of all ADVs were synchronized.

3.2.4. Verification of the data

During the installation of the ADVs the coordinates were manually obtained using a GPS device. From these GPS measurements the coordinates of the ADVs themselves and the direction of the ADV head were obtained. This was repeated during the removal of the ADV installations. These coordinates have been compared in Figure 3.8 and from this figure, it can be seen that the ADVs hardly moved and rotated during the measurement campaign.

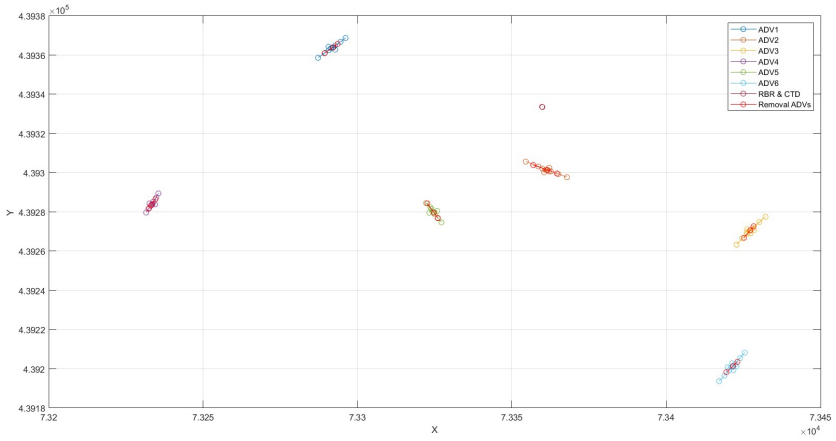

Figure 3.8: Coordinates from the GPS obtained during the installation and removal of the ADVs, in Rijksdriehoek coordinates.

To remove the error spikes from the raw ADV data a despike function has been used. The despike function uses the method of Goring and Nikora (2002) for detecting and replacing the spikes. Most of the errors occur when the ADV heads are above the water level. From Figure 3.9 can the remove points be seen. This significant clustering of the peaks is primarily found in between tides at the lowest water levels.

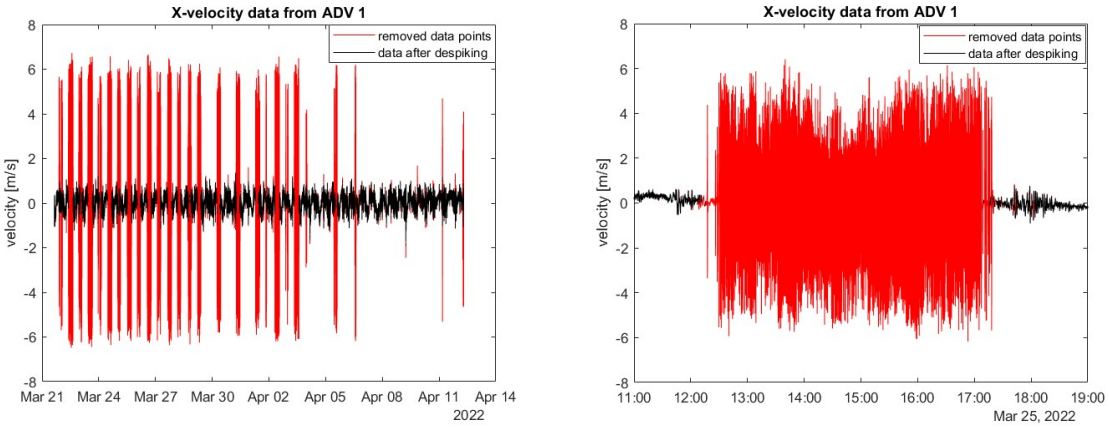

(a) (b)

Figure 3.9: Raw data from ADV number 1, the despiked function has been obtained from the university. The removed data is shown in red. In (a) the full data set is shown and (b) a low tide.

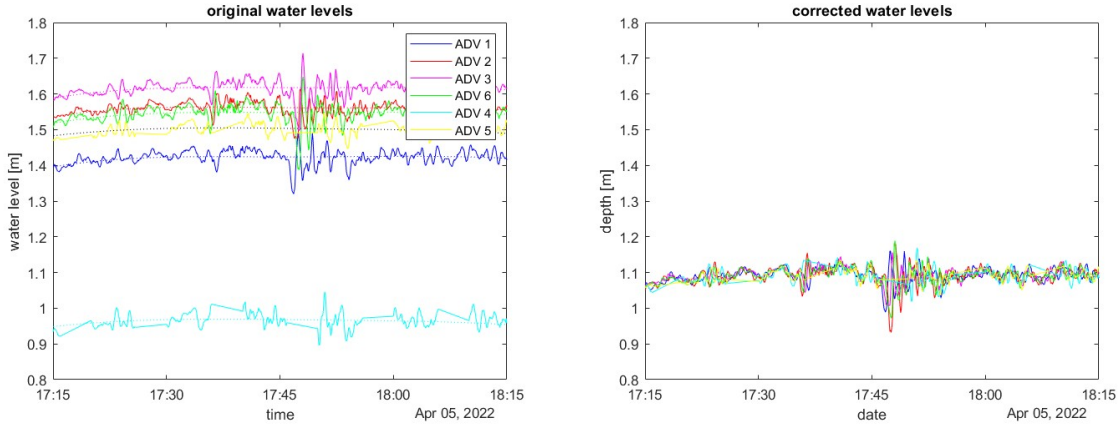

(a) (b)

Figure 3.10: The section of data used to correct the GPS heights. (a) The water levels using the original GPS heights. (b) Water levels using the corrected GPS heights.

The measured ADV heights will be checked with the water levels for each ADV. In Figure 3.10a it can be seen that the difference between the water levels is up to 20 cm between ADV 1,2,3,5 and 6, while the difference to ADV 4 is even larger. These significant differences are due to measuring errors for example tilting of the antenna or height mistakes due to underwater measuring. The ADV heights have been corrected by taking the difference average excluding ADV 4. This has been done with data from the 4th of April at 17:35 for a pressure signal averaging over 30 minutes. The average water level with the exclusion of ADV 4 has been used, which can be seen in Figure 3.10b and in table 3.2 can the corrected heights of the ADVs be found.

Table 3.2: Custom correction of the water levels due to human errors with GPS heights.

ADV number	water level correction
1	+ 0.034 m
2	- 0.096 m
3	- 0.192 m
4	+ 0.395 m
5	- 0.116 m
6	- 0.024 m

3.3. Second measurement campaign

The second measurement campaign data on the changes in the flow during the different stages of one tide has been obtained. During this tide, a more detailed analysis of the changes in the velocities over several cross-sections of the groyne area can be made.

3.3.1. Equipment

The ADCP was placed on a floating board facing downwards. This board had a hole in the middle specially designed for the ADCP. The fins at both sides of the board helped straighten the sailing path. The ADCP used during this measurement is the Sontek Riversurveyor 5. The board was not motorized, so it was attached to the jet ski to sail between the reference poles. This mount consisted of a two-meter pole attached to the side of the jet ski facing forward and a second pole attached to the first pole as shown in Figure 3.11. The combined length of the two poles ensured that the board was not colliding with the jet ski during sailing. The board was attached with a rope to the mount from the pole. With the rope, the board can pitch, and roll independently of the jet ski. The ADCP contains software and a compass to compensate for the pitching, rolling and turning.

Figure 3.11: Jet ski with the attached ADCP and floating board.

The ADCP measures the velocity over the depth in the same three directions as the ADV. It measures in four beams and with the River Surveyor computer software is this data converted into three directions. The ADCP can use its compass to convert the data to N-E-S-W. With the beam, the bed topography underneath the ADCP will also be mapped. The coordinates of the ADCP could not be obtained because there was no GPS linked to the ADCP (*RiverSurveyor S5/M9 System Manual Firmware Version 4.02*, 2016).

3.3.2. Measuring paths

The locations of the reference poles have been marked with GPS. The distances between these poles are the theoretical sailing paths. In reality, the sailed path differs from this theoretical path due to human error and the maneuverability of the jet ski. The ADCP records its traveled distance and shape of its path. To link this to coordinates, the assumption is made that starting point of each of the measurements is always at a refence pole like the paths shown in Figure 3.13. In practice, this was different for the starts and ends of each measurement due to human error and the reaction speed of the device. For every row, the measurement will be repeated four times in succession. This will compensate for the effect deviations in sailing paths during the measurements on the results.

There are certain criteria for selecting the position of the rows:

1. The jet ski requires a minimum depth. If the water depth is insufficient, sediment will be sucked into the jet ski damaging its engine.

2. To get the most information about the groyne area, the reference poles has to be as close to the dam and the bank as possible to maximize the length of the obtained cross sections. Maximizing the lenght of the row will capture most of the activity in the groyne area. As told above the lines traveled are often not straight and if the distance between the rows is too small, the measurements will overlap.

3. The rows must have a minimum width due to the jet ski's maneuverability. If the width is too small, the jet ski won't be able to maneuver around the poles because of its turning cycle and the influence of the flow itself.

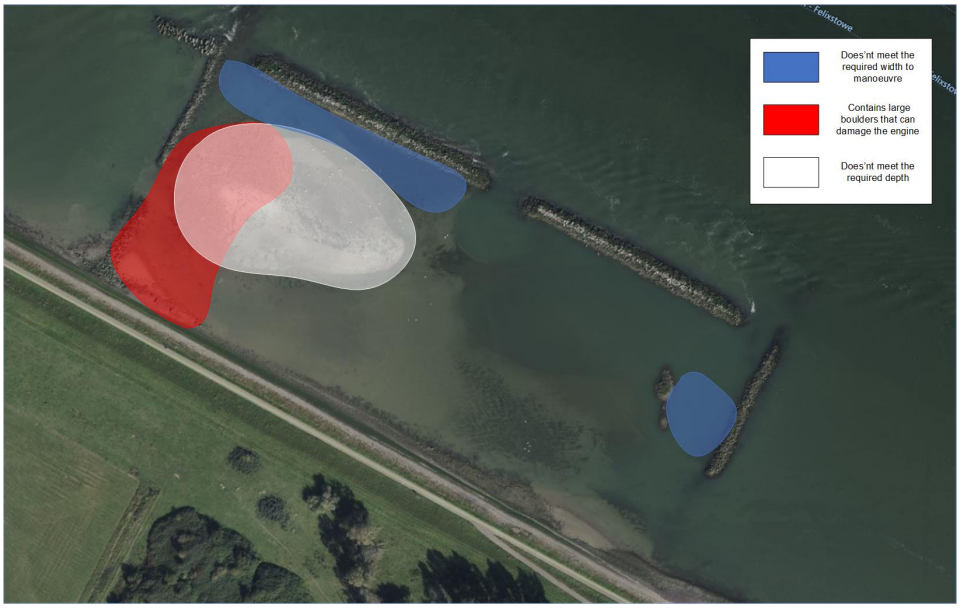

Figure 3.12: Zones that don't meet the requirements for the ADCP measurements.

Figure 3.12 shows the areas which don't meet the requirements. The interesting zones for this expedition are the same as for the first measuring campaign.

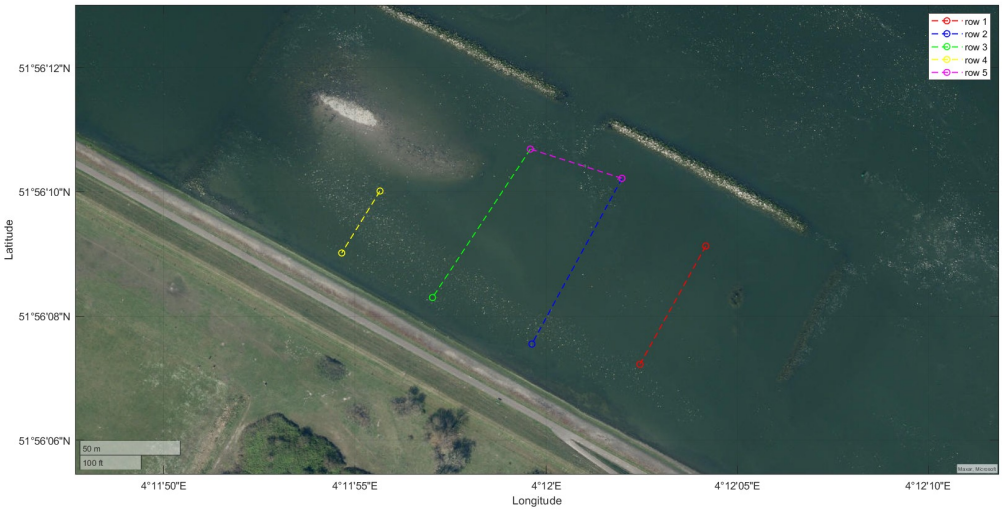

Figure 3.13: Sail paths from between the reference poles.

Figure 3.13 shows the final placement of the rows. The rows must be perpendicular to the flow to ensure optimal results. Row number 5 is in line with the entrance in the middle of the dam. This location has been chosen to observe the in and outflow through the dam. This in and out flow through the dam is perpendicular to the flow in the river. For that reason is row 5, parallel to the river

3.4. Sediment sampling

Sediment samples have been taken from the soil at the locations of all six ADVs. plastic sampling tubes have been used to obtain these samples. The tubes have been inserted 15 to 20 cm into the soil and multiple samples were taken at every ADV location.

Multiple techniques can be used for determining the composition of the soil. For this research the technique used is laser diffraction. Laser diffraction has a limit range of particle sizes that can be detected, so particles larger than $1\,\mathrm{mm}$ are removed from the sample to maximize the accuracy of the laser diffraction. The equipment used for laser diffraction is a sensitive piece of equipment. The results can be influenced by particle sizes that exceed the range and the flocculation of the particles. These larger particles can obstruct the tubes of the equipment and cause stoppages. Flocculated particles have a larger area than the individual particles of which they consist. This causes a distorted sieve curve with an increased d_{50}.

Another technique that could have been used is sieving of the samples. Samples were then dried and fed through a series of vibrating sieves. The weight of the material that can't pass through the sieve is then measured and a sieve curve is made. Unfortunately, the samples with higher percentages of clay and silt became hard solid structures after drying, comparable to a brick. Because of this, the choice was made not to use this technique.

For this analysis the Malvern Mastersizer 2000 is used in the Geolab of Deltares. With laser diffraction, the dispersed sediment particles will pass through a laser beam. When the particles pass through this beam the different angles of the scattered light will be measured. Smaller particles will scatter with relatively large angles in comparison with larger particles. The software will analyze this scattering intensity and with the use of the Mie theory a size is found for that particle (*Mastersizer 2000 User Manual*, 2007).

(a)

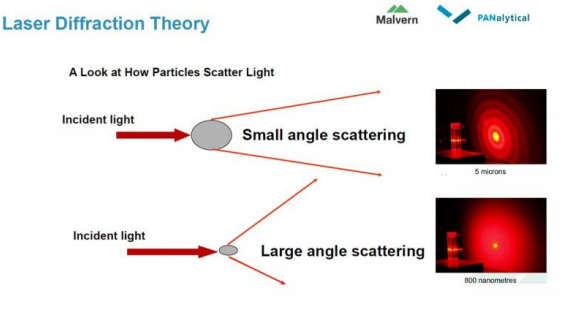

(b)

Figure 3.14: (a) The Malvern Mastersizer 2000 setup used for the experiment. (b) The principle of the method used to identify the different particle sizes (*Mastersizer 2000 User Manual*, 2007).

Before the sediment samples will be fed into the Malvern they will be sieved to $1\,\mathrm{mm}$. The Malvern can measure up to $2\,\mathrm{mm}$ particles, but unfortunately, this sieve was not available. A sieve of $1\,\mathrm{mm}$ was used instead. The sediment samples have been stirred before using, to mix samples taken at the same location together. Background scattering will be measured from the beacon with clean water before the sediment is added. This background scattering will automatically be accounted for in the results. After the background scattering measurement is completed, the sieved sample is added to this water beacon until the obscurity is between 10 and 20 percent. The particles in sediment compositions in which clay is present will be first put through the ultrasonic setting for 30 to 40 seconds to break up any flocculated particles. From every location, multiple samples will be measured in the Malvern. After every sample that is measured, the Malvern will be cleaned by feeding clean water into the system to wash out the leftover sediment particles in the system. During the washing process, the beacons will be checked manually and if there is no sediment present in the beacon from washing, a new beacon containing a mixture of water and a sediment sample will be placed and the measurement will start.

For the sediment measurements with the Malvern the obscuration is an important parameter. Obscuration is the light fraction that is lost due to scattering or absorption (*Mastersizer 2000 User Manual*, 2007). To get the best results this obscuration has to be between 10 and 20 percent. Table 3.3 shows the obscuration percentages for the different samples. All the samples are in the ideal obscuration range.

Table 3.3: Obscuration percentages for every sediment sample, measurements for these samples have been averaged per location.

sample	obscuration percentage
1	17.5
2	15.9
3	16.9
4	19.7
5	16.4
6	14.3


ADV gps locations
Location 1 in the text corresponds to the location of ADV 1
ADV 1
ADV 2
ADV 3
ADV 4
ADV 5
ADV 6
51°56'14"N
51°56'12"N
51°56'10"N
51°56'08"N
51°56'06"N
Latitude
4°11'50"E
4°11'55"E
4°12'E
4°12'05"E
4°12'10"E
Longitude
50 m
100 ft

4 | Hydrodynamic conditions

The results from the data obtained during the measuring campaigns will be shown and explained. A deeper understanding of some methods can be found in appendix B. A short explanation will follow when the method is essential for understanding the graphs and tables displayed in this section. In this chapter numbers will be used to indicate specific locations in the groyne area. These numbers correspond with the numbers of the ADVs, for example location 1 is the location where ADV number 1 is placed. Figure 3.15 shows a map of these locations.

4.1. Different effects on the groyne area

Different mechanisms from the river influence the flow in the groyne area. The different influences that will be discussed in this section are the tide, the river discharge, the effects from shipping, local wind and storms at sea. An overview will be given of the effects from these different influences on the groyne area. The most significant influences will be discussed more thoroughly in the following sections and the other influences will not be investigated further.

4.1.1. Tide

The tidal influence in the river at the location of the groyne area is considerable because the groyne area is positioned close to the delta. The effect of the tide can be seen back in the water level and the velocity signals. From these signals, it can be observed that the velocity follows the trend of the water levels. The Ebb flood cycles as well as the spring neap cycle can be clearly distinguished in the velocity signals as shown in Figure 4.1. This figure shows that the velocities are mainly caused by the tide and follow the same trend, so there are positive X-velocities during flood and negative X-velocities during ebb.

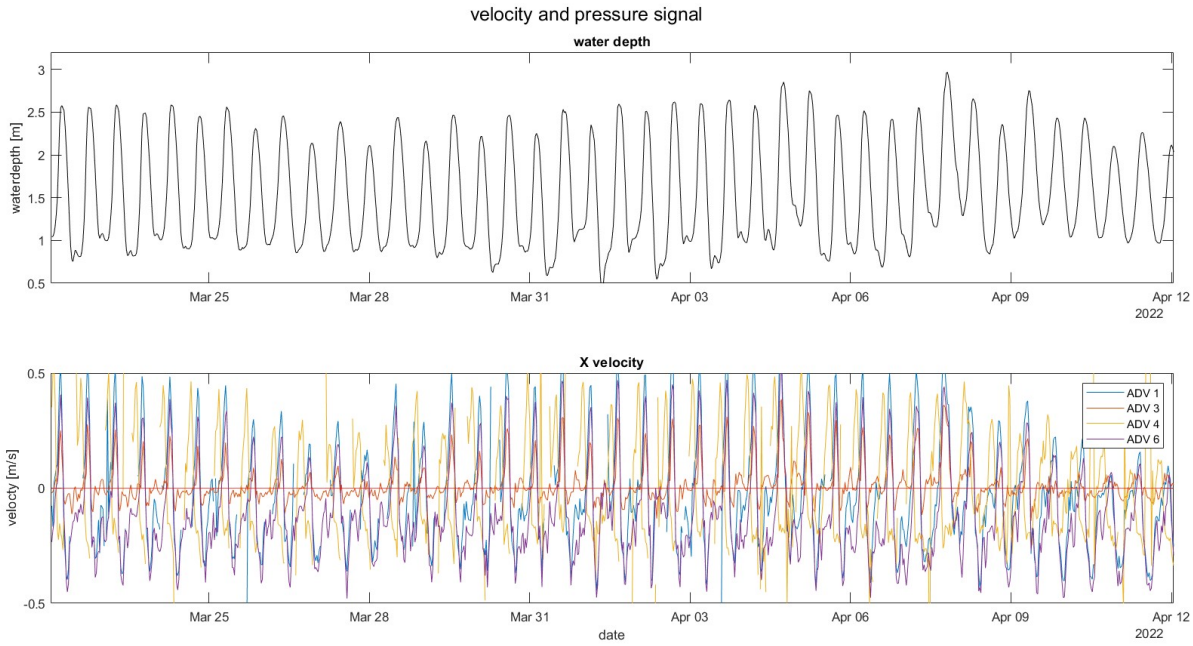

Figure 4.1: The X-velocities and the water depth averaged over 30 minutes.

4.1.2. River discharge

The controlled opening of the Haringvliet dam and the incoming discharge from the river influences the river's discharge. At Lobith the incoming discharge is measured from the Rijn. It takes roughly

estimated four to five days for this water to reach the Nieuwe Waterweg. Due to this complex system with the Haringvliet dam, predicting the discharge at Nieuwe Waterweg is complicated because the discharge in the river does not directly follows the trend at Lobith.

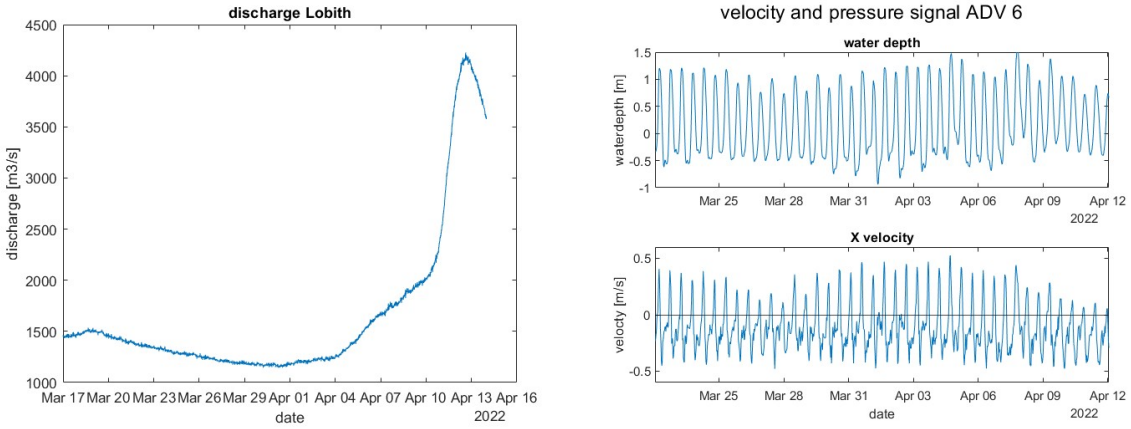

(a) (b)

Figure 4.2: The changes in discharge compared to the changes in velocity. (a) Discharge from Lobith obtained from data collected by Rijkswaterstaat. (b) Velocity and the water depth to ADV 6, averaged over 30 minutes.

Figure 4.2a shows the discharge at Lobith. From April 4^{th} until April 7^{th} the discharge increase with around $500\,\mathrm{m^3\,s^{-1}}$. This increase will be felt at the Nieuwe Waterweg around April 9^{th} to 12^{th}. Figure 4.2b shows that in that period in the Nieuwe Waterweg the X-velocities during ebb increase and during flood decrease, but other factors could have an influence as well.

4.1.3. Shipping

Shipping influences the groyne area due to the waves created by the passing ships. These ship waves have a distinctive signal from which the shape can easily be recognized. This is mostly the case for larger ship waves. The smaller ship waves can be more difficult to recognize. These waves can have wave heights from a few centimeters up to $60\,\mathrm{cm}$ depending on the other external influence on these waves like the characteristics of the ships from which they come. From observations, during the measurement campaigns it could be observed that ship waves impact the groyne field even with shallow water levels. This impact is shown in the photos of Figure 4.3.

Figure 4.3: Ship waves breaking in the adjacent groyne.

4.1.4. Local winds and storms at sea

wind waves grow in size with an increased fetch length (Holthuijsen, 2007). The fetch length is limited for wind waves that enter the groyne area. This is due to the dams and the groynes. So the main directions for wind waves to have a maximum fetch are in the direction of the river pointed either downstream or upstream to the river and perpendicular to the dam. The fetch is at its maximum during the submergence of the groynes and during the emergence of these groynes is the fetch limited to the distance to the next groyne. The perpendicular fetch length of the wind waves is limited to the river's width. Figure 4.4 shows the pressure signals from two different periods and the wind velocities combined with whether the wind is in a favorable direction. Figure 4.4c shows that during the period of Figure 4.4a the wind has a relatively high velocity in a favorable direction. However, this is not the case in Figure 4.4b. Figure 4.4a meets the conditions for the maximum fetch length and Figure 4.4b is during a calm period. These Figures show that the difference is negligibly small.

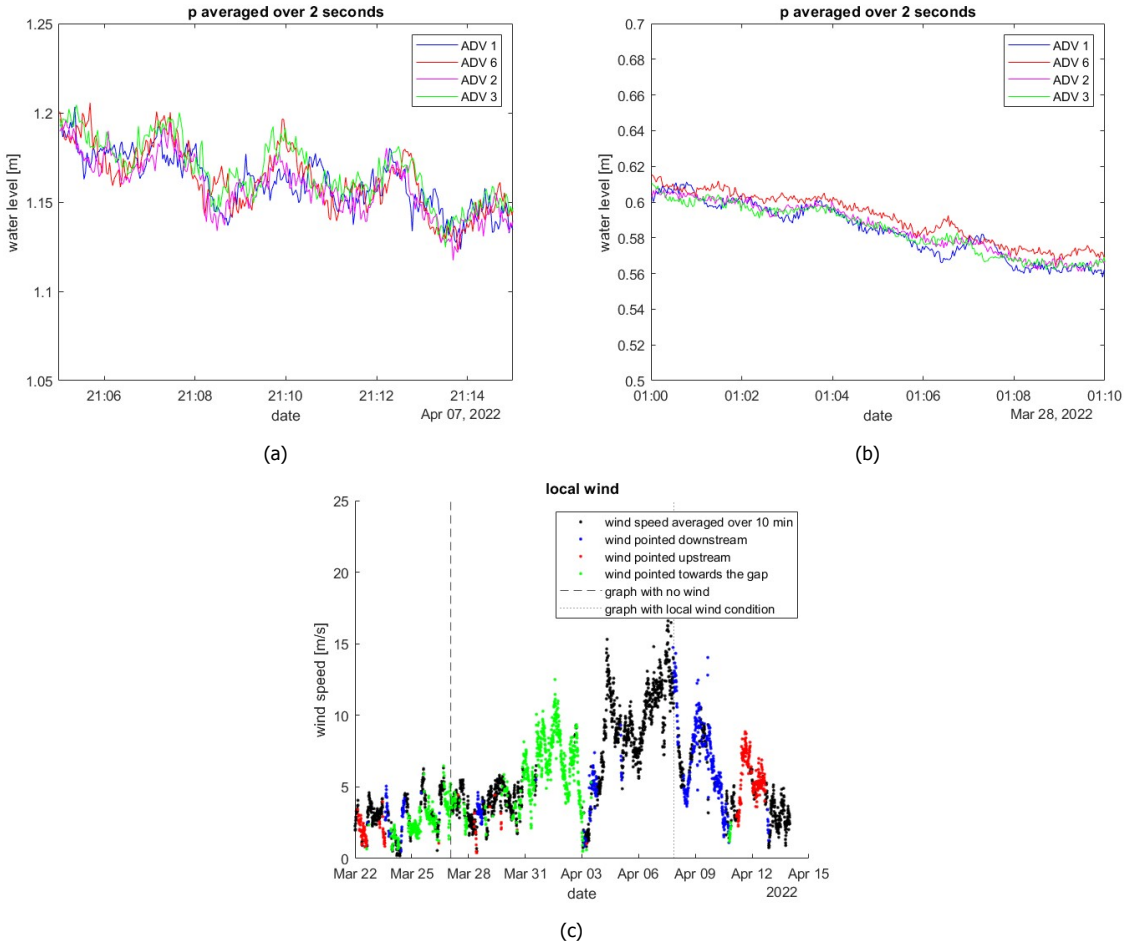

Figure 4.4: The pressure signals are averaged over two seconds and the wind signals are obtained from Rijkswaterstaat. (a) During strong local winds with a large fetch. (b) During a period with calm winds. (c) The local wind velocities from the measuring station at the Maeslantkering.

If there is a storm offshore of the estuary, the fetch can cause a set-up at the shore or in this case in the river. This setup causes an increase in water level and an increase in flood velocity. According to the data from Rijkswaterstaat there was a storm at sea on March 21^{st}, but this didn't show up in the velocity or water depth data from Figure 4.2b.

4.1.5. Comparison of the influences

The tide, ships and the wind directly affect the groyne area. The most considerable effects are from the ship waves and the tide. The analysis will include these two parameters because of their significant effects. From the parameters, the tide and ship influence have a much more considerable impact on the flow than the wind. These local winds create smaller oscillations than approximately $2\,\mathrm{cm}$. Because of the small size of the oscillations compared to waves created by ships, the wind waves will be neglected in the analysis. The influence of the river discharge is difficult to directly link to the data on the flow inside the groyne area because of the Haringvliet dam and the limited stations where they measure the discharge. For this reason, it is decided also to neglect the river discharge in the analysis.

4.2. Tidal flow

The tide is one of the main drivers of the flow through the groyne area, as discussed in Section 4.1. The tide controls the water level and gives the groyne area a flow in two directions. This is necessary for creating an intertidal zone. The locations are numbered from downstream to upstream 1 to 3 at the dam and 4 to 6 at the river bank.

4.2.1. Flow direction

The ADVs measure the directions and velocities of the flow at each of the 6 locations. The flow directions in the groyne area are governed by the flow in the main channel and the modifications to the groyne area. In a tidal rose, all the velocity vectors are shown together for different stages of one tide giving an overview of the changes that occur from flood to ebb. For the tidal rose graphs, the length of the tides has been manually selected. Each vector represents the average velocity over 30 minutes. The vectors have been scaled due to their velocity magnitude and the colors of the vectors represent the moment in time for an individual tide. A tidal cycle starts at low water followed by the rising stage of the tide and after the peak is reached, the water level descends and the tide ends at the next low water.

Figure 4.5 shows the tidal roses for three different tides. From these tidal roses, it can be observed that for some of the locations, vector colors are missing. Disturbances cause this missing data due to low water levels or by filtering the data.

(a)

(b)

(c)

Figure 4.5: Tidal roses of tides on different days during the measurement. The ADVs are numbered from downstream to upstream in the length of the groyne area, close to the dam from location 1 to 3 and close to the bank from 4 to 6. (a) The tidal range is 1.74m and a peak water level of 1.58m. (b) The tidal range is 1.39m and a peak water level of 0.93m. (c) The tidal range is 1.40m and a peak water level of 1.06m.

The graphs show that the ebb and flood directions per tide are consistent at locations 1, 4 and 6. At location 3 it can be observed that during flood the flow direction is pointed to the groyne and the direction stays constant, while during ebb the direction is changing and the velocities are low. This indicates that during flood when a threshold water level is reached to flow over the groynes, water does not exclusively exit through location 6, but also through location 3. During the majority of the ebb tide, enters the flow through location 6 instead of location 3. From location 2 the ebb flow seems to be directed to the opening in the middle of the dam while the flood flow has a broader range of directions.

Figure 4.6 shows an overview of the average flow directions in the groyne area during ebb and flood. During flood, the configuration of the entrance in the downstream groyne causes the water to start significantly flowing through the groyne area after the groynes are submerged. This means that during flood the flow does not prioritize between locations 3 and 6 or 1 and 4. After the flow reverses the larger section of the water flows through location 6 instead of location 3 and when the ebb flow is at its highest velocity, the water flows almost exclusively through location 6.

When the flow profile of Figure 4.6 is compared to the flow patterns in a typical emerged groyne area shown in Figures 2.4a and 2.4b, the influence of the adjustments is visible. In a typical emerged groyne area which doesn't contains the dams the flow in the main channel of the river causes eddies between the groynes. The placed dams limits the interacting with the main channel and the groyne, but eddies can still occur in the dead zones of the groyne area. These dead zones are places where there is no direct flow. Because of the nourishment, no dead zones are located between locations 1, 2, 4 and 5. In the area at location 3 there is a possibility of the emergence of eddies. This could be explained by observing the low velocities and changing directions during ebb at this location.

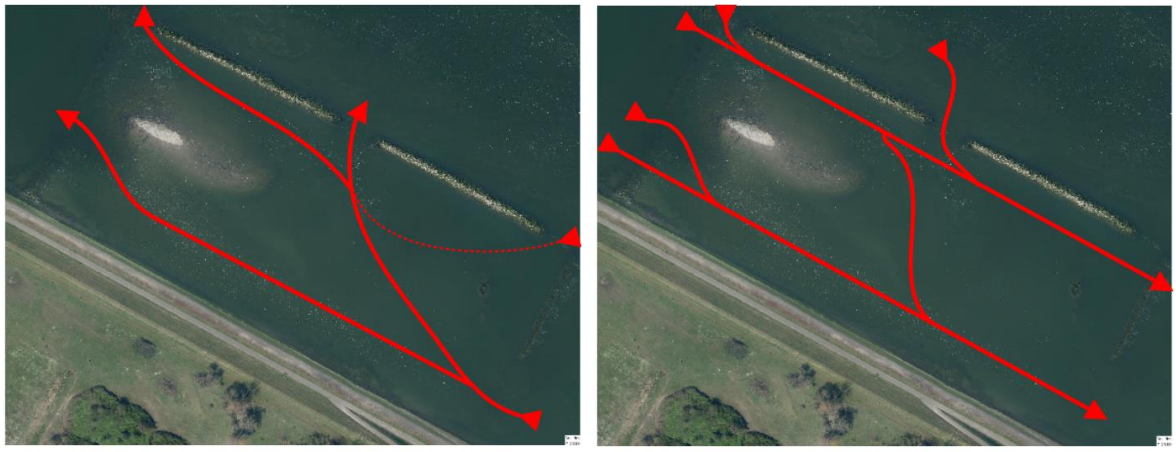

(a) (b)

Figure 4.6: Flow directions during ebb at (a) and flood at (b).

4.2.2. Tidal flow velocities

The X and Y directions for the velocities can be seen in Figure 4.7. The direction of the X-axis has been chosen to give positive velocities during flood and negative velocities during ebb. Figure 4.8 shows the velocity signals during the descending part of a tide. At location 6 during this period the average X-velocity is $-0.3\,\mathrm{m\,s^{-1}}$, while the average Y-velocity is $0.05\,\mathrm{m\,s^{-1}}$. From the flow directions, it is seen that the flow at location 6 is mostly directed in the X direction. This confirms the difference between the X and Y-velocity. Because of this large difference, the focus will be on the X-velocity for this location as well as locations 1, 2 and 3 where there is the same velocity distribution. At location 2 it can be seen that the average X-velocity is $-0.05\,\mathrm{m\,s^{-1}}$ and the average Y-velocity is $0.2\,\mathrm{m\,s^{-1}}$. The focus of location 2 will be on the y-velocity, because although the difference between the velocities is smaller, the average Y-velocity exceeds the X-velocity at this location. The Y-velocity at this location gives information on the in and out flow through the opening in the middle of the dam. Although for location 5 the X-velocity is larger than the Y-velocity, does the Y-velocity contain as much information over the flow as the X-velocity. This is because the Y-velocity is for the water distribution between the two main flows.

Figure 4.7: River-coordinate system.

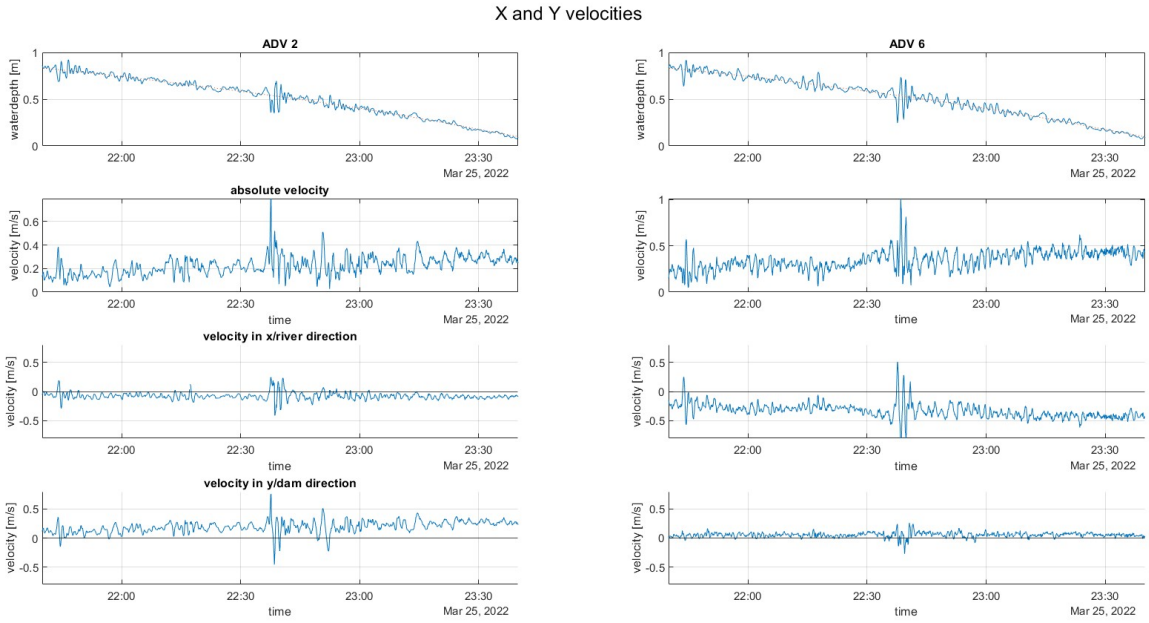

Figure 4.8: X and Y-velocities for a regular tide. The velocity is averaged over 5 seconds.

To obtain the velocities caused by the tide, the velocity has been averaged over 30 minutes as shown in Figure 4.9 for the velocity profiles of two tides. In Figure 4.10 are 10000 random data points in time taken from the measurement data. For these data points, the tidal velocity and water level have been obtained. Every single data point represents a random time during the measurement. For such a data point, the velocity and water level have been obtained that occurs during that time. These velocities and water levels from all the random points in time have been plotted together in these graphs for every ADV. These graphs show the relations between the velocities and water levels that occur during a tide and with 10000 data points, this gives an accurate representation of this. All these graphs show that the higher velocities occur at locations 1, 4, 5 and 6, while at locations 2 and 3 the velocities are lower. Lower velocities indicate a more significant amount of fines at the bed, which matches Table 5.2 in Section 5. That table shows that the d_{10} at both locations 2 and 3 has a lower value than at the other locations, indicating a larger percentage of fines in the sediment composition.

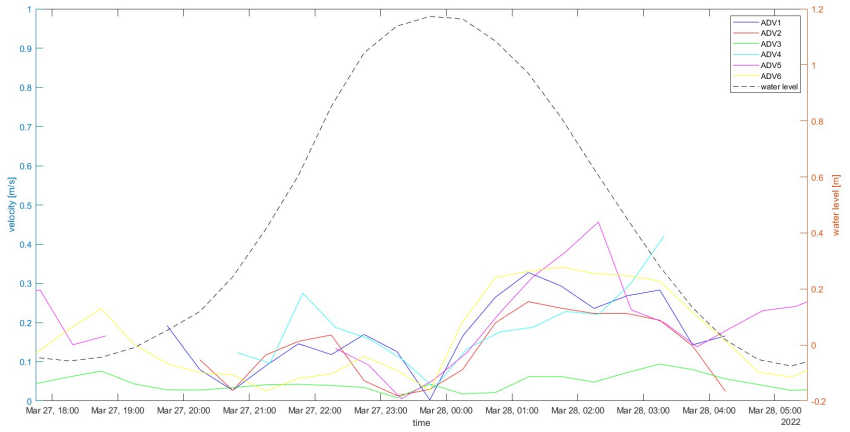

(a)

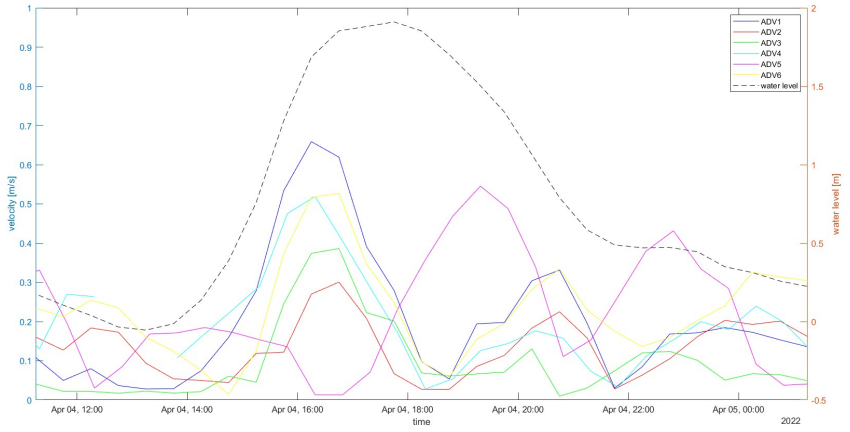

(b)

Figure 4.9: Velocities at every ADV during two different tides. (a) Tide with a peak water level of $1.17\,\mathrm{m}$. (b) Tide with a peak water level of $1.91\,\mathrm{m}$.

From the velocity signals can be seen that the velocities of locations 1 and 4 follow the same shape, while location 1 has a consequently larger flood velocity and location 4 has a larger ebb velocity. This indicates that both locations are subjected to similar flow conditions as shown in Figure 4.9. Figure 4.10 shows for these locations that the flow velocities during flood increase with increasing water levels, while this is not the case at ebb. The ebb flow velocities at location 1 show a regular tidal flow where the highest velocities occur in the middle of the ebb tide. In theory, the velocity is the time derivative of the water level. This slope of the water level from a regular tide is at its maximum in the middle of the rising and descending stage of that tide. In such a regular tide the slope of the water level is 0 at the peak and trough of the tide. This is the moment that the flow changes direction. Such a regular tidal shape can be observed in Figure 4.10a for the ebb flow. This means that during floods with lower water levels, the flow of water through the groyne area is minimal. An explanation for this could be the area of the downstream gap compared to the upstream gap. The bed level at the downstream gap is higher and the width of the opening is smaller than upstream. This means the flow is minimal through this gap, but when the water levels are high enough the groynes are submerged and the water flows over the submerged groynes into the groyne area.

Location 3 shows only peak velocities during flood after reaching the water level threshold. From Figure 4.9b ebb flow at this location shows flat profiles which indicate limited use of this location by the ebb flow, which has also been observed in the tidal roses. Only during high water levels at ebb can higher flow velocities at this location be observed in Figure 4.10c. Also from the data can be

seen that the dominant direction is to the north while the highest velocities are all pointed in the flood direction.

At location 2 the highest velocities occur during ebb. These velocities have a positive Y-velocity meaning that the water flows out of the groyne area at this period, flowing through the opening in the middle of the dam. This is also shown in the tidal roses. Figure 4.10b shows that the ebb velocities follow the typical shape of a tide while the flood velocities remain constant during the tide.

At location 5 the velocity and flow depend on the conditions at the other locations. This means that location 5 follows the trend at flood mostly of locations 1 and 4 and during ebb it follows the trend of location 6, which can be seen in Figure 4.9. Location 5 is responsible for water exchange between the main flow between 1 and 3 and the other main flow between 6 and 4. During ebb flow, the velocities follow the same pattern as for the other locations. During floods below the water level threshold, the velocities at this location are very low which means there is a minimal exchange of flow before this time, shown in Figure 4.10e.

Location 6 shows ebb velocities which are in most cases slightly higher than the flood velocities. The majority of the flow goes through the gap at location 6 during ebb and flood. The incoming water at flood is limited due to avoiding the groyne area at lower water levels. This can be seen in Figure 4.10f for location 6 as well where the velocity increases when the threshold is reached. During ebb flow a typical tidal flow pattern can be seen at location 6, which is enhanced by the fact that from a higher threshold water level, the upstream groynes are submerged as well and the incoming water gets more divided over the width of the groyne area. This is why the steep decline of ebb velocities with increasing water levels.

During ebb, the incoming flow from location 6 is divided over locations 1 and 4. This causes a high exchange of water between these main flow directions, which is indicated by the higher ebb velocities at locations 2 and 5.

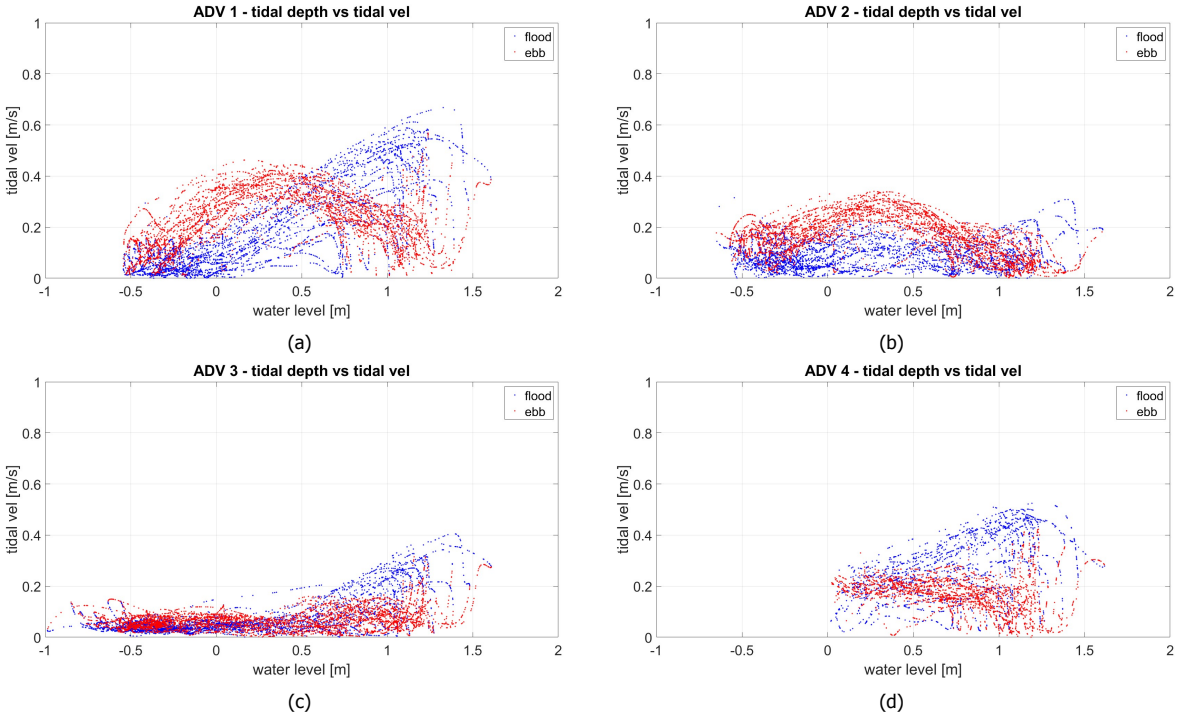

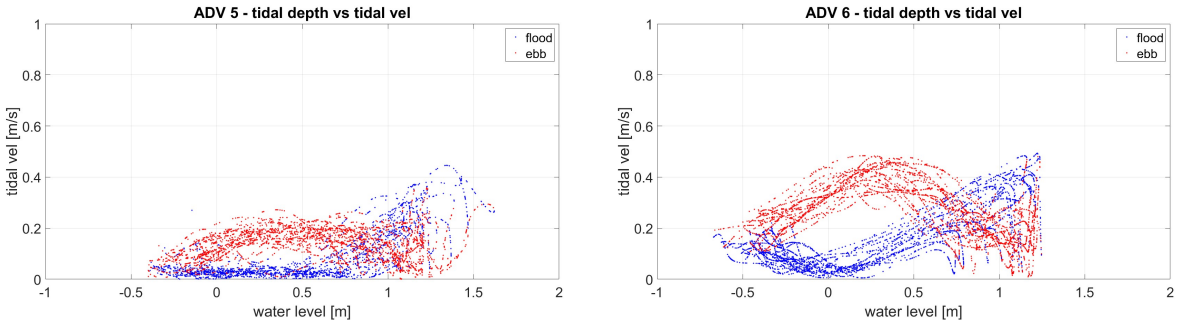

(e) (f)

Figure 4.10: The tidal velocities and water levels for 10000 random moments. Red dots represent the ebb moments and the blue dot the moments during flood. The tidal velocities and water levels are averaged from the signal every 30 minutes to filter the smaller oscillations.

Figures 4.11c and 4.11d show the depth average velocities that have been obtained from the ADCP measurements. The X-axis shows the path that has been sailed with the ADCP. The start position of this axis is located to the left in the downstream position, so the sailing path is from the river bank to the dam. The velocities from this graph are relatively low compared to Figure 4.10 for the same water level, meaning that no direct information has been obtained from the depth average velocities. From the depth average directions in Figure 4.11c and 4.11d it can be observed that the difference in flow direction at the rising tide is less than during the descending tide. However, the depth average velocities are in the same order of magnitude. This confirms that the behavior is consistent with the behavior found in the tidal roses and velocity data. Figures 4.11a and 4.11b show the color plots for the same paths as in Figures 4.11c and 4.11d. These color plots confirm that during flood there is a flow at both locations 6 and 3, while during ebb water flow at location 3 is minimal compared to location 6.

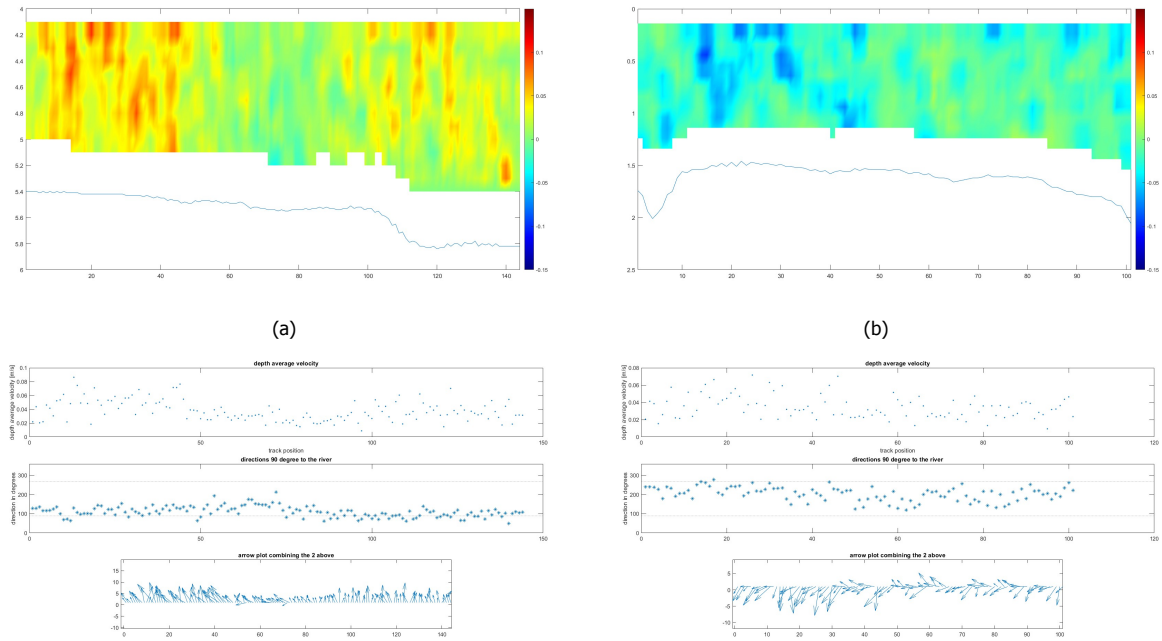

(a) (b)

(c) (d)

Figure 4.11: The difference during a tide's rising and descending stage. The height of the peak was about $0.8\,\mathrm{m}$. (a) Color plot of the velocities during rising tide from row 2. (b) Color plot of the velocities during descending tide from row 2. (c) Depth average velocities for the rising tide. (d) Depth average velocities for the descending tide. The axis for the vector plots is pointed upwards for the X/flood direction and to the right for the Y/dam direction.

4.2.3. Neap and spring tide

From the water levels in the groyne area, it can be observed that the tide behaves as a semi-diurnal tide. This can be seen from the deviation between two consecutive tides. Figure 4.12 shows the X-velocities and the water levels at location 1. The X-velocity has the same direction as the flow in the river, where the positive direction is the direction of the flood. For locations 2 and 5, the Y-velocities have been observed, where the positive Y-velocity is pointed from the land to the dam. Two moments have been singled out from the graphs. These moments are during the spring and neap tides. Because of other influences which have been discussed in 4.1 the neap and spring tides are distorted. This makes it difficult to see the exact dates of both spring and neap tide. In order to obtain the dates for the neap and spring tides, the astronomical tide chart of Maassluis from the website of Rijkswaterstaat has been used. In the astronomical tide chart, all other influences to the water levels are filtered, making it less difficult to spot the neap and spring tide dates.

From Figure 4.12 it can be seen that both the flood and ebb velocities are affected by the neap spring cycle. The ebb velocities show a velocity increase of around $0.15\,\mathrm{m\,s^{-1}}$ from neap to spring tide, while for the flood velocities this increase is around $0.45\,\mathrm{m\,s^{-1}}$. For the other locations with the exception of location 2, the difference in flood velocities during neap and spring tide is significantly larger than during ebb. At location 2 no relation between velocity changes and the neap spring tidal cycle can be observed.

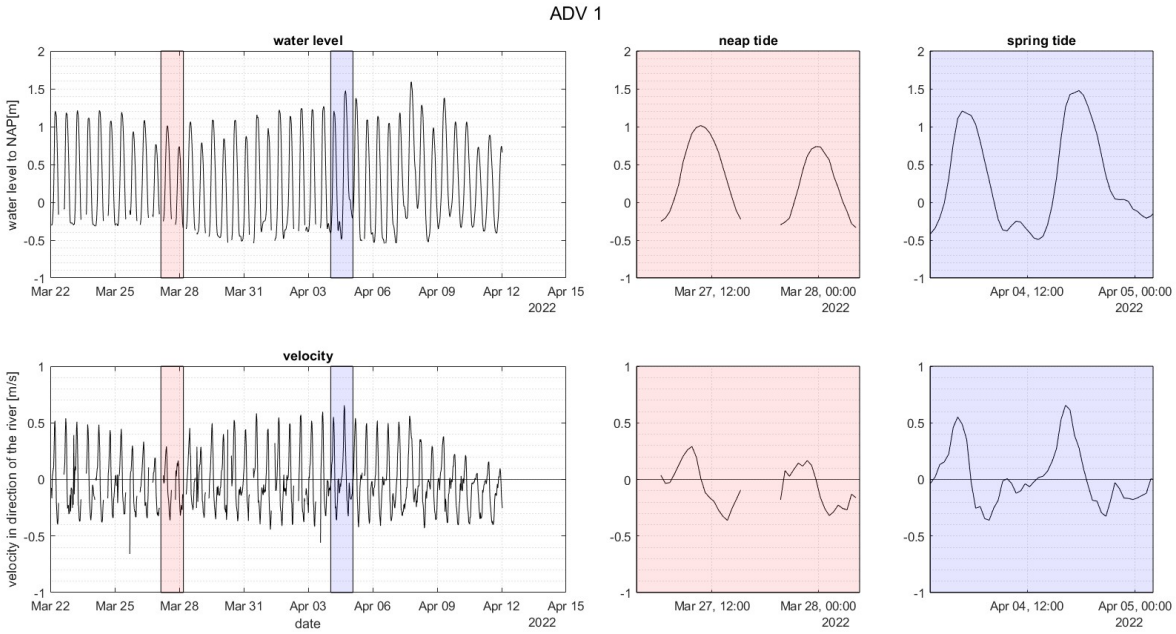

Figure 4.12: The velocity and pressure signal of location 1 for neap and spring tide.

The flood velocities in the groyne are more affected by the neap spring tidal cycle than the ebb velocities. This causes the flood velocities to increase for all locations from neap to spring, while the ebb velocities remain constant. This makes the flow flood dominant during spring tides, with higher flood velocities in comparison to the ebb velocities. When the tides change from spring to neap this flood-dominant system transforms into an ebb-dominant system with higher ebb velocities over flood velocities.

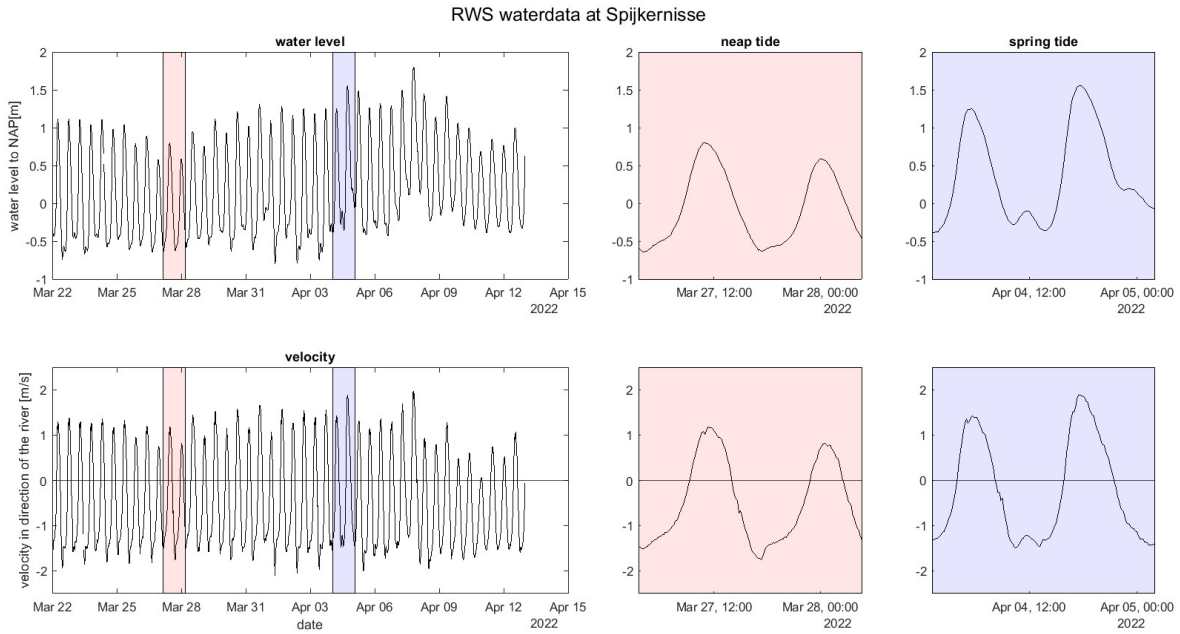

Figure 4.13: The velocity and pressure signal at the measuring station near Spijkernisse for neap and spring tide. The data has been obtained from Rijkswaterstaat.

Figure 4.13 shows the flow velocities and water levels during the same period as the measurements in the groyne area. The measurement station is located at a bridge over the Oude Maas between Rotterdam and Spijkernisse. Both the Oude Maas and the Nieuwe Maas flow into the Nieuwe Waterweg, meaning that the measurement station is upstream of the groyne area. This figure shows the same behavior as the flow inside the groyne area. There is an increase in the flood velocities from neap to spring tide while the ebb velocities remain relatively constant. The high ebb velocities in Figure 4.13 cause the ebb velocities to remain constantly higher than the flood velocities, while this is not the case for the velocities in Figure 4.12. This shows that the reaction of the flow to the neap spring cycle in the groyne area is partly caused by the modifications to the groyne area. The similarities between the signal of the groyne area and the signal at Spijkernisse show the characteristics of the river itself.

4.3. Shipping influence

From observations, it has been seen that waves originating from has a passing ship have a considerable influence on the groyne area. Those waves travel through the entrances in the groynes and the dam into the groyne area. For the analyses of tides in Section 4.2, the data was averaged over 30 minutes. The event of a ship wave propagating through the groyne area has a considerably smaller time scale. From observing a number of individual ship waves it was seen that their wave periods ranged between 55 to 120 seconds. Further information about these individual ship waves can be found in Appendix B. The time difference between a ship passing the groyne area and the first waves of this ship reaching the groynes ranges between 2 minutes before to 4 minutes after the ship has crossed the groyne area, depending on the velocity of the ship and other parameters. The calculation for this time can be found in Appendix B. The calculation made gives an indication of the time difference between the arrival of the wave and the ship crossing the groyne area. These times are not exact because of the assumptions that are made. The AIS has provided the ship data. From all ships passing the groyne area, the data has been collected. Ships with a velocity below 6 knots have been discarded because it has been seen from observations that the waves created by those ships have a minimal impact on the groyne area.

In most cases ship waves can be recognized in a pressure signal due to their distinctive wave shape. As discussed in Section 2.3.3, ship waves are not just a single wave, but they consist of a primary wave

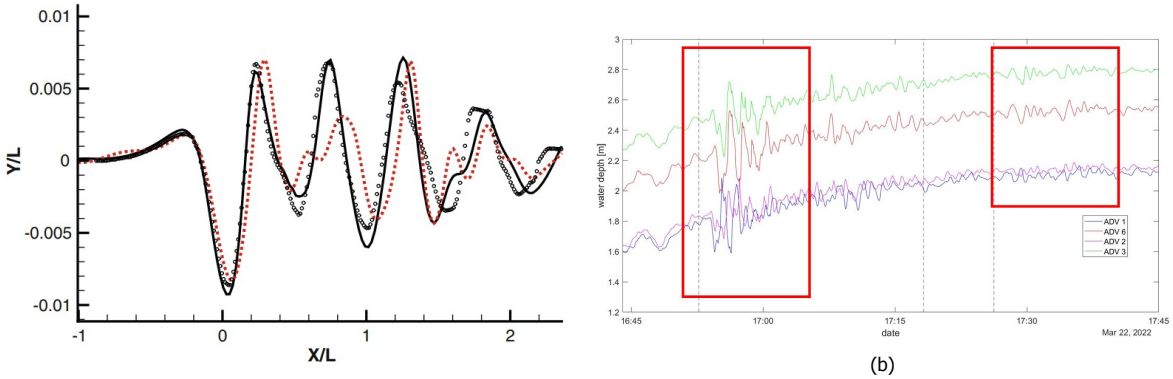

(a) (b)

Figure 4.14: In Raven (2010) is looked at the relation between the hull form properties and ship wave patterns. Waves were computed using the approaches from this research and compared to experimental data. Comparing the wave shapes obtained from Raven (2010) to the wave shapes found in the groyne area similarities in shape can be observed. (a) The computed data (dotted and straight line) and the experimental data (markers) from Raven (2010). (b) Ship wave patterns in the ADV pressure data from the tide of the 22^{nd} March.

and secondary waves with a water level drop in front of the primary wave. Figure 4.14 shows a typical ship wave moving through the groyne area. In Figure 4.14 ship waves computed by Raven (2010) are compared to the ship waves found in the data. Raven (2010) computed ship wave data and compared the computed waves to obtained experimental wave data. Comparing the figure of Raven (2010) to the ADV pressure data shows that the shape of the ship wave pattern in the groyne area is consistent with the ship wave shape found by Raven (2010). This ship wave pattern together with observations from inside the groyne area confirms the effect of ships inside the groyne area.

4.3.1. Movement of a single ship wave through the groyne area

In this section six single ship waves will be analyzed. These are waves from six different situations are shown in Table 4.1. With these single wave analyses, the wave can be more thoroughly analyzed and more details can be seen.

Table 4.1: Six different single waves analyzed.

Propagation direction	moment during the tide
flood direction	flood
ebb direction	flood
flood direction	peak of the tide
ebb direction	peak of the tide
flood direction	ebb
ebb direction	ebb

Ship waves propegating through the groyne have been analyzed with animated quiver plots. The quivers show how the ship influences the flow in the groyne area. Figure 4.14 shows the general shape of the ship waves and the drawback. While the waves cause a velocity in the direction of the wave itself, the drawback cause a velocity in the opposite direction. The waves have the same direction as the ship from which they originate.

looking at a ship that is sailing to the sea (ebb direction) or the port of Rotterdam (flood direction), the primary ship wave first enters the groyne area at location 3 and 6. At these locations, a velocity increase in the direction of the wave propagation can be observed. The primary wave then propagates through the groyne area, while also entering at location 2 through the gap in the middle of the dam. Before the primary wave, the water is pulled out of the groyne area through the drawback, causing a drop in the water level. This moves through the groyne field the same as the waves but causes a velocity in the opposite direction of the wave. After this drawback, the secondary waves move through

the groyne field, which behaves like the primary wave but with a smaller wave height. In some cases, a wave moving through the groyne field also causes outflow at location 2. This outflow from a wave propagating through the groyne area, depends on the timing of the outgoing wave, which has traveled through the groyne area and exits at location 2 and the incoming wave directly from the ship at this location.

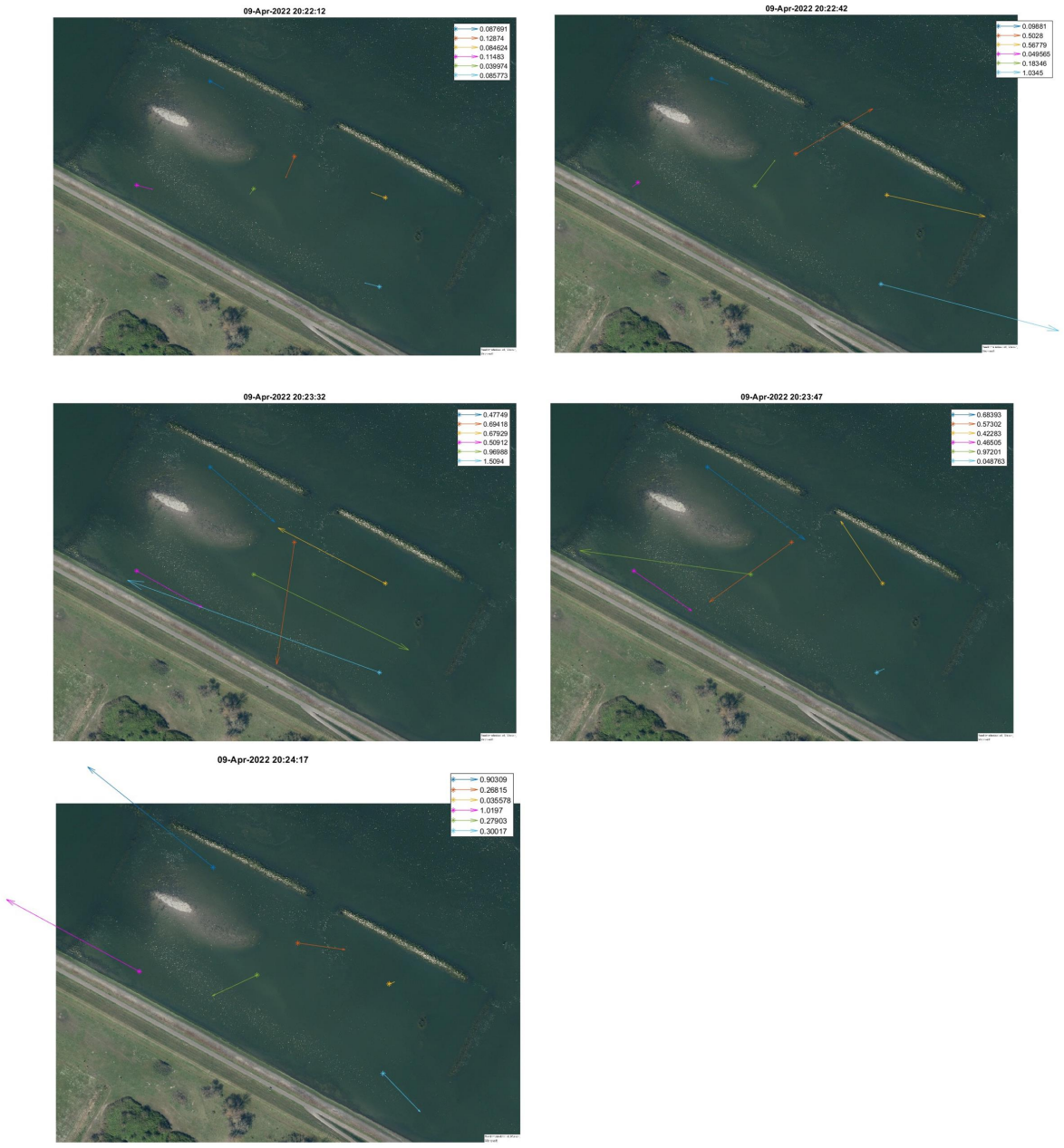

Figure 4.15: The different colors represent the different locations: location 1 is blue, location 2 is orange, location 3 is yellow, location 4 is pink, location 5 is green and location 6 is light blue.

Figure 4.15 shows the velocity vectors when a ship passes the groyne area. The numbers of the enumeration correspond to the moment in the figure. The time of each moment can be seen in the title of each figure. The ship and its waves propagate in the ebb direction.

1. The ship has not passed the groyne yet, so the influence of the ship is not visible yet in the velocities. The tide is at its peak, which means the direction of the tidal velocities is changing. Hence the low flow velocities and the opposite directions of the flow between location downstream and upstream sections of the groyne area.

2. The ship is starting to pass the groyne area and the drawback pulls the water towards the ship. This can be seen in all locations except location 4.

3. The primary wave enters at the upstream side of the groyne area and through the opening changing the direction in the ebb direction in this location. The downstream locations are still submitted to the drawback giving the velocities at those locations an opposite direction to the locations where the wave comes in.

4. The incoming waves through the dam and from the upstream locations meet at location 2, changing their direction slightly. The waves are also passing location 5.

5. The primary wave has reached the downstream locations. The smaller primary waves and oscillations in the water constantly change the direction of the water at the other locations.

Figure 4.16 shows the velocity of three different waves passing through location 6. Table 4.2 shows the characteristics of each of the waves.

Table 4.2: Characteristics of the analyzed waves.

Number of the wave	propagation direction	moment during the tide
1	flood direction	ebb
2	flood direction	flood
3	flood direction	peak of the tide

A wave traveling in flood direction adds a flow velocity to the tide in this same direction as its propagation. The drawback, which can be observed as the wave's low trough, adds a negative velocity to the flow in the opposite direction. This is shown in Figure 4.16. Waves 1 and 3 propagate in flood direction during the ebb part of the tide, which means their velocities are in the opposite direction of the tidal velocity. Wave 1 has a $3\,\mathrm{cm}$ lower wave height, a $0.04\,\mathrm{m\,s^{-1}}$ higher tidal velocity and a $30\,\mathrm{cm}$ lower mean water level than wave 3. The difference between the X-velocity signal of waves 1 and 3 shows that wave 1 cannot change the direction of the flow while this is happening during the passage of wave 3. This suggests that these conditions determine whether or not the wave's velocity reaches the bed and influences the flow direction close to the bed.

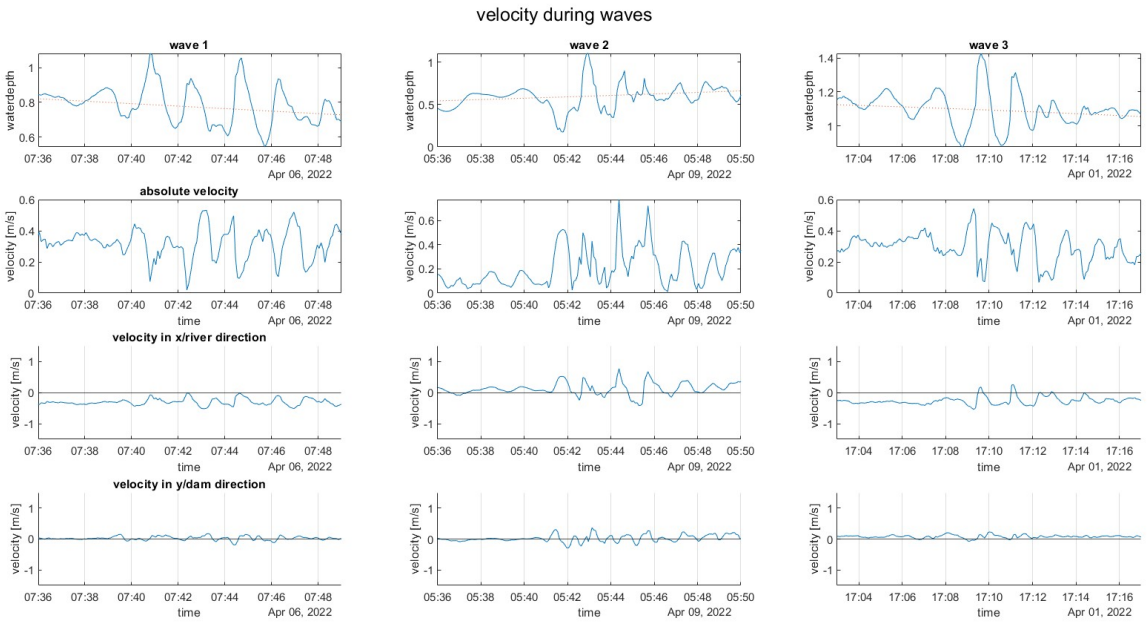

Figure 4.16: The velocity signals in X and Y direction of 3 different waves at location 6.

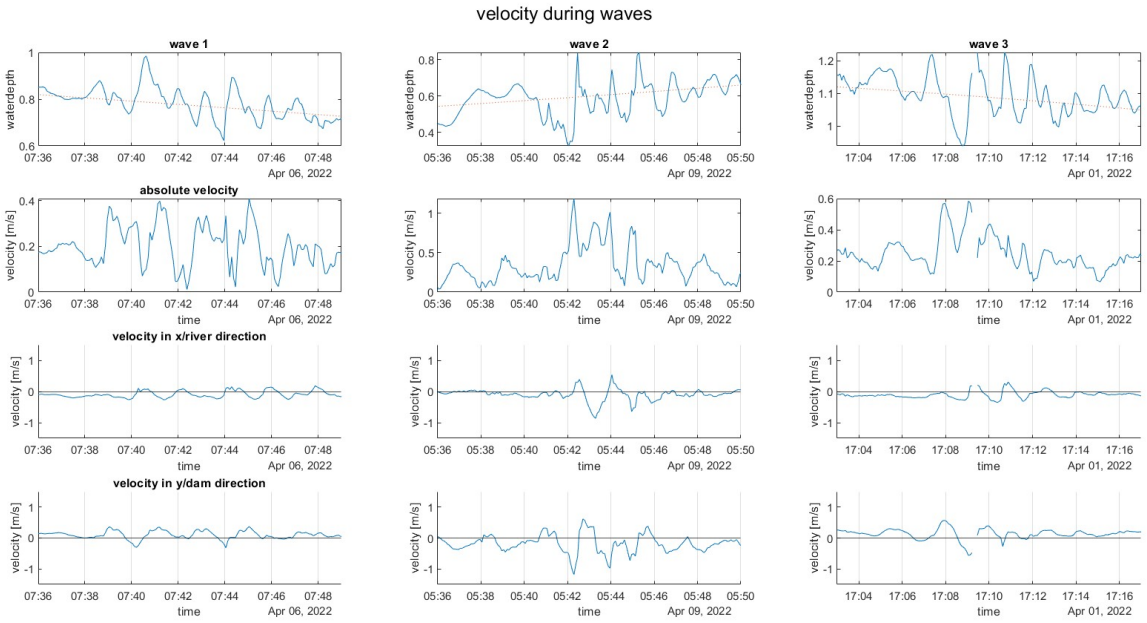

Figure 4.17: The velocity signals in X and Y direction of three different waves at location 2.

From the movement of a ship wave through the groyne area, the waves from the same ship pass two different times through location 2. Waves entering the groyne area through the opening in the dam pass through location 2 with a higher Y-velocity from the absolute velocity. When the wave comes from location 1 this wave has a higher X-velocity. Figure 4.17 shows the same waves as for the wave analysis of location 6. The incoming wave has a negative Y-velocity when it enters through the opening in the dam and a positive X-velocity when it comes from location 2. Comparing the pressure signals of the

three waves between location 2 and location 6, it can be observed that the signal of location 6 looks like Figure 4.14a. The different parts of the ship wave like the primary wave, the return flow and the secondary waves can easily be identified, while this is not the case for location 2. Comparing the water depth signals from location 2 and location 6, it can be observed that the same wave passes location 2 on two occasions. At location 6 the typical shape of a ship wave can be recognized in the signal, but the shape of the signal from the same wave at location 2 indicates an interference with another wave. This signal of location 2 contains extra peaks and troughs in the wave signal itself indicating two colliding waves. From the velocity signals, the velocity increase is first visible only in the Y direction. In contrast, the influence in the X direction is visible after a particular time. This could indicate that the first wave arrives at this location through the opening in the dam and the other wave from location 1. The collision of these two waves was also observed from the vector plots, which indicate the directions of the velocity during the waves.

4.3.2. Wave properties and influence

Waves cause a significant increase of velocity over a short time, as seen in Figures 4.16 and 4.17. These velocity peaks can be observed in the velocity signal accompanied by a peak in the water depth. From the ADV data, the peak velocities are obtained for all ships passing the groyne area. The peak values for the velocities due to the waves have been obtained from the maximum velocity in the period between 3 minutes before and 5 minutes after the passing of a ship. To ensure that waves from different ships do not interact with each other, a ship will only be used in the analyses if the previous ship passed the groyne area more than 10 minutes before the current ship. To analyze the velocities caused by waves, the mean velocity averaged over 30 minutes is subtracted from the peak velocity to get the increase in velocity due to the passage of a ship. With this method, only the primary waves will be targeted because these waves will give the most prominent peak in both velocity and water depth. Table 4.3 shows the velocity increases for locations 1, 2, 3 and 6. Due to the burst type measurements from ADV 4 and 5, only a section of the time has been measured. When a ship waves occur during the time that the ADV is not measuring, the method still finds a peak velocity, although this is not from the ship wave. This makes it very difficult to verify whether the obtained ship wave data is correct at these locations. Because of this, the accuracy of the analysis for both locations is unknown. For this reason, the choice has been made not to include the data from ADV 4 and 5 in the ship wave analyses.

Table 4.3: Velocity increase due to ships waves at every location.

Location	average velocity increase
1	0.23 m/s
2	0.19 m/s
3	0.11 m/s
6	0.18 m/s

Table 4.3 shows the average increase of velocity due to waves. The increase in velocity due to waves at location 3 is lower than for the rest of the locations. Location 3 is sheltered on two sides with the groyne and the dam when the groynes are emerged. Waves can reach this area through a small gap between the dam and the groyne, this means that the waves most likely enter the groyne at an other location. At high tide, the wave travels over the submerged groyne. Because the waves travel over the submerged groynes, the waves are weakened when they arrive at location 3.

Figure 4.14b shows that there are also waves outside of the zone for the ship waves. These waves can be caused by wind or other external sources, but the exact source of these waves is unknown. These waves are visible for extended periods of time and can influence the computations for the ship wave analyses. Using a too narrow time interval between the passing of a ship and the arrival of the wave from this ship will detect these smaller oscillations instead of the larger ship waves. This will cause the mean wave heights and wave caused velocity increases to decrease. In order to minimize these smaller oscillations getting misrecognized as the waves from a ship, different intervals have been tested. Increasing the interval will be limited by the computation time, which will increase exponentially. The mean wave heights and velocity increases can be observed in Table 4.4, for the different intervals. The mean velocity increase due waves, grows with an increasing time interval. However, it can be seen

that the mean wave height does not increase in the time intervals, from the last two rows in the table. Ship waves causes a more significant increase in velocity in comparison with other smaller oscillations. This means that for the largest mean velocity increase, a higher percentage of waves caused by ships have been detected. Because of this the time interval of 3 minutes before and 5 minutes after has been used for ship wave analyses.

Table 4.4: Mean velocity increase and wave height for different intervals for ship waves passing ADV6.

Interval	mean velocity increase	mean wave height
1.5 minutes before and after a ship	0.13 m/s	0.04 m
2 minutes before and after a ship	0.14 m/s	0.05 m
2 minutes before and 4 minutes after a ship	0.16 m/s	0.06 m
3 minutes before and 5 minutes after a ship	0.18 m/s	0.06 m

Due to the analyzed waves in Section 4.3.1, it was observed that their wavelengths are more than 40 to 200 times larger than the water depths. Because of this, it can be assumed that all the waves are shallow water waves. For shallow water, kd goes to 0, so $tanh(kd) \rightarrow (kd)$ (Holthuijsen, 2007) see Equation 4.3.1. In this Eqation $c = wave\ velocity\ [m/s]$, $g = Gravitational\ constant\ [m^2/s]$, $omega = angular\ frequency\ [Hz]$, $k = wave\ number\ [m^{-1}]$, and $d = water\ depth\ [m]$. This means that according to linear wave theory, the velocity of the wave itself depends on the water depth. The total amount of detected ships that have crossed the groyne area in the time is 1805 ships. For the tidal velocities and mean water levels, the signal has been averaged over 30 minutes to remove all the smaller oscillations and waves. The wave heights and increases in velocity have been obtained by subtracting these from the signals which are averaged over 5 seconds.

$$c = \frac{g}{\omega}\tanh(kd) = \sqrt{\frac{g}{k}\tanh(kd)} \tag{4.3.1}$$

$$\hat{u} = \frac{\omega a}{kh} = c\frac{a}{h} = \sqrt{gh}\frac{H}{2h} \tag{4.3.2}$$

The orbital velocity of the wave is a rotating velocity that causes multiple rotations over the water depth. Equation 4.3.2 shows the orbital velocity for a shallow water wave. In this Equation $\hat{u} = orbital\ velocity\ [m/s]$, $a = wave\ amplitude\ [m]$, and $H = wave\ height\ [m]$. This velocity depends on the water depth and wave height for a shallow water wave, as shown in Equation 4.3.2.

This shows that the wave height positively correlates with the orbital velocity, while the water depth has a negative correlation. The orbital velocity from the wave causes the velocity increase in the signal. Figure 4.18 shows the measured velocity increases with the wave heights and the water depths for each ship's passing. From these figures, it can be seen that there is a correlation between wave height and increased velocity, which is expected from the orbital velocity. Figure 4.18b shows the influence of the water depth and the wave height on the velocity increase. The water depth as a ratio of the wave height is displayed on the X-axis. The figure shows that the velocity increase is more significant when the water depth decreases in comparison with the wave height. Figure 4.18b shows that for the different locations between a ratio of 20 and 30 the slope decreases significantly. At location 1 it can be seen that the ratio does not go to zero. A possible explanation for this can be the breaker index by Miche (1944). This breaker index is the minimum water level over wave height ratio before the wave breaks, which is found to be between 2 and 2.5. The minimum value for the measured ship waves is 3, which is correct according to the theory.

Correlations have been found to the increase in velocity from both the water depth and the wave height. Figure 4.18c shows the relation between the increase in velocity and the tidal velocity. No direct correlation can be observed in this figure. The tidal velocity does not feature in the formulas for the orbital or wave velocity. Although, it has been seen in Section 4.2 that the tidal velocity is correlated to the water depth. From Figure 4.10 it is known that the correlations between the water level and the tidal velocity differ per location. This results in a variation in shapes between the different locations in Figure 4.18c.

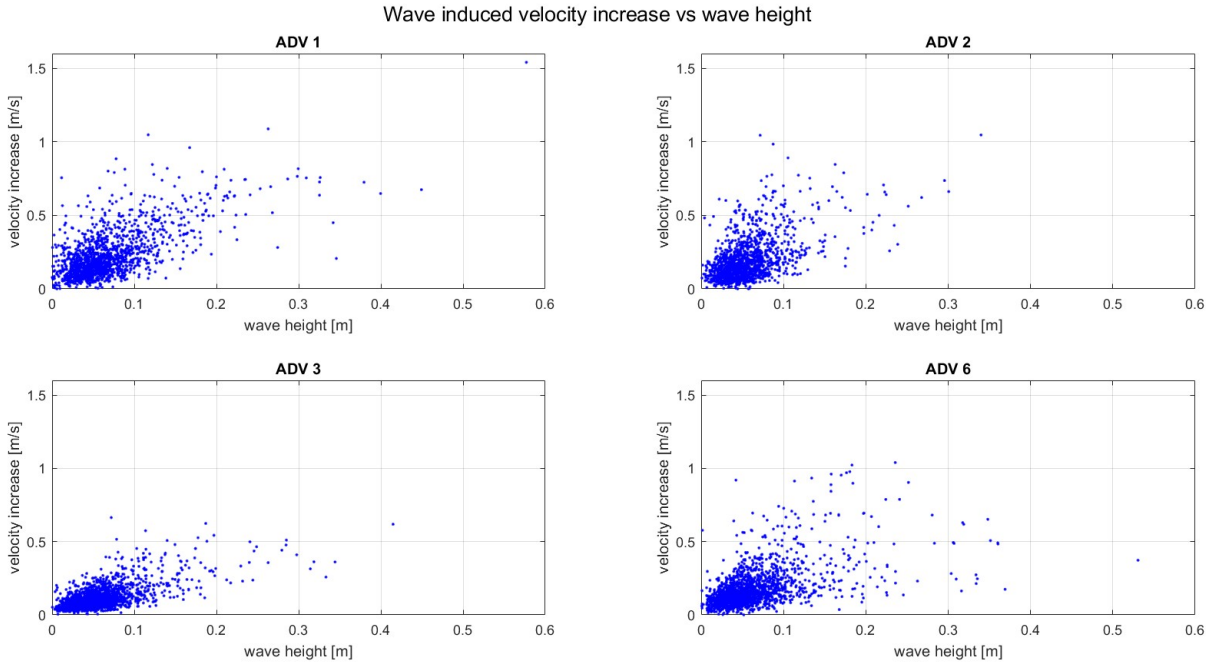

(a)

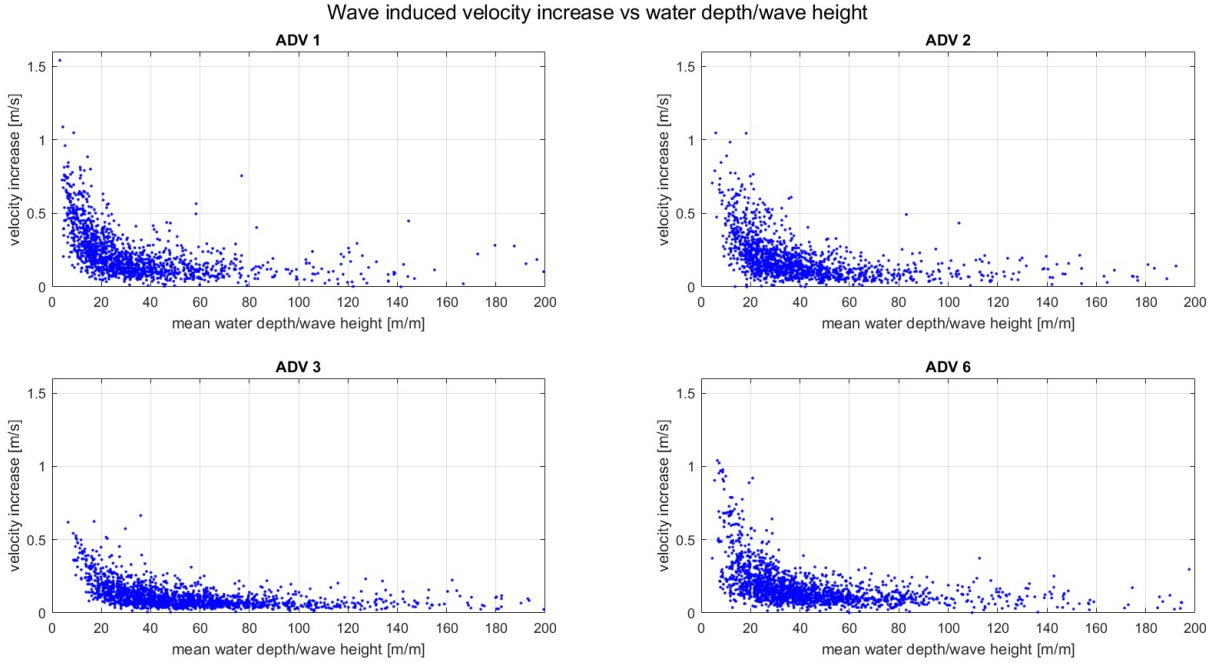

(b)

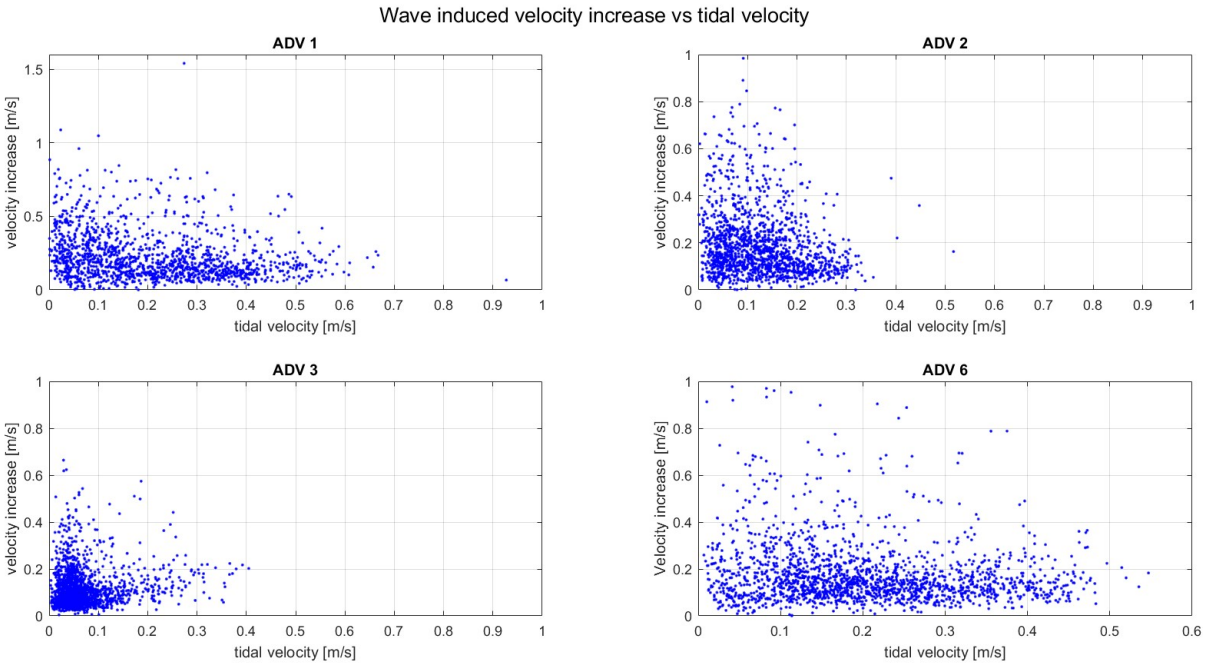

(c)

Figure 4.18: The same ships have been used for all analyses. The data for these ships have been obtained from the AIS. Every data point represents a ship passing the groyne area, with no other ship passing closer than 10 minutes before and after the ship has passed. The ships have been found using the data from the AIS. The waves from the same ships have been used in all three graphs.

4.3.3. Secondary waves and oscillations

Figure 4.14b shows that besides the sizeable primary wave, smaller oscillations are also present in the signal. These smaller oscillations are caused by the secondary ship waves and their reflected waves, which cannot be isolated perfectly from the first primary wave with the method used in Section 4.3.2. Reflection of these waves from the dam and groynes cause reflected waves that could appear as small oscillations in the area. Another cause for the small oscillations is wind waves, as seen in Section 4.1. However, the fetch length when the water level is below the groyne height is minimal so that the wind will have an almost negligible impact during this time.

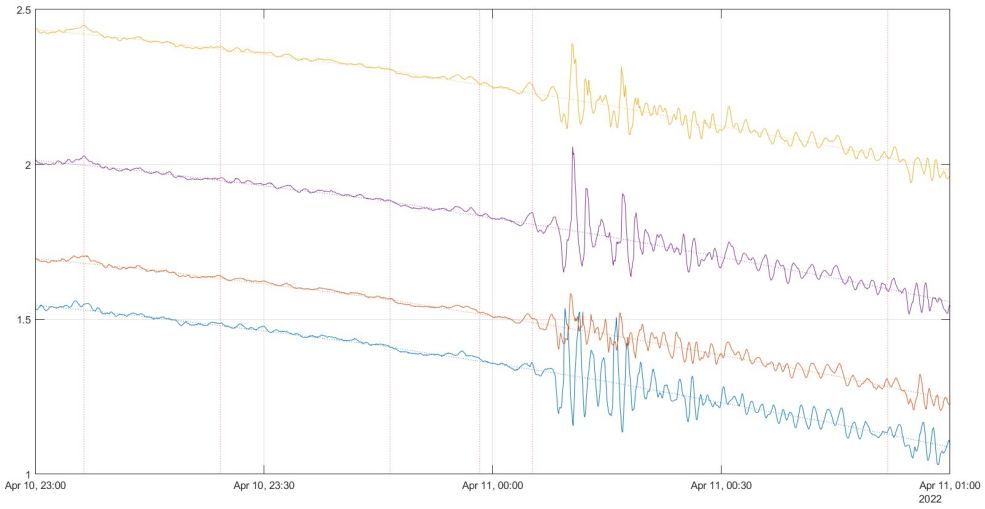

Figure 4.19: Calm water disturbed by a ship wave obtained from the pressure data.

Figure 4.19 shows a moment in time during measuring when there are almost no oscillations in the pressure signal. This means that the oscillations in the signals are not continues. The oscillations can be seen to start again after a large ship wave disturbs the water. This section of the signal containing the oscillations has a lower water level than the calmer section in the signal. If the calmness of the water were caused by sheltering due to the water level dropping under the height of the groynes, the calmer water would show up during a higher water level. The data shows that the oscillations caused by the first ship wave last until a second ship wave arrives at the end of the signal. According to their waves, the time between these ships is approximately 30 to 40 minutes. Because this is a busy shipping route there are almost no calm periods in the signal.


ADV gps locations
Location 1 in the text corresponds to the location of ADV 1
ADV 1
ADV 2
ADV 3
ADV 4
ADV 5
ADV 6
50 m
100 ft
51°56'14"N
51°56'12"N
51°56'10"N
51°56'08"N
51°56'06"N
Latitude
4°11'50"E
4°11'55"E
4°12'E
4°12'05"E
4°12'10"E
Longitude

5 | Sediment behavior

In Section 4, the data collected during the measurement campaigns was analyzed. The analyzed data gives an overview of the hydrodynamic conditions inside the groyne area. The parameters obtained from the analyses are needed to predict the behavior of the sediment. The predictions are based on calculations for the threshold of motion and sediment transport because of the number of uncertainties.

5.1. Sediment characteristics

Sediment gives a quick indication of the characteristics of the flow. The sizes and shapes of the sieve curves can indicate the origin of the particles and whether the bed is active due to the velocities at the bed. In the project area, there is a distinctive difference between the original sediment and the nourished sediment. According to the dredging report, the deposited sediment is mainly sandy material with a d_{50} of $0.23\,\mathrm{mm}$ (Wensveen, 2019). This coarse material was used to minimize the unwanted spreading.

There are two different analyses done on the sediment samples. The first analysis has been done during the measuring campaigns. These first observations are made by walking through, feeling and seeing the sediment. This will give a first impression of the soil and difference within the project area. The second analysis has been made by sieving the material with the Malvern which is explained in chapter 3.4. The sieving curves will give a complete overview of the range of particle sizes.

Table 5.1: Classification for different types of sediment present in the project area (Verruijt, 2001).

sediment type	size range
gravel	$> 2\,\mathrm{mm}$
sand	$2\,\mathrm{mm}$ - $63\,\mu\mathrm{m}$
silt	$63\,\mu\mathrm{m}$ - $8\,\mu\mathrm{m}$
clay	$< 8\,\mu\mathrm{m}$

5.1.1. Observations

During the measurement campaigns observations were made about the difference in sediment. While walking through the project area it was felt that at locations 1 and 4 the bed was hard and impressible. At locations 3 and 6 the bed felt very slippery and loose. In the area with the loose and slippery bed the ground would compress for around $10\,\mathrm{cm}$ under the weight of a person. The transition between the different sediment was felt at locations 2 and 5.

When driving in the poles for the ADV mounts the different sediment types gave different resistances. At the more muddy bed at locations 3 and 6, less force was required to put in the poles. Especially at location 3 the resistance of the soil was low. However, at location 4 the Resistance was very high and it was felt when driving in the poles that the bed contained larger stones at different places and depths.

5.1.2. Sieve curves

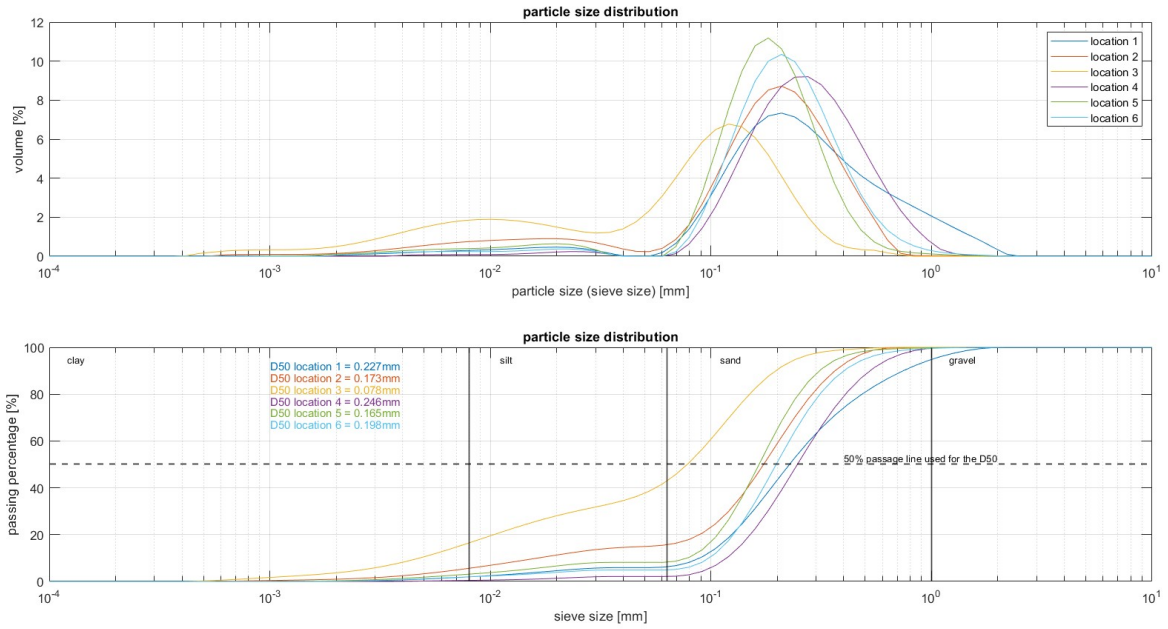

Figure 5.1: Particle sizes obtained from the Malvern.

Figure 5.1 shows the particle size distributions for the different locations. The top graph in the figure shows the percentages in which the particle sizes are present in the sample and the bottom graph shows the cumulative particle sizes. Because of the technique used by the Malvern to analyze the size of a clay particle, it is possible to obtain two different sizes for the same particle. This is caused by the shape of clay particles, which is often different from a sphere-like shape of a sand grain. For example, plate-like shapes have very different two-dimensional areas depending on which side is looked at and the non-uniformity of the bed. This can result in a second peak in the particle size distribution graph. The different d_{50} for each location can be seen in the cumulative size distributions. The sample at location 3 has the lowest d_{50} and the lowest d_{10}, which means that this soil contains the highest percentage of silt and clay particles. This is consistent with the observations about the slippery bed and the looser soil. The samples from locations 1 and 4 show a low percentage of small particles and a high d_{50} compared to the other locations. The locations with a higher percentage of sand in the soil compared to the other locations are consistent with the observations of high resistance during the walk. The sample from location 6 shows a distribution with a high d_{50} and a small percentage of smaller particles, which is different from the observations made in the same area. This difference can be caused by a small layer of organic slimy material which can cause the bed to be slippery. Another cause could be that smaller particles escaped into the water while collecting the sample, which can cause a larger d_{50} and more uniform sediment.

Table 5.2: The coefficient for uniformity of the different samples.

location	d_{10}	d_{50}	d_{60}	Cu=d_{60}/d_{10}
1	89.08 µm	226.91 µm	289.59 µm	3.25
2	16.40 µm	173.36 µm	202.59 µm	12.37
3	4.77 µm	71.01 µm	99.77 µm	20.90
4	117.94 µm	246.47 µm	286.72 µm	2.43
5	78.33 µm	165.23 µm	183.14 µm	2.34
6	98.29 µm	197.53 µm	224.31 µm	2.28

table 5.2 shows the different Uniformity coefficients. These coefficients represent the distribution of particle sizes, so a lower coefficient means a more uniform soil. The table shows that only at locations 2 and 3 the coefficient of uniformity is above 6, which is considered the threshold for sand to be well graded (Verruijt, 2001). The sediment at the other locations can be considered poorly graded or an uniform soil. The Low uniformity coefficient at locations 1 and 4 and the high d_{50} indicate that the samples consist mostly of the deposited sediment. This deposited sediment contains a higher d_{50} than the naturally deposited material and the d_{50} resembles the d_{50} that is mentioned in the dredging report. This means there is a low deposition of smaller natural sediment and a small amount of erosion of the deposited material. The high percentage of silt and clay in the sample from location 3 indicates low flow velocities at this location, while the smaller percentages of these finer sediments at the other locations indicate larger flow velocities.

5.2. Movement of the sediment

The flow velocity at the bed causes the movement of sediment. This flow velocity depends on the mean flow velocity, the water depth and the friction at the bed. Although the velocity and pressure at the ADV are measured, it is impossible to get the precise values for the mean velocity and friction. This means that the values obtained will indicate where the sediment will move when it is between the boundaries. Therefore, no distinction is made in this section in the kind of sediment movement.

5.2.1. Initiation of motion

Shields (1936) can be used to find the critical velocity for the initial motion of the sediment. However, Shields's approach has a number of limitations. This method does not consider the effects of shadowing for smaller particles by larger particles and other effects due to sediment size differences. This means that this method is more accurate for uniform soils. From 5.2 it can be seen that locations 1, 4, 5 and 6 have an uniform soil while the other two locations have a more extensive spread in sizes.

Shields (1936) initially uses the shear velocity in his formula and later van Rijn (1984) rewrote this to use the non-dimensional grain size. The non-dimensionless grain diameter can be obtained using Equation 5.2.1 (van Rijn, 1984). In this Eqation $d_* = dimensionless\ particle\ parameter\ [-]$, $d_{50} = median\ sediment\ grain\ size\ [m]$, $\Delta = (\rho_s - \rho)/\rho \rightarrow \rho_s = mass\ density\ of\ the\ particle\ [kg/m^3]$, $\rho = mass\ density\ of\ the\ surrounding\ fluid\ [kg/m^3]$ and $v = kinematic\ viscosity\ coefficient\ [-]$. Table 5.3 shows the estimated dimensionless particle sizes for every location with the d_{50} obtained from the sieve curves. The kinematic viscosity has been used, is for clean water with a temperature of 10 degrees. From the CTD data, water temperatures can be seen shifting between 8 and 13 degrees during the period of the ADV measurements. These smaller changes in the temperature are caused by the exchange of seawater and river water in the groyne area, which can be seen in Section B. These two types of water often have different temperatures depending on the conditions at the source of the water. Although, small temperature differences will have a limited effect on the critical velocities. For this reason, a water temperature of 10 degrees is sufficient.

$$d_* = d_{50} \left(g\Delta / v^2 \right)^{1/3} \tag{5.2.1}$$

Table 5.3: Based on the CTD temperature data the kinematic viscosity is obtained for a water temperature of 10 degrees, which gives $v^2 = 1.307 * 10^{-6} m/s^2$ (Habib et al., 2019), $g = 9.81 m/s^2$ and $\Delta = 1.65$.

location	d_{50}	d_*
1	0.23 mm	4.80
2	0.17 mm	3.67
3	0.08 mm	1.78
4	0.25 mm	5.22
5	0.17 mm	3.50
6	0.20 mm	4.18

van Rijn (1984) modified the shields graph with its dimensionless grain size. Van Rijn's formulas for calculating the critical Shields parameter with the non-dimensional grain size can be found in Figure 5.2. Using these formulas for the d_* the critical Shields parameter is obtained for the different locations and temperatures as shown in Table 5.4.

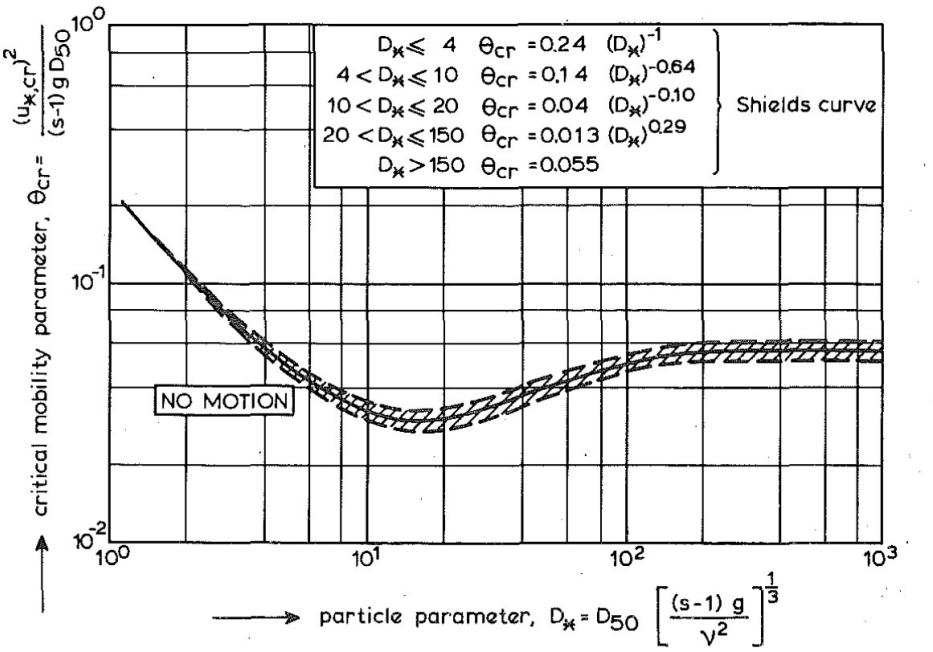

Figure 5.2: In the modified shields graph, the Reynolds shear stress is replaced with the dimensionless grain size. (van Rijn, 1984)

Table 5.4: Critical shield parameters for 10 degrees.

location	θ_{cr}
1	0.051
2	0.065
3	0.135
4	0.049
5	0.069
6	0.056

5.2.2. Bed friction an roughness height

According to Q. Zhu et al. (2016), the roughness height can be obtained using the vertical velocity profile. When assuming a logarithmic boundary, Equation 5.2.2 can be used to describe this verticle velocity profile, where $\kappa = Von\ Karman's\ constant\ [-]$. The rewritten equation with constants A and B that replace the variables, can be used to fit the vertical velocity profiles to the ADCP data. From the ADCP, velocities over the water depth have been obtained at every measurement along a sailing path. With the fit function from Matlab, a curve has been fitted through all these profiles using the method from Q. Zhu et al. (2016). The z_0 can be obtained from coefficients A and B using equation 5.2.3.

$$U(z) = \frac{U_*}{\kappa} \ln\left(\frac{z}{z_0}\right) \tag{5.2.2}$$

$$u = A\ln(z) + B \rightarrow\ A = \frac{u_*}{\kappa},\ B = -(\frac{u_*}{\kappa}\ln(z_0)) \tag{5.2.3}$$

The data can only be used for this method if it passes the criteria of the internal consistency analysis (Collins et al., 1998). For this analysis, the ADCP data will be tested on two criteria: The B coefficient should be close to zero and the correlation coefficient between the fitted curve and the data from the ADCP should be above 0.9. When these two criteria are met the z_0 can only be used if the value is between $0.03\,\mathrm{mm}$ and $7\,\mathrm{mm}$. These criteria should be met for at least four profiles in a data set. Unfortunately, this is not the case for the ADCP data, so this method could not be used.

Because a value for z_0 could not be obtained from the method due to the criteria off the internal consistency analysis, the value for z_0 must be approximated. A cf value often used for river beds is 0.003. Using this cf value, the shear velocity u_* can be obtained using equation 5.2.4. The ADCP data shows that the vertical velocity profile doesn't have a logarithmic profile. This means that the velocity measured at the ADVs can be used as an estimate for the mean vertical velocity. The critical shields parameter from Table 5.4 can be used to obtain the critical velocity for all locations using Equations 5.2.4 and 5.2.5. There is also an uncertainty of the Shields parameter itself. According to (Van der Wal, 1990), this uncertainty is around 15%. This will give a lower and an upper bound for the threshold of motion.

$$u_*cr = \sqrt{\theta_{cr}\Delta g d} \tag{5.2.4}$$

$$u_*cr = \sqrt{cf}\cdot\overline{u_{cr}} \tag{5.2.5}$$

Table 5.5: Critical velocities using a cf of 0.003.

Location	upper bound	u_{cr10°	lower bound
1	$0.29\,m/s$	$0.25\,m/s$	$0.21\,m/s$
2	$0.29\,m/s$	$0.25\,m/s$	$0.21\,m/s$
3	$0.28\,m/s$	$0.24\,m/s$	$0.20\,m/s$
4	$0.30\,m/s$	$0.26\,m/s$	$0.22\,m/s$
5	$0.29\,m/s$	$0.25\,m/s$	$0.21\,m/s$
6	$0.28\,m/s$	$0.24\,m/s$	$0.20\,m/s$

5.2.3. Critical velocities during tides

Figure 4.10 shows the tidal velocities compared to the water levels at every location. When these graphs are combined with the found critical velocity values for the threshold of motion, it can be seen whether transport can occur during ebb and flood. Also shown in the graph is at which stages of the tide movement of the sediment start and ends. This is shown in Figure 5.3

At the majority of the locations, there is an inequality between the ebb and flood velocities which exceed the threshold of motion. These differences between ebb and flood can indicate the mean direction for the sediment transport at the location.

At location 2, the ebb velocities are in between the bounds for the critical velocities during the descending stage of the tide. The flood velocities only cross the lower bound during the peak of extremely high tides at this location. However, this is only at a few occasions the case. This means these few moments during flood can be neglected in comparison to the number of occasions when the ebb velocities exceed this boundary.

At location 3, the critical velocity is only reached during flood, close and during the peak of the tide. The same situation takes place at location 5, where the ebb velocities are between the critical velocity boundaries and the flood velocities exceed the upper boundary of the critical velocity during higher water levels.

At location 4, the flood velocities exceed the upper boundary of the critical velocity during the majority of the tide, while the ebb velocities only exceed the upper boundary during the higher water levels.

The rest of the locations follow the same pattern where during ebb the critical velocity is reached in

the middle of the descending stage of the tide, while during flood the critical velocity is reach close to the peak of the tide. The number of occasions that the critical velocity is reached during ebb compared to flood is similar for these positions.

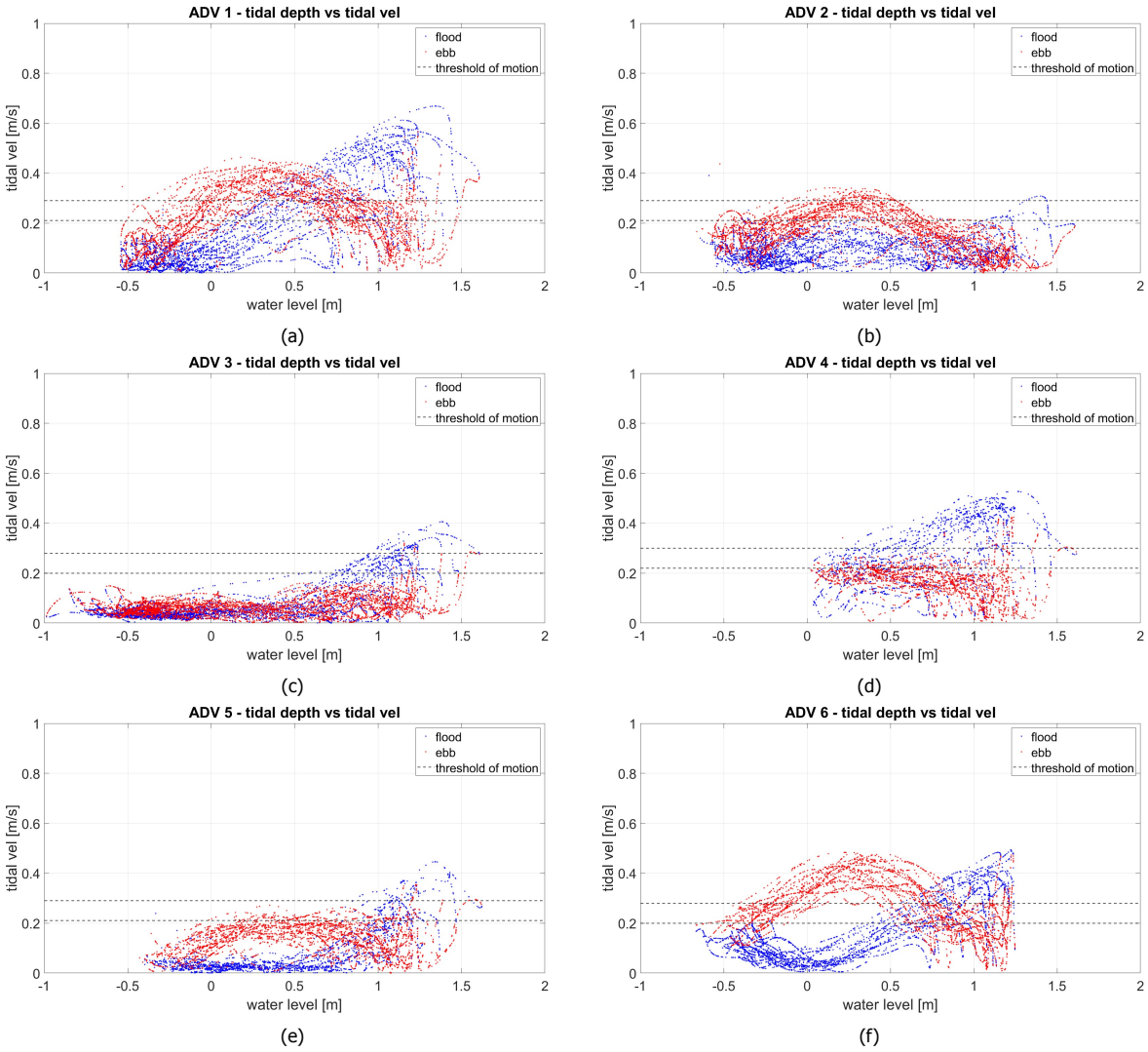

Figure 5.3: The critical velocities have been combined with Figure 4.10. The upper and lower boundaries represent the threshold of motion.

5.2.4. Critical velocity at a smooth bed

Although, location 3 has a smaller d_{50} than the other locations, indicating a smoother bed as discussed in Section 5.1. The apparent difference in bed friction is unknown. In van Rijn and Grasmeijer (2018), different chezy values were found for the original Ems river in Germany. The average value used was a Chezy value of $70\,m^{0.5}/s$, which translates to a cf of 0.002. Using this value, a critical velocity is obtained of $0.30\,m/s$ with an upper and lower boundary of $0.35\,m/s$ and $0.26\,m/s$. Figure 5.4 shows the critical velocity plotted with a cf of 0.002. Comparing this to Figure 5.3c it shows that a change in the friction parameter significantly impacts the threshold of motion. At the smooth bed, transport is only possible at the highest flood velocities and the upper boundary is only exceeded for several moments. As explained above, due to failed internal consistency analyses with the vertical velocity profiles found with the ADCP, no cf values could be obtained for this bed.

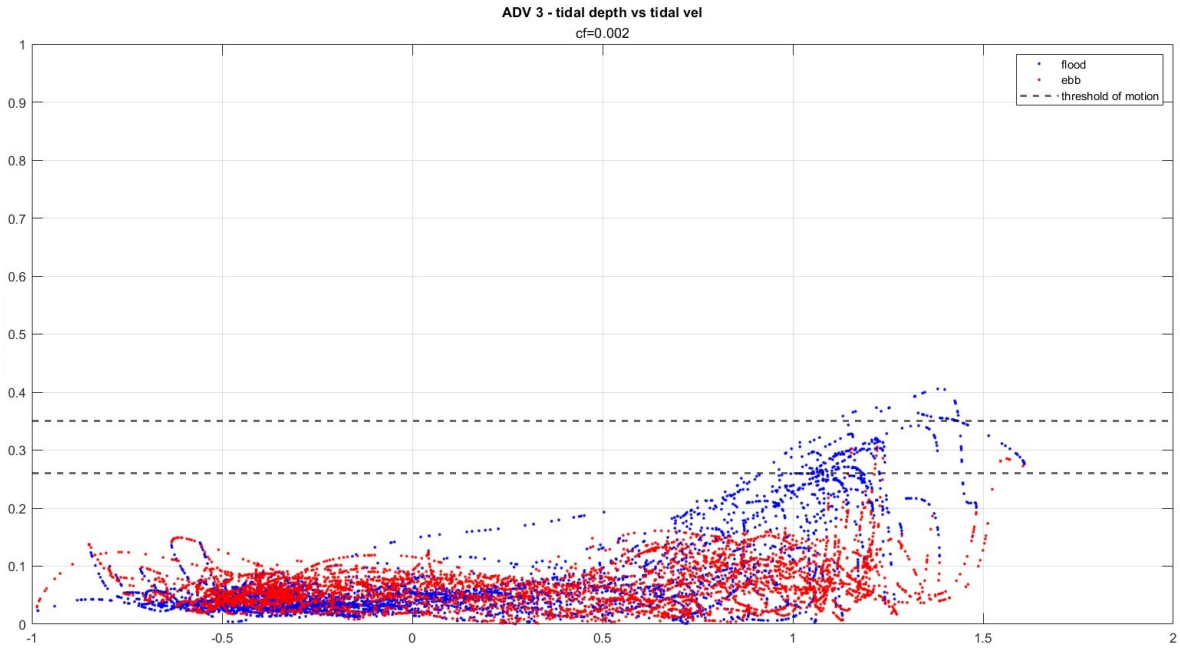

Figure 5.4: Threshold of motion at location 3, assuming the bed is smooth.

5.3. Sediment transport

To calculate the sediment transport, the formula of Engelund and Hansen (1967) will be used. This method gives the best results for a sorting coefficient below 1.6 and diameters larger than $0.15\,\mathrm{mm}$. Data within that range has been found to give no significant deviations from the method (Engelund and Hansen, 1967). The sorting coefficient at different locations is however between 2 and 10, so the actual sediment discharge will be larger for the lower sediment discharge rates. The large sediment suspension in the water column will influence the velocity distribution for sediment with a smaller diameter than $0.15\,\mathrm{mm}$. This means that this effect can influence the sediment discharge.

Equation 5.3.1 shows the formulation for the sediment transport according to Engelund and Hansen (1967), where $\mathrm{q_T} = sediment\ discharge\ [m^2/s]$, $s = relative\ density\ of\ sediment\ grains\ [-]$, and $d = particle\ diameter\ [m]$.

$$\mathrm{q_T} = \Phi\sqrt{(\mathrm{s}-1)g\ \mathrm{d}^3} \tag{5.3.1}$$

The Einstein coefficient Φ can be calculated using Equation 5.3.2. However, in the original formula, there is a friction factor. This friction factor has been replaced with $2 * c_f$.

$$\Phi = \frac{0.05}{c_f}\theta^{5/2} \tag{5.3.2}$$

Rewriting Equations 5.2.4 and 5.2.5 and changing the critical velocity with the mean velocity gives the formula for the Shields coefficient. The calculated $\mathrm{q_T}$ gives the total sediment discharge per unit width. because of the limitations of the method and the differences between the soil conditions in this analysis, the ratio's between the transport of different locations and conditions are of more importance than the exact numbers.

5.3.1. Sediment transport caused by the tide

The sediment transport in the direction of the river is negative when it is in the ebb direction and positive if transported in the flood direction, using the same coordinate system as in Section 4. The highest transport rates can be seen at location 1, while the lowest transport rates can be seen at locations 2 and 5. Locations 1, 3 and 4 all show a similar behavior to each other. The transport peaks can be seen mainly from the flood velocities at these locations. The transport difference between ebb and flood at these locations can differ from one to several orders of magnitude. The peaks increase from neap to spring tide. At location 3 the transport during neap tides is neglectable compared to the transport during spring tides, so the transport is almost exclusive in flood direction. At location 2, the transport peaks are primarily from the ebb velocities and in this location, no influence is showing from spring or neap tide. This is also the case for location 5, with the difference being that the transport peaks are located during the flood section of the tides. Location 6 is the only location with comparable values for the transport peaks during ebb and flood. The transport rates at location 6 are shown in Figure 5.5. This Figure shows an increase in transport from neap to spring tide, while the transports during ebb remains more constant.

At the downstream section of the groyne area, the most sediment is transported into the groyne area. At location 2 and 3 this sediment transport is directed out of the groyne area, for location 2 out of the gap in the dam and in location 3 in flood direction where the exact exit point is unknown.

At location 6 the outflow and inflow due to the sediment transport is equal, meaning that in normal conditions, the sediment transport direction is dominated by flood. During spring tides this behavior of the standard sediment transport conditions is reinforced. Approaching neap tide, flood-directed sediment transport decreases for all locations, while the ebb-directed sediment transport into the groyne area at location 6 stays constant. Because of this, the sediment transport direction changes and transport is mainly driven by the ebb-directed sediment transport from location 6.

The sediment transport of the other locations except for location 2 decreases towards neap tide, making the sediment transport at that time almost neglectable. The ebb and flood sediment transport at location 2 stays constant, meaning that at this location, the sediment transport does not change during neap and spring tide.

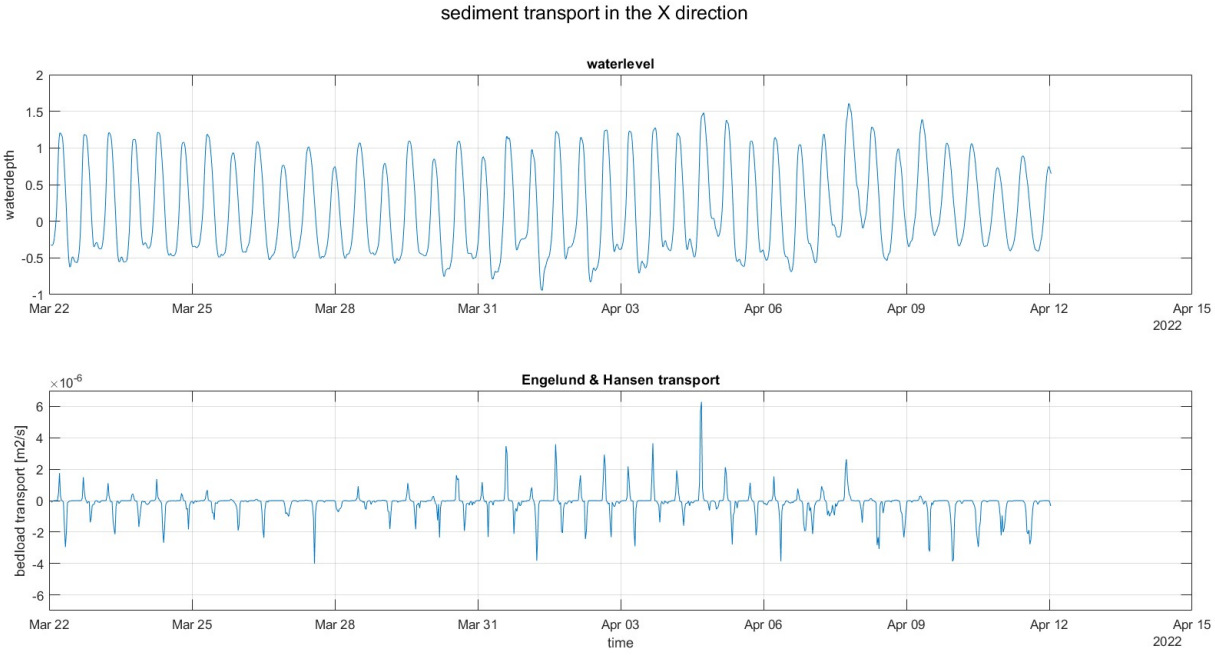

(a)

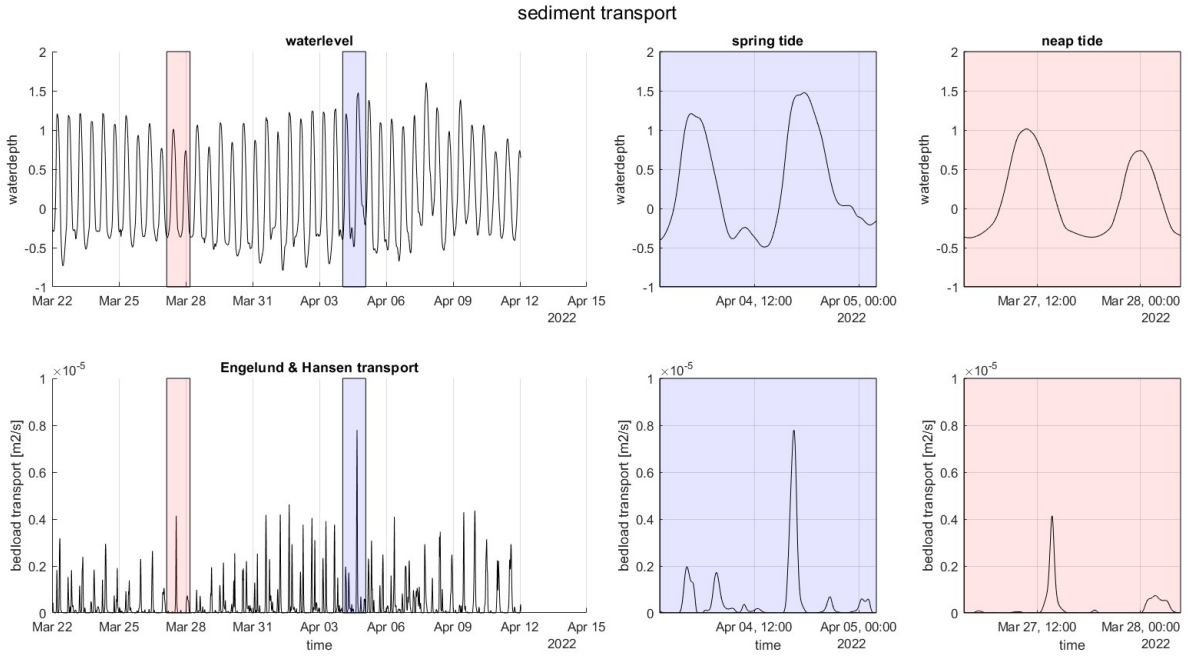

(b)

Figure 5.5: Transport due to the tide at location 6. (a) Transport in the direction of the river. (b) Absolute transport during neap and spring tide.

5.3.2. Sediment transport caused by the waves

The sediment transport due to three different waves caused by ship passage has been analyzed. The first wave travels in flood direction during the ebb part of the tide with a wave height at ADV 6 of $0.31\,\mathrm{m}$. The second wave is a wave traveling in flood direction during the flood part of the tide, with a wave height of $0.51\,\mathrm{m}$. And the last wave occurs near the end of the peak of the tide and travels as well in the flood direction. This last wave has a wave height of $0.34\,\mathrm{m}$. The rest of the characteristics of the waves can be found in Appendix B. The sediment transport from these waves has been analyzed for locations 1, 2 and 6. For locations 1 and 6 the absolute transports have been compared to the sediment transport in X direction, while at location 2 this is compared to the sediment transport in Y direction. For locations 1 and 6 the sediment transport peaks are located at different stages of the waves, so there is no clear indication of which stage of the wave has the most influence on the sediment transport. The sediment transport at these 2 locations has peaks in the direction of the flow, even if this is opposite to the direction in which the wave travels. This can be observed for the wave at location 6 in Figure 5.6.

At location 2, the direction of the peak coincides with the stage of the wave. A peak in the positive Y direction occurs during the rising stage of the wave, while a negative peak occurs during the descending stage, as shown in Figure 5.7. During the second wave, there are no positive peaks present for the Y transport. Figure 4.10b shows that the flood velocities during the rising stage in the middle of the flood are significantly higher than the velocities during ebb. During ebb, the tidal velocities are not high enough to counter the velocities created by a wave traveling in the opposite direction. Because of this, the transport peaks are in both directions during ebb. During the rising stages the tidal velocities are high enough to counter the velocities from waves travelling in opposite directions, which means that the transport of the sediment is only in the direction of the tidal flow.

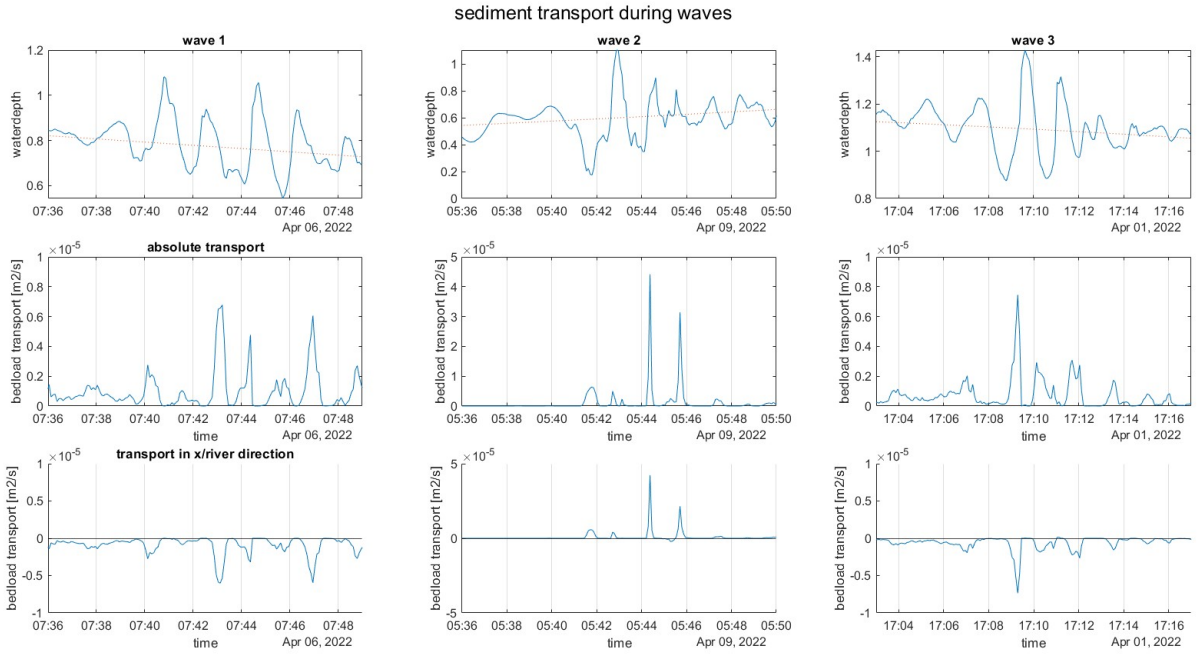

Figure 5.6: The absolute sediment transport and in X direction for three different waves at location 6.

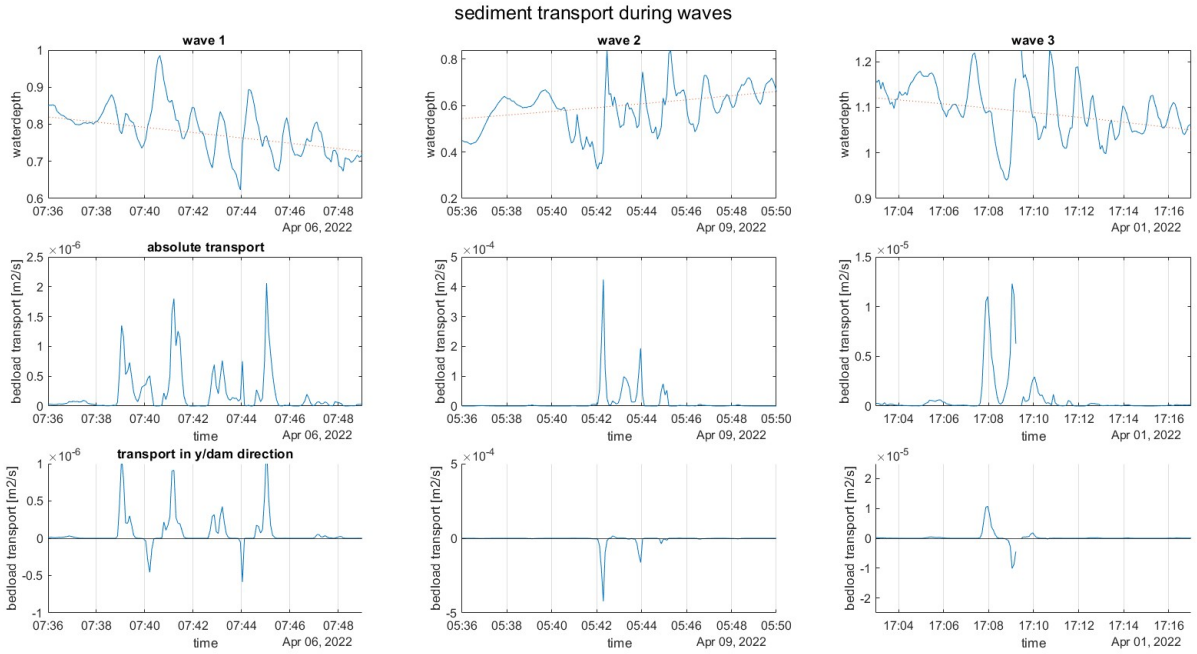

Figure 5.7: The absolute transport and in the Y direction for three different waves at location 2.

6 | Discussion

The data have shown that the tide and waves caused by shipping significantly influence the flow inside the groyne area. In addition, the flow pattern inside the groyne area is changed due to the modifications to the groyne area, which causes the flow to differ between ebb and flood. The wave impact is related to the wave height and water depth. Sediment in the groyne area is still active at some locations, and sediment transport direction is affected by the neap and spring tidal cycle. In this section, a deeper insight will be given into these key findings and the limitations of this research.

6.1. Emergence and submergence of the groynes

Comparing typical emerged groyne areas to this modified groyne area during emerged conditions is only possible for a specific section of the tide, where the water levels are too low to flow over the groynes. Previous literature about flow through an emerged groyne area like in (Bouwmeester, 1987) and (Przedwojski et al., 1995) shows that eddies are formed in a traditional open groyne area. A typical example can be seen in the data of (Brouwers, 2022), where two eddies are created in such a groyne area in the Waal. Flows in such open groyne areas are dominated by these eddies, which depend on the groyne area's water depth, velocity and shape. However, the data in this research did not show eddies in the modified groyne area. The modifications like the entrances in groynes and the dam cause the water to flow through the groyne area, entering and exiting mainly through these entrances. There is limited water exchange through the dam because of the size of the opening. In a typical groyne area, the lack of entrances in the groynes prohibits water from flowing directly through the groyne area. Instead, water from the river flows adjacent to the groyne creating the eddies with the differences in flow velocities from the river and the groyne area. This is in line with the results from the model of (Nijhuis, 2021). Although the modifications in that model had no entrances in the groynes, opening in the middle of the dam and larger openings where the groynes meet the dam, the typical eddies inside the groyne area where not present in the model.

During the emergence of the groynes, water flows laterally through the groyne area. The velocities at location 3 are significantly lower than the velocities of the adjacent locations. This could indicate the presence of an eddy or a mixing layer at that location during the emergence of the groynes. These eddies are formed the same way as they would be formed in an open groyne area where there is a significant velocity difference between water in the groyne and the main channel. The direction of the flow at location 3 is directed at the dam and constantly changing, whereas the directions at the other locations are relatively constant. However, this eddy has not been seen directly in the velocity data or the bed topography.

A re-circulation zone is formed behind a weir or submerged groyne from the flow over such a structure. In the researched groyne area at the downstream groyne the majority of this layer is blocked by the nourished island, but at the upstream groyne the layer has only a small pile of rip rap behind the groyne as an obstacle. As seen on the map in Figure 6.3, ADV 3 and 6 need to be located closer to the groyne to measure this re-circulation layer. From the bed topography of the groyne area it can be seen that upstream groyne has scour holes both in and outside of the groyne area next to the groyne itself. This scour is an effect of the submerged groyne and shows the significant effect of the weir flow on the sediment transport in the groyne area. This indicates significantly high velocities located at the upstream groyne.

6.2. Waves and oscillations

Oscillations are present in the majority of the measurements, but from the data it has been seen that there are certain periods of calm water. These periods can be disturbed by shipping waves, which create the smaller oscillations that can last for an extended period of time. One of these calm periods is shown in Figure 4.19. This period was at the peak of the flood and with submerged groynes. Reflection and secondary ship waves can explain these oscillations. Waves can be reflected from the bank and the dam. This reflection of the wave will show as an out of sync oscillation between the pressure signals of ADV 1 and 3 because these reflected waves do not travel in the X direction. On the other hand, secondary ship waves travel in the same direction as the primary ship waves. This means that these secondary ship waves are in sync oscillations between the pressure signals of ADV 1 and 3.

6.3. Scope and applicability

The scope of this research is focused on the flow and activities within the groyne area. The activities of the river itself were not measured during the measuring campaigns. The impact of natural or artificial changes to the river will impact the flow in the groyne area. For example, changing depths or widths in the river due to dredging or erosion will alter the flow inside the river, which could impact the exchange of water between the main channel and the groyne area per tide. In addition, the amount of water flowing through the groyne area affects the flow patterns, flow velocities and sediment movement.

This research can be used as a basis for further research into other locations, groyne area and dam designs. However, the direct applicability of this research to other locations and other groyne area and dam designs is questionable. Ships can be seen to have a significant impact on the groyne area. Waves come in from both upstream and downstream openings in the groynes. The waves can travel undisturbed through the adjacent groyne areas because, these are not protected by dams. When an adjacent area closes off with a dam, waves are expected to lose part of their energy, which would drastically decrease the impact in the groyne area. The tidal flow through the groyne area will also decrease. This will cause an increase in resistance for the flow resulting in less water flowing through the groyne area.

Even though the specific situation of this modified groyne area, the extremely limited research on modified groyne areas makes that this research gives an overview of how the modifications can change the flow of a typical groyne area. This means that the knowledge gained from this research could be used in the designs of new groyne area modification projects. In addition, for this groyne area, the data of this research could be used as a baseline measurement for future modifications.

6.4. Limitations

6.4.1. Data acquisition

Batteries for the ADVs were in limited supply, so having all 6 ADVs measure continues during the whole experiment was impossible. The choice was made to let two of the six measure in bursts of 6 minutes for every 10 minutes. When analyzing the wave data, it was seen that some of the ship waves were lost due to the timing of the burst. This can be seen in Figure 6.1. The method used for analyzing the ship waves was also not applicable for in burst measured data. This resulted in missing the wave data at two of the locations. Location 4 is one of the locations where burst measurements have been done. This location is in line with location 6 where the waves enter in the upstream groyne and this is the closest location to the entrance in the downstream groyne. The waves at this location contain essential information due to their position.

There was no GPS linked to the ADCP during the measurements. Because of this, the precise locations of the measurements were unknown. To compensate for this, reference poles were placed and their coordinates mapped with the GPS. The sailed paths were assumed to start precisely at the location first pole and in a straight line to finish at the next pole. In reality, this was not the case. The starting and ending points differ per measurement and the straightness of the path can be affected by the flow. This causes difficulties in obtaining the locations of the observed events and the comparison of events from different measurements.

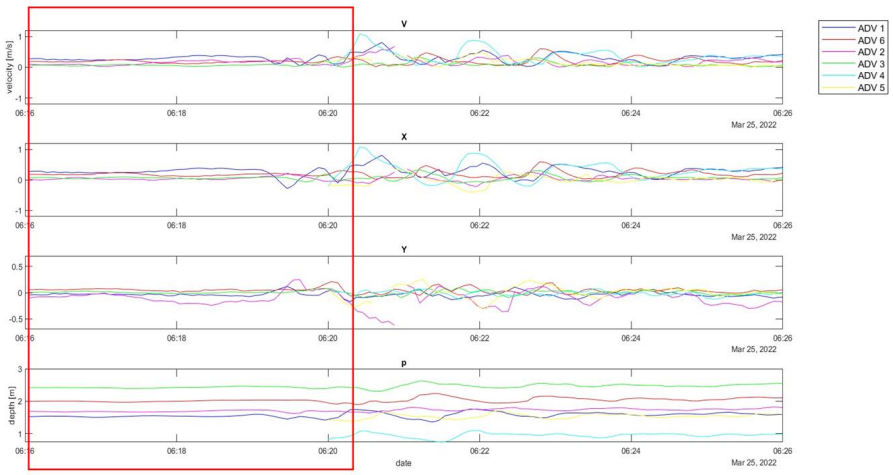

Figure 6.1: The missing data from ADV 4 5 is highlighted. The data can be seen as missing in all graphs due to the burst.

6.4.2. Data handling and analyses

The primary ship waves are detected by locating the most significant water level difference between the water depth and the averaged water depth. This maximum deviation is searched for 3 minutes before and 5 minutes after a ship passes the groyne area. However, this method can't distinguish between the shape of a primary ship wave and other types of oscillations. This means that some of the recognized ship waves could be wind waves or small oscillations caused by ships, as discussed in 6.2. This can be seen from the relatively large section of waves smaller than $5\,\mathrm{cm}$. This time frame in which the waves are detected is calculated from the wave velocity, which can be found in Appendix B. For this wave velocity, an assumption was made for the channel depth and because the bed is not flat average depth was used. The vessels were also assumed to sail in the middle of the channel. This has an impact, or the moment the wave arrives, when this is outside the time frame the waves are undetected. As a result, the mean height and increase in velocity decreases for ship waves.

6.4.3. Equations, calculations and parameters

The bed composition is assumed to be a homogeneous bed. When looking at the sediment curves, it can be seen that some locations deviate further from this assumption than other locations. The critical bed shear stress and the mean particle size have a linear relationship for poorly graded soils. A larger particle has a higher critical bed shear stress. For well graded soils this is not the case. The larger difference in size causes hiding effects between the soil particles, caused by smaller particles sheltering behind larger particles. For locations 1 and 4, the larger rip rap stones in the bed reinforce this. These effects cause the linear relationship to change into a nonlinear relation, where the smaller particles have a higher critical bed shear stress. The threshold of motion for smaller particles in a bed with a significant variation of particle sizes increases. This effect increases when the percentage of medium size particles decreases and the percentages of larger and smaller particles increases. This means that this has the largest effect on the transitioning zones at location 2 and 5.

The assumption was made to use the same roughness coefficient for the calculations of the threshold of motion and the sediment transport. This would imply that the bed is fully submitted to the same conditions. From the sediment curves and the observations in the field, this is known to be not true. For example, the difference in the mean grain size indicates a difference in roughness height. The difference between hydraulic smooth and rough conditions is the roughness height and roughness coefficient essential factors to determine the flow conditions over the bed. This will influence the difference between the movement of the sediment at the different locations.

The ADVs measure the velocity at one certain height. This height differs per location. The assumption was that the velocity measured at the ADV was the same as the depth average velocity. Figure 6.2 shows the measured velocity in the velocity column over the water depth for two different water levels.

It can be seen that the difference between the measured velocity and the depth average velocity changes over time. This difference impacts the shield parameter, which uses this depth average velocity. ADCP data suggest a relatively significant velocity difference over the water depth at different locations, so the observed velocity depends on the installation depth of the ADV.

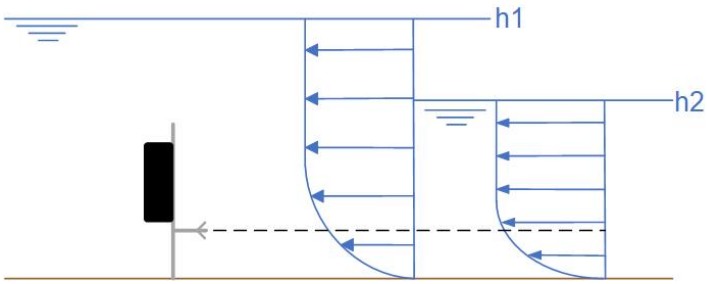

Figure 6.2: A sketch of the difference in velocity at the height of an ADV from two different water levels. The vertical velocity profiles are assumed to have a logarithmic shape.

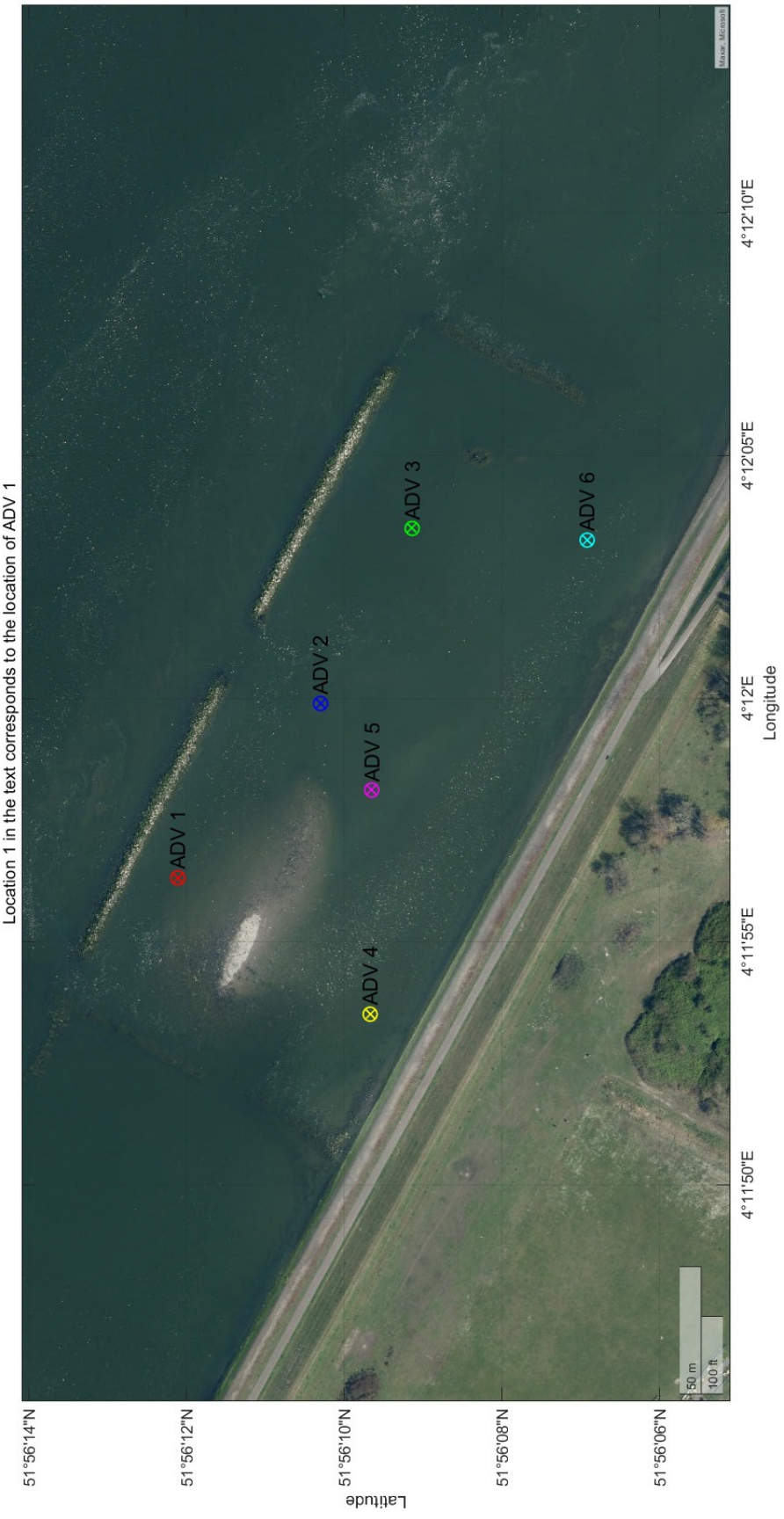
ADV gps locations
Location 1 in the text corresponds to the location of ADV 1
ADV 1
ADV 2
ADV 3
ADV 4
ADV 5
ADV 6
51°56'14"N
51°56'12"N
51°56'10"N
51°56'08"N
51°56'06"N
Latitude
4°11'50"E
4°11'55"E
4°12'E
4°12'05"E
4°12'10"E
Longitude
50 m
100 ft

7 | Conclusion

In this section, an answer will be given to the research question: *What is the influence of the groyne area modifications to the flow characteristics inside this area?* This answer to the research question has been found by combining the answers of the sub-questions to the found literature of the groyne area. A map can be found in Figure 6.3, which shows the positions of the different locations within the groyne area.

1. *What is the effect of physical processes to the flow inside the groyne area ?* → Section 7.1.
2. *What is the effect of passing ships on the flow inside the groyne area?* → Section 7.2.
3. *What are the effects of the hydrodynamic conditions on the behavior of the sediment?* → Section 7.3.

7.1. Physical processes

From the different natural processes, only the local winds and the tide can be seen to have an effect in the data. The local winds causes small oscillations in the water, but have no visible impact on the flow velocities. On the other hand, the shape of the flow velocities can seen to be heavily related to the shape of the tide in pressure data. This means that the tide is the leading physical driving force for the flow in the groyne area.

With the openings in the groynes and the dam, water can flow through the groyne area at different water levels. This flow has two main flows channels within the groyne area, located at either side of the nourished island and in direction of the river. The exchange of water between these main flow channels differs between ebb and flood. During flood, the flow from the river starts flowing through the groyne area when a threshold water depth is reached. At ebb, this flow through the groyne area is not dependent on the water level and flows through the groyne area during the complete ebb period. However, from neap to spring tide the threshold is reached at an earlier stage in flood flow, affecting the difference between the ebb and flood flow.

The tidal velocities are related to the water levels in the groyne area. The ebb velocities behave like a typical tidal flow, where the maximum velocities are reached in the middle of the descending stage of the tide. However, the velocities during flood differ from the ebb flow and increase with the water level, reaching their maximum velocities at the end of the rising stage of the tide. At some of the locations, this velocity increase comes after a threshold water level has been reached. The rise in water level from neap to spring tide changes the groyne area from an ebb-dominant to a flood-dominant system, where the highest velocities are reached during flood.

7.2. Shipping influence

Shipping causes the most significant wave action in the groyne area. A typical movement pattern was recognized in the movement of these waves through the groyne area. Waves propagate from either side through the groyne area in the same direction as the ship from which they originate. The wave also enters through the gap in the middle of the dam where both waves interfere with each other. After the wave has passed a location, oscillations from later secondary waves and reflection of the wave are still present in that location.

From a ship passing the groyne area, the primary wave and the drawback have the most considerable impact on the velocity. On average this increase in velocities due to primary ship waves ranges from $0.11\,\mathrm{m\,s^{-1}}$ to $0.23\,\mathrm{m\,s^{-1}}$ for the different locations of the groyne area. It has been seen that this increase in velocity is correlated to the wave height and the water depth. However, no clear correlation was found with tidal velocity and the increase in velocity due to the ship waves.

7.3. Sediment behavior

From the sediment samples and the observations during the excursions, it have been seen that the nourished sediment hasn't been transported to all the locations. The areas next to the nourished island have similar sizes for the d_{50}. The size of the sediment decreased when moving away from the nourished island. Although lower than sediment sizes found next to the nourishment, the size at the upstream groyne entrance has a slight increase compared to the sediment in the middle of the groyne and a large increase compared to the upstream location close to the dam. These results correspond with the observations made of a more rigid and less compressible bed at the downstream groyne in comparison to the upstream section of the groyne.

During a tide the velocity is able to reach the threshold of motion for the sediment at every location, indicating that movement is possible for the sediment at every location. For the majority of the locations, this threshold of motion has been reached during ebb as well as flood. At the location at the entrance in the middle of the dam the critical velocity is only reached during the ebb tide. The critical velocity is only reached during flood at the location where the upstream groyne meets the dam.

The neap-spring cycle greatly influences sediment transport in the groyne area. During spring tide, the average sediment transport is directed upstream. When the tide gradually changes from spring to neap tide, the average sediment transport direction changes from upstream to downstream. The direction of the sediment transport between the gap of the dam is unaffected by the neap-spring cycle.

The velocity increase caused by ship waves significantly impacts the sediment transport. These ship waves causes visible peaks in the sediment transport. Peaks that are caused during the passage of the primary and secondary wave are directed in the same direction as in which the waves propagate, while the peaks caused by the drawback are directed in the opposite direction. When the wave and the tide are in opposite directions the transport direction during the passage of a wave depends on the difference between the tidal velocity and the increase in velocity due to the wave. In some cases, this causes the tidal velocity to completely counter the velocity increase from the wave, which can be seen back in the transport directions.

7.4. Answer to the research question

The flow in the groyne area has changed due to the dam and the nourishment. Typical flow in an emerged groyne field with the eddies is unrecognizable during lower water levels in the modified groyne area. The exchange of water between the main channel and the groyne area is through the gap in the dam, which removes the mixing layer that separates the groyne and the main channel during submerged conditions. The flow in this groyne area is lateral and divided into two main flows along either side of the nourished island. Rocks and a higher entrance in the downstream groyne compared to the entrance in the other groyne, gives the groyne area different flow velocities between ebb and flood. The neap and spring tidal cycle enhances Ebb and flood differences in the groyne area even more. These velocities differences also impact the sediment transport and its absolute direction in the groyne area. The dam also helps reduce the wave influence on the groyne area, although these waves still significantly influence the velocities. Waves also propagate in a lateral motion from groyne to groyne through the groyne area. The water can move material from the nourishment, but the spreading of this material is limited to a number of locations in the groyne area. For the largest part, the nourished material is still at the location where it is deposited.

8 Recommendations

Field measurements add extra challenges to a research. There are multiple approaches to the practical problems that present during the data analysis. In this section, recommendations for further research are discussed.

8.1. Physical processes

Because of the interaction between the sea water and the river discharge, salinity is an important factor for describing the flow and sediment transport. Baroclinic effects influence the exchange between water in the main channel and water in groyne area because of their difference in salinity during a tide. This variation of salinity in the groyne area during has been observed with the CTD mounted at the entrance in the middle of the dam. Because salinity was not in the scope of this project this data is not been further analyzed. It is recommended to determine the impact of the salt freshwater exchange on the groyne area and its effect on the flow and transport of sediment.

The river discharge and the wind impact on the groyne area have not been treated. The data showed that the wind causes small continuous oscillations in the water. These oscillations are small waves. The impact of a single oscillation on the velocity increase and bed erosion is negligibly small. However, the continuous impact of the oscillations could cause erosion in the groyne area. The river discharge has an impact on the water levels in the river. This research shows that the water level has a significant impact on the flow in the groyne area. These two effects are recommended to be further analyzed by using the data from Rijkswaterstaat and comparing the wind and discharge data to the velocity and pressure data. The river discharge analyses should be prioritized with its shown effect on the ebb velocities.

The experiment with the mounted ADCP was done during a neap tide, which caused low flow velocities. This caused the measuring window to be smaller and the differences in velocity to be very small. The color plots lacked details because of the small horizontal and vertical velocities which occurred during the measuring period. In addition, the vertical flow profiles couldn't be obtained due to these low velocities and water levels. The jetski required a minimum water depth to perform measurements and because of the lower water levels only a small portion of the flood and the ebb tide was in the measuring window. Doing the experiment during a higher tide gives better velocity distribution results over the groyne area's cross-section, as the flood velocities were seen to increase in Figure 4.10. Because of this, it is recommended to repeat the experiment during normal or spring tides.

A computer model is recommended as a tool to fill in the gaps between the data from the ADVs. The ADVs have done point measurements at six different locations at a fixed height above the bed. The behavior captured by the data is limited to the conditions during the measuring period. In this research, assumptions have been made for the behavior between the different ADV locations. A computer model uses a grid over the groyne area and calculates the flow behavior from a grid point to next grid point, giving a more accurate description of the flow between the locations. This model uses the data obtained during the field campaigns. From such a model, different conditions are simulated such as an extremely large river discharge or an extreme storm. Such specific conditions are extremely difficult to capture during a measurement campaign and these conditions have not been encountered during this particular research.

8.2. Shipping influence

Ship waves have a very distinctive shape. To optimally identify and locate these waves that are caused by shipping, it is recommended to use another method. With the technique used in this research the shape of the wave has not been accounted for, because the technique works with the assumption that the ship waves are always more prominent than the oscillations in the water level. A wavelet analysis

recognizes the shape of waves that could be identified as ship waves. The wavelet analysis will be less dependent on the AIS data as well. The accuracy of this AIS data is questionable as seen from Brouwers (2022), who used this same AIS data. This would increase the probability that the measured oscillation is the primary ship wave.

8.3. Sediment composition and transport

Only sediment samples inside the groyne area were obtained after the groyne was modified and nourished. Therefore, there is limited information about the original sediment in the groyne area, the sediment of the adjacent groyne areas and the sediment in the channel itself. Because of this there is no knowledge and data of the exchange of sediment between the groyne area and the adjacent areas. The sediment transport is limited to within the boundaries of the groyne area, so it is recommended to obtain and analyze the samples of the adjacent areas. This will help further understand the pilot's role in the river's morphological system.

Sediment transport formulas such as from Shields (1936) and Engelund and Hansen (1967) have been used to predict sediment transport. Due to the complicated conditions in the field, the accuracy of predicting sediment behavior is limited. Using specialized equipment to measure erosion and sedimentation at specific locations in the groyne area is recommended. A well calibrated Seapoint Turbidity Meter can measure the sediment flux at one location.

8.4. The pilot

In the long run, one of the pilot's main goals is to create an intertidal area, which also attracts new flora and fauna. There has not been a specific ecological goal for this project such as the amount of new species they want to attract, which species they want to attract and the percentage of area they want to be covered in vegetation eventually. This research has focused only on the abiotic conditions of this groyne area, but it is unclear which requirements are needed for the success of this project. Because these goals are unclear, no advice can be given in this research. An ecological study of the groyne area and clear guidelines for the desired biotic and abiotic conditions are essential for determining the goal of this project. A basis for this further study can be de Jong (2023), who discusses the potential for ecological development in this area is discussed.

Traveling ship waves significantly impact the groyne area in the current configuration. This means the adjacent groyne areas are open and don't contain dams to shelter them from the impacts of the river. The intention of the pilot is to close all of the groyne areas in that section of the channel. This means that the results give a distorted view in the impact of waves and the tide. Therefore, testing should be done to multiple adjacent groyne areas with the same modifications. There are multiple ways to do these tests: by building a second and third pilot area next to the existing one, with a small-scale laboratory test or computer simulation. It is recommended to do the computer simulation because of its simplicity and duration compared to the testing.

This research focuses on the situation where the groyne field is modified, and only one of the two nourishments has occurred. This is a specific situation, but it is essential in understanding the influence of the adjustments on such a groyne area. The second nourishment occurred on December 20^{th} in 2022. To fully understand the effect of this pilot on the flow, two different measuring campaigns have to be performed. First, a measuring campaign of a situation where the groyne area is modified and the nourishments have not yet been done. This will give a more profound understanding of how the heightened groynes and the dam will affect the flow in the groyne area. Measurement campaigns at groyne areas with other configurations will also give more knowledge into the effects of the dam on the groyne area. For example, two groyne areas with different modifications used for this pilot are found upstream from the groyne area. Secondly, measurements must be done in the situation of the finished pilot after the second nourishment. A measurement campaign in the finished situation is recommended to see if the pilot has a desirable outcome and as a baseline measurement to measure the long-term effects of the groyne area.

The goal of the project is to create an intertidal area within the groyne area that gives a habitat to the flora and fauna of the region. From this research, it has been shown that the modifications have a direct impact on the flow and the wave action within this groyne area. The changes that occur to flow are especially beneficial for the fauna in the region. The different gullies that have been created at both the river bank and the dam are beneficial for the fish migration from salt to fresh water and reverse. Another positive change regarding the fish migration are the more sheltered areas with lower flow velocities, such as location 3 during ebb. During the fish migration, these fish need sheltered areas to rest and get used to the water's salinity change. The flora has unfortunately not benefited yet from the modifications due to the high wave impact within the groyne area. As discussed before, the waves enter from the openings in the groynes due to the adjacent groynes being open. It is expected that when the adjacent groynes are closed with a dam the wave impact will significantly drop and the possibility comes for flora to develop in the area. Because of the positive impact on the fauna and the potential for the development of the flora, it is recommended to continue this project and extend it from one single groyne area to multiple groyne areas or even to the majority of the groyne areas in the Nieuwe Waterweg.

References

Ali, S. (2013). *Flow over weir-like obstacles*.

Altenburg, W., Arts, G., Baretta-Bekker, J. G., van den Berg, M. S., van den Broek, T., Buskens, R., R. Bijkerk, H. C. C., H. van Dam, G. v. E., Evers, C. H. M., Franken, R., Higler, B., T. Ietswaart, N. J., de Jong, D. J., Joosten, A. M. T., Klinge, M., Knoben, R. A. E., Kranenbarg, J., van Loon, W. M. G. M., Noordhuis, R., … Backx, J. J. G. M. (2021). *Referenties en maatlatten voor natuurlijke watertypen voor de kaderichtlijn water 2021-2027*. Stichting Toegepast Onderzoek Waterbeheer.

Ambagts, L. R. (2019). Flow over and around submerged groynes: Numerical modelling and analysis of a groyne flume experiment.

Bennett, A. S. (1976). Conversion of in situ measurements of conductivity to salinity. *Deep Sea Res Oceanogr Abstr*, *23*, 157–165. https://doi.org/10.1016/S0011-7471(76)80024-1

Bosboom, J., & Stive, M. J. F. (n.d.). Coastal dynamics. https://doi.org/10.5074/T.2021.001

Boskalis en van der kamp baggeren nieuwe waterweg: Nu geschikt voor grootste mammoetschepen. (2018).

Bouwmeester, J. (1987). *Flexibele waterbouwkundige constructies*. Delft University of Technology.

Brolsma, J. et al. (1988). Six-barge pushtow trials. *PIANC, Den Haag*.

Brouwers, S. V. (2022). The effect of vessels on the flow pattern inside a groyne field.

Chassagne, C. (2021). *Introduction to colloid science*. Delft University of Technology open.

Collins, M. B., Ke, X., & Gao, S. (1998). *Tidally-induced flow structure over intertidal flats*.

The comprehensive manual for velocimeters. (2019). Nortek.

Coomans, M. (2018). *Uitbaggeren nieuwe waterweg kan beginnen*. RTV Rijnmond.

De aanleg van de nieuwe waterweg. (n.d.).

de Jong, B. (2023). Brakwatergetijdennatuur in de groene poort: Proeftuin sediment rijnmond.

de Vet, P. L., van Prooijen, B. C., Schrijvershof, R. A., van der Werf, J. J., Ysebaert, T., Schrijver, M. C., & Wang, Z. B. (2018). The importance of combined tidal and meteorological forces for the flow and sediment transport on intertidal shoals. *Journal of Geophysical Research: Earth Surface*, *123*, 2464–2480. https://doi.org/10.1029/2018JF004605

Elger, D. F., LeBret, B. A., Crowe, C. T., & Roberson, J. A. (2012). *Engineering fluid mechanics*. John Wiley & Sons.

Engelund, F., & Hansen, E. (1967). *A monograph on sediment transport in alluvlal stream.*

Goring, D. G., & Nikora, V. I. (2002). Despiking acoustic doppler velocimeter data. https://doi.org/10.1061/ASCE0733-94292002128:1117

Habib, A., Kabir, & Imran, S. M. D. (2019). *Applied fluid mechanics lab manual*.

Hans, H., & Benoit, C. (2007). Closed form solution for threshold velocity for initiation of sediment motion under waves. https://doi.org/10.1061/40926(239)2

Helmer, J. (2013). *Groene poort verbetert leefgebied rotterdamse havendelta*. ARK Natuurontwikkelingen.

Holthuijsen, L. H. (2007). *Waves in oceanic and coastal waters*. Cambridge university press.

Klijn, F., van Velzen, E., ter Maat, J., & Hunink, J. (2012). *Zoetwatervoorziening in nederland: Aangescherpte landelijke knelpuntenanalyse 21e eeuw*. Deltares.

Kranenbarg, J., Houben, B., & Brevé, N. (2017). *Voorstudie rijn actieplan europese steur: Noodzakelijke acties en actoren met het oog op een herintroductieprogramma in de rijn*. Stichting RAVON.

Mastersizer 2000 user manual. (2007). Malvern Instruments Ltd.

Miche, M. (1944). Mouvements ondulatoires de la mer en profondeur constante ou décroissante. *Annales de Ponts et Chaussées, 1944, pp (1) 26-78,(2) 270-292,(3) 369-406*.

Nijhuis, L. W. (2021). Tidal parks in the rhine-meuse estuary case study groene poort.

Przedwojski, B., Blazejewski, R., & Pilarczyk, K. W. (1995). River training techniques : Fundamentals, design and applications : A literature survey.

Ramin, B., Hossein, A., & Subhasish, D. (2015). Effects of relative submergence and bed slope on sediment incipient motion under decelerating flows. *Journal of Hydrology and Hydromechanics*, *63*. https://doi.org/10.1515/johh-2015-0039

Raven, H. C. (2010). Validation of an approach to analyse and understand ship wave making. *Journal of Marine Science and Technology*, *15*, 331–344. https://doi.org/10.1007/s00773-010-0102-1

Riversurveyor s5/m9 system manual firmware version 4.02. (2016). SonTek, a Xylem brand.

S. AI Ani, I. K. R. D., & Huntley, D. A. (1991). *Measurement of the influence of salinity on floc density and strength*.

Schiereck, G. J., & Verhagen, H. J. (2012). *Introduction to bed, bank and shore protection*. VSSD.

Shields, A. (1936). *Application of simalarity principles and turbulance research to bed-load movement.*

Sigel, L. (2021). Effect of an artificial oyster reed on a wave attenuation.

Soulsby, R. L., & Clarke, S. (2005). *Bed shear-stresses under combined waves and currents on smooth and rough beds produced within defra project fd1905 (estproc)*.

Soulsby, R. L., Hamm, L., Klopman, G., Myrhaug, D., Simons, R. R., & Thomas, G. P. (1993). *Wave-current interaction within and outside the bottom boundary layer*.

Stolk, R., de la Haye, M., & Kers, B. (2015). Toestand en herstel unieke getijdennatuur langs de nieuwe waterweg. *Vakblad natuur bos landschap*.

Van der Wal, M. (1990). Heranalyse van m1155 onderzoeksresultaten. *Delft Hydraulics report Q902*.

van Rijn, L. (1984). *Sediment transport, part i: Bed load transport*.

van Rijn, L., & Grasmeijer, B. (2018). Effect of channel deepening on tidal flow and sediment transport—part ii: Muddy channels. *Ocean Dynamics*, *68*, 1481–1501. https://doi.org/10.1007/s10236-018-1205-1

Vellinga, N., van der Vegt, M., Hoitink, A., & Hoekstra, P. (2014). Discharge distribution and salt water intrusion in the rhine-meuse river delta network. *Proceedings of the International Conference on Fluvial Hydraulics, RIVER FLOW 2014*, 229–234. https://doi.org/10.1201/b17133-35

Verruijt, A. (2001). *Soil mechanics*.

Wensveen, M. (2019). Proef om gebiedseigen baggerspecie toe te passen.

Wolters, M., Garbutt, A., & Bakker, J. P. (2005). Salt-marsh restoration: Evaluating the success of de-embankments in north-west europe. *Biological Conservation*, *123*, 249–268. https://doi.org/10.1016/j.biocon.2004.11.013

Yossef, M. F. M. (2002). *The effect of groynes on rivers*. Delft University of Technology.

Zhu, Q., van Prooijen, B. C., Wang, Z. B., Ma, Y. X., & Yang, S. L. (2016). Bed shear stress estimation on an open intertidal flat using in situ measurements. *Estuarine, Coastal and Shelf Science*, *182*, 190–201. https://doi.org/10.1016/j.ecss.2016.08.028

Zhu, Z., Bouma, T. J., Zhu, Q., Cai, Y., & Yang, Z. (2021). Effects of waves and sediment disturbance on seed bank persistence at tidal flats. *Frontiers in Marine Science*, *8*. https://doi.org/10.3389/fmars.2021.728065

A | Field research and method

In order to formulate an answer to the research question, two separate measurement campaigns have been carried out. During the measurement campaigns specialized measuring instruments have been used in the groyne area to carry out on-site measurements. Figure A.1 shows the position of the Groyne area and other important places and structures that define the area.

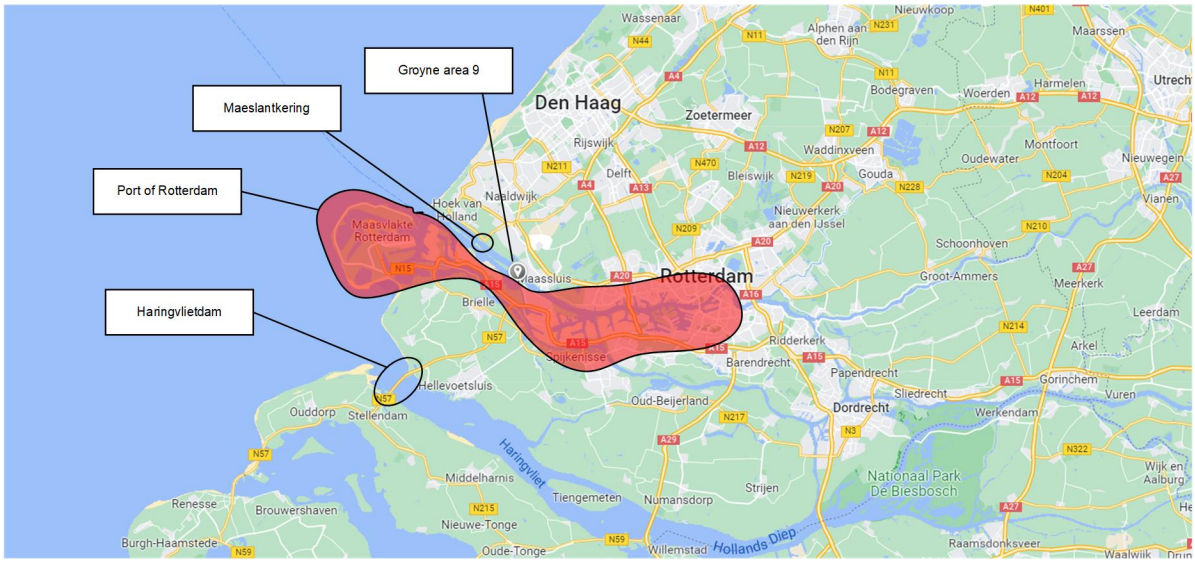

Figure A.1: Map including both flood defences and the Port of Rotterdam.

A.1. First measurement campaign

The goal of this measurement campaign was to install and uninstall the ADVs and take samples from the sediment. The campaign was carried out on two separate days. The first trip was used to install the ADVs and the second trip was to pick up the ADVs. The setup consisted of a pole with the ADV and battery canister attached, a metal extension piece to hold the flexible head of the adv in a fixed vertical position away from the setup and a second pole for stability and to prevent rotation. The poles have been put into the ground at different depths depending on the strength and composition of bed at the specific location. The poles were carefully hammered into the ground using a sledgehammer. The poles were hammered into the ground to a depth until rotation and movement by hand were impossible. The ADVs were attached with braces to the mounts, which were then attached to the poles. To ensure the ADVs would not be damaged in the braces or rotate rubber strips would be put between the braces and the ADVs. The external battery canisters were prepared at the university and attached to the on-site ADVs. A special lube was used to make the attachments from the battery to the ADV waterproof. The RBR and the CTD have been attached to a separate pole. This pole was not supported by another pole because this was not possible at the position of the RBR and CTD. Another CTD was used to measure the air pressure, which was placed discreetly on land several meters away from the groyne area.

The team consisted out of six people: Bram van Prooijen, Kees Sloff, Pieter van der Gaag, Steven Brouwers and Tors Kouwenhoven.

Figure A.2: Photos taken by Kees Sloff during the first measurement campaign.

A.1.1. Program

The ebb tide on the day of the placement was at its lowest water level at 10:10. The height of the ebb tide was $-0.75\,\mathrm{m}$ NAP. With this low ebb tide it was possible to enter the groyne area around 8:30 and the installation had to be done before 15:30. The research team left the university at 7:00 with an 20-minute drive to the groyne area. The ADVs were transported in their cases and attached to the poles and the external batteries on site. During installation, the tide was low enough for the groyne area to fall almost completely dry. Because of this, the installation depth could be chosen for every height and there was more freedom for positioning the instruments. In Figure A.3 the 3D map of the ADVs can be seen from different angles.

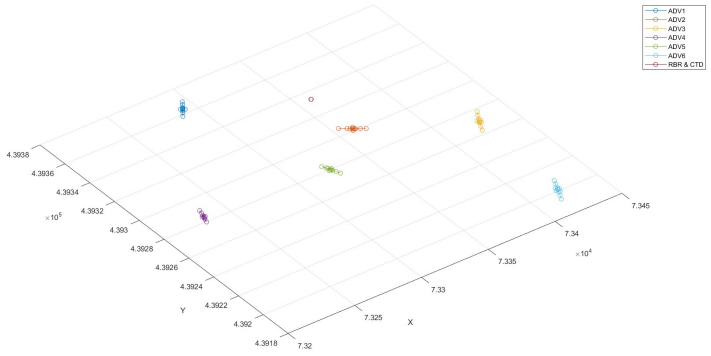

(a)

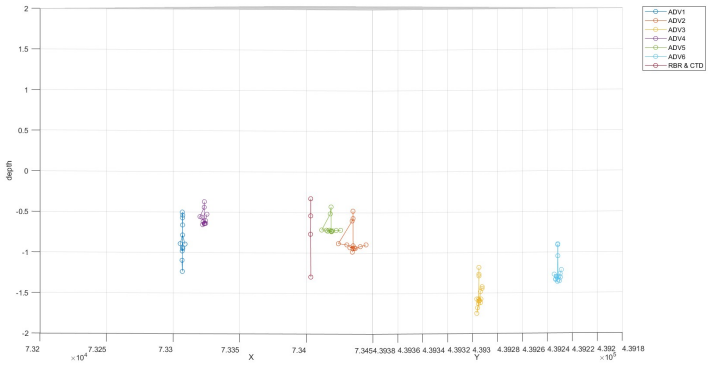

(b)

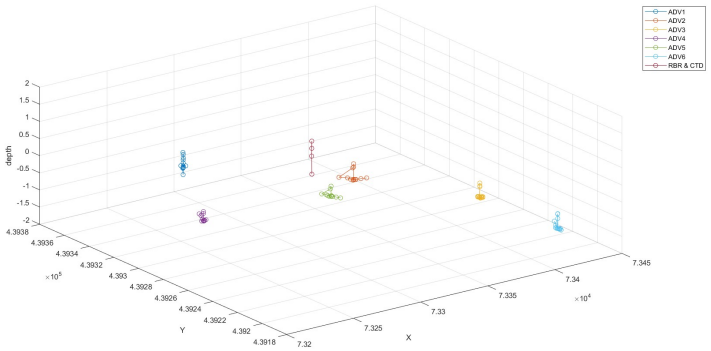

(c)

Figure A.3: All the views of the 3D map of the GPS coordinates. (a) Top view of the 3D map of the instruments. (b) Front view of the 3D map of the instruments. (c) 3D map of the instruments.

A.1.2. Equipment settings

All the research equipment was adjusted and programmed at the university. The type of ADV that was used was the Nortek Vector. The CTD that was used was the CTD-diver and the for the RBR the RBR solo.

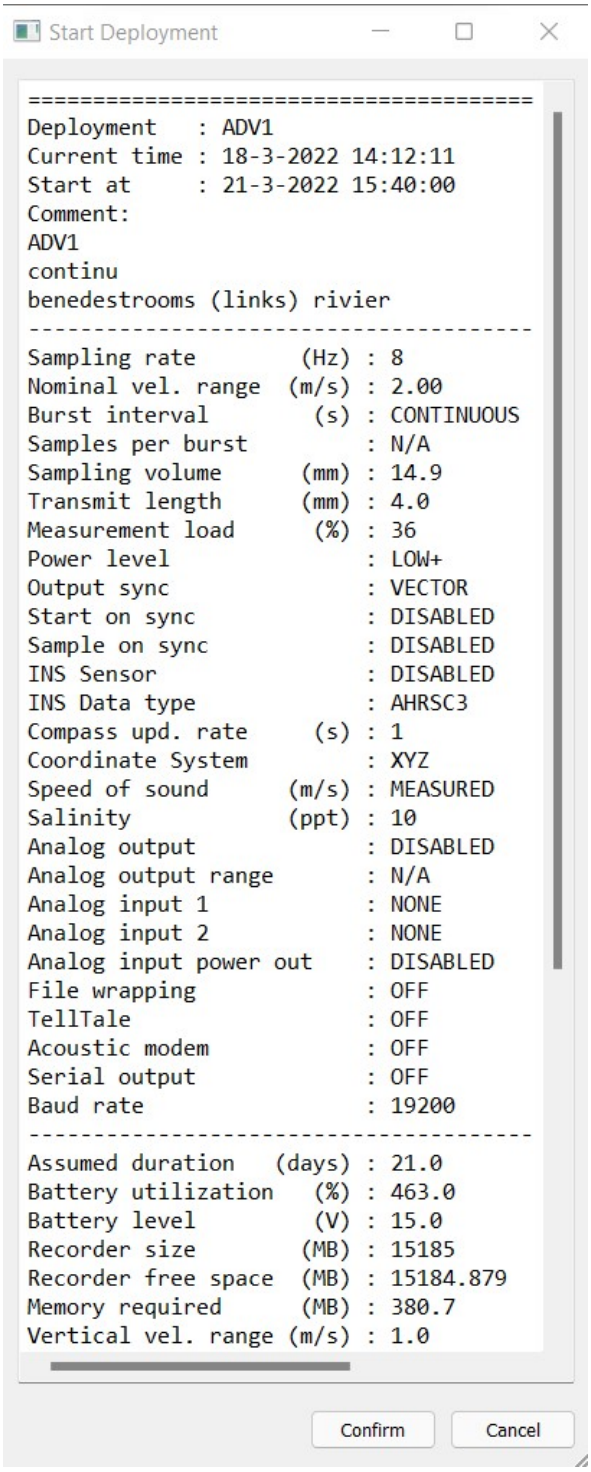

(a)

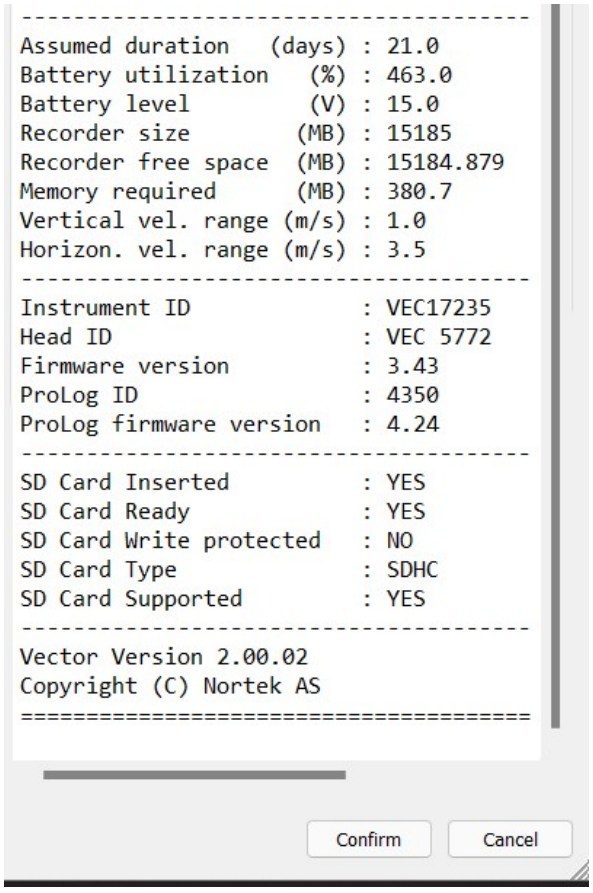

(b)

Figure A.4: Settings for ADV at location 1. All continues ADVs have the same settings.

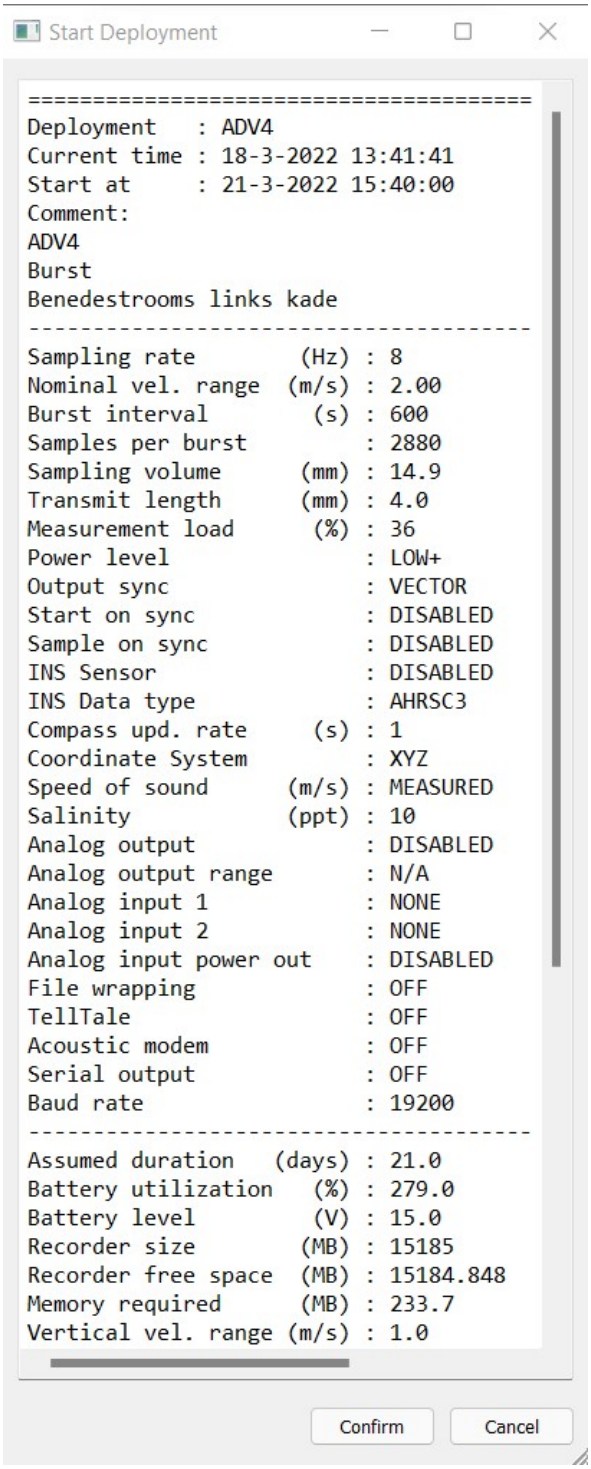

(a)

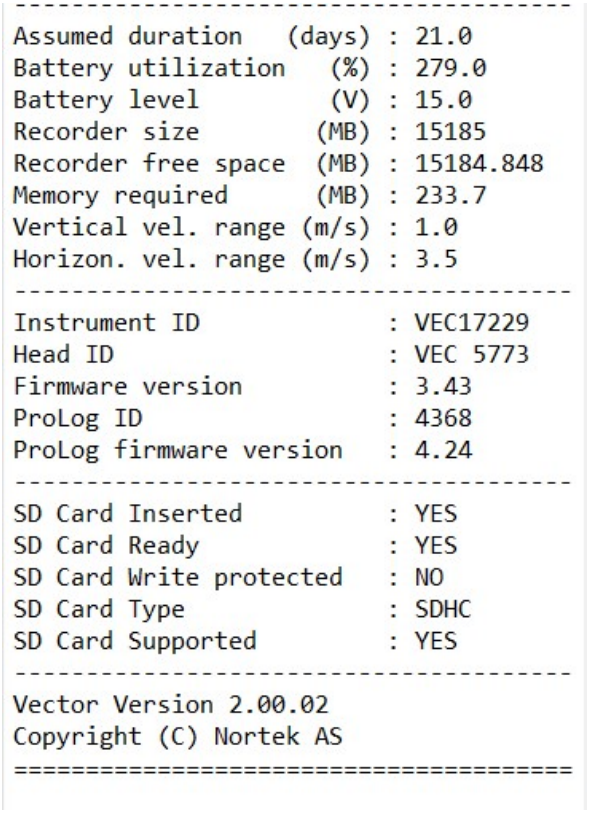

(b)

Figure A.5: Settings for ADV at location 4. Both burst ADVs have the same settings

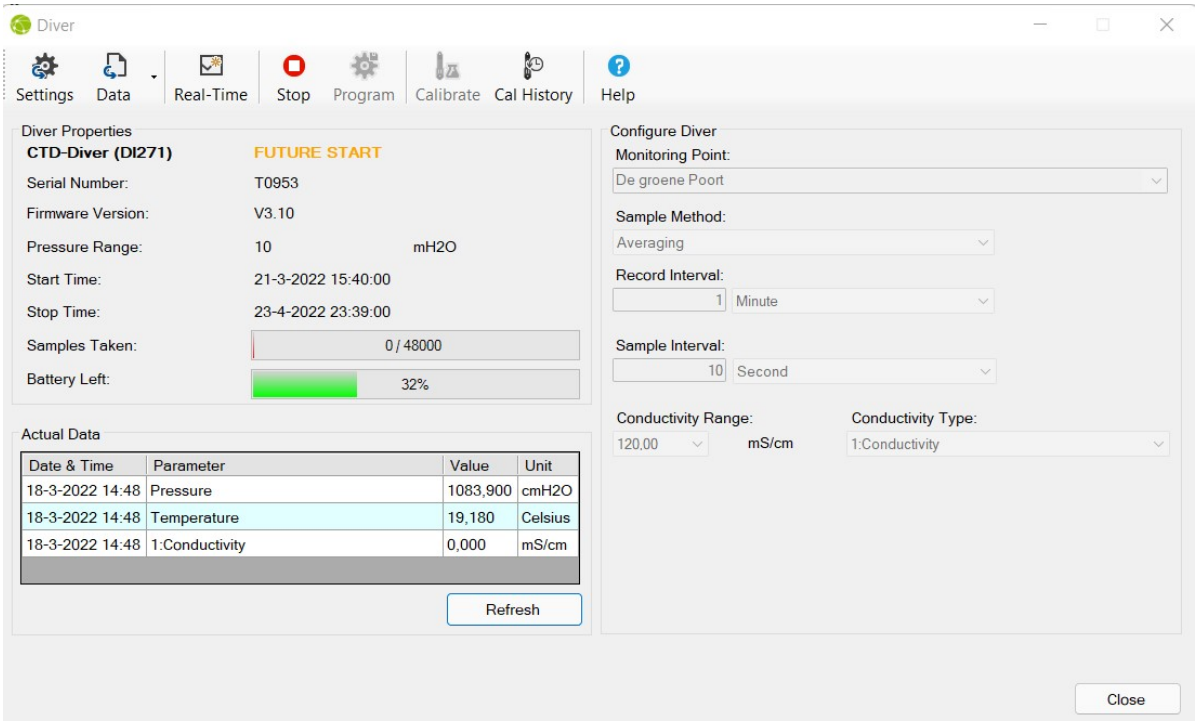

Figure A.6: Settings CTD. Both CTDs have the same settings

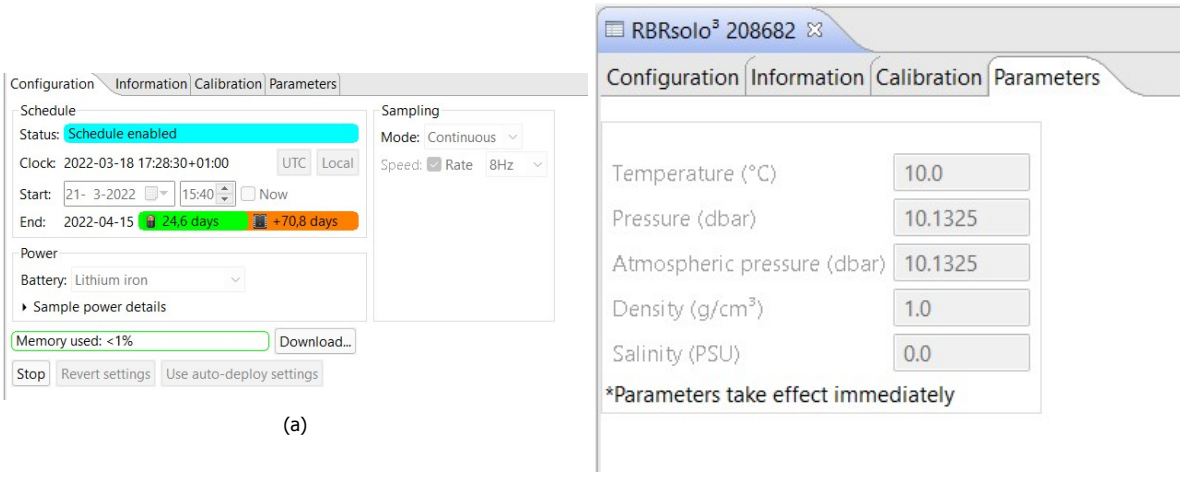

(a)

(b)

Figure A.7: Settings for RBR

A.2. Second measurement campaign

This measurement campaign aimed to obtain data using the ADCP in the groyne area. The ADCP was attached to a floating board which was specially designed for the ADCP. The board contained a hole where the ADCP could be placed and could freely look down facing the bed. The board contains two fins placed at either side to improve the board's stability and ability to sail in a straight line. The board was attached at the front with a rope to an extension on the jet ski. The extension on the jet ski consisted of two poles that are connected to each other, they both have a length of two meter. The first pole was attached to the jet ski and the second pole was attached to the first pole. The extension poles were tidily attached to the jet ski, which minimized the movement between the pole and the jet ski. The jet ski would sail between from one reverence pole to the other reverence pole with an average of around velocity of $0.75\,\mathrm{m\,s^{-1}}$. The maximum sail velocity has been $1.6\,\mathrm{m\,s^{-1}}$ and the minimum $0.3\,\mathrm{m\,s^{-1}}$.

The team consisted out of six people: Kees Sloff, Pieter van der Gaag, Arie van der Vlies, Arno Doorn, Eveline van der Deijl and Tors Kouwenhoven.

Figure A.8: Photos taken by Kees Sloff during the second measurement campaign.

A.2.1. Program

The expedition took place on August the 23^{rd}. Low water was at 7:40, so the groyne area could be entered between 5:30 and 10:30. The university was left at 7:15. During low water the reference poles were placed in the water and mapped with the GPS. The jet ski was put into the water around 11:30. This was done at the ramp for the ferry in Rozenburg that sails between Rozenburg and Maasluis. During the time that the jet ski was put into the water, the ADCP was calibrated at the groyne area. This calibration was done away from large structures that could interfere with the signal. The measurements took place between 12:25 and 14:46 and a total of seventy measurements were done. When the measurements were done the poles were removed and the jet ski lifted out of the water.

A.2.2. Equipment settings

The ADCP that was the Sontek RiverSurveyor.

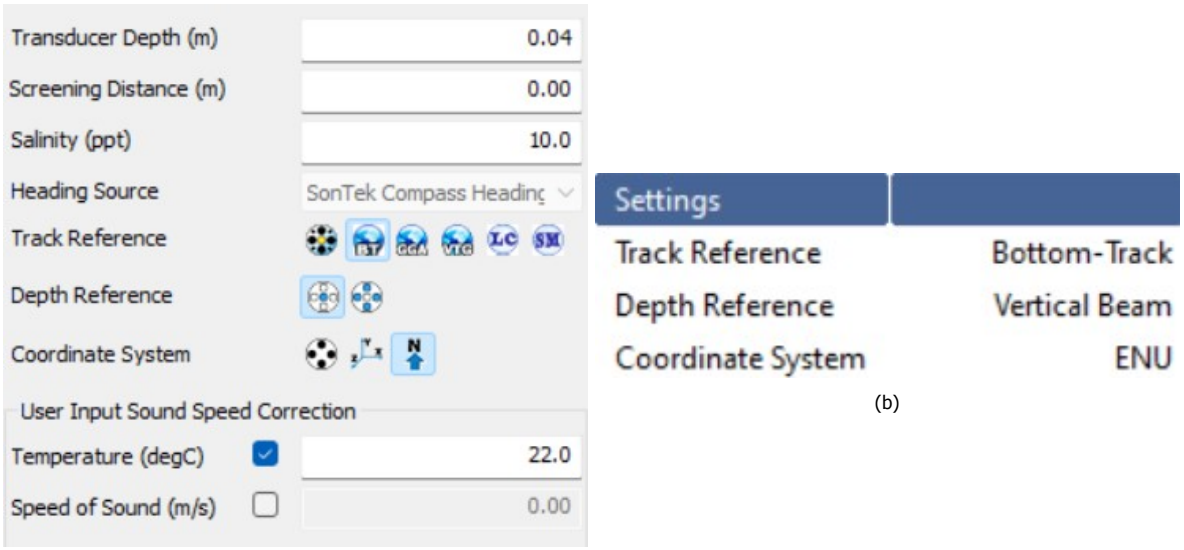

(a) (b)

Figure A.9: Settings for ADCP.

A.3. Sediment analysis

The results as obtained from the Malvern. Outlying results were later removed before taking the average. Such outlying results can be seen clearly in A.10d where two sediment curves are far off from the rest of the curves. Human errors can cause these outliers during the transport of the sediment from the location to the Malvern or due to insufficient cleaning of the machine before use.

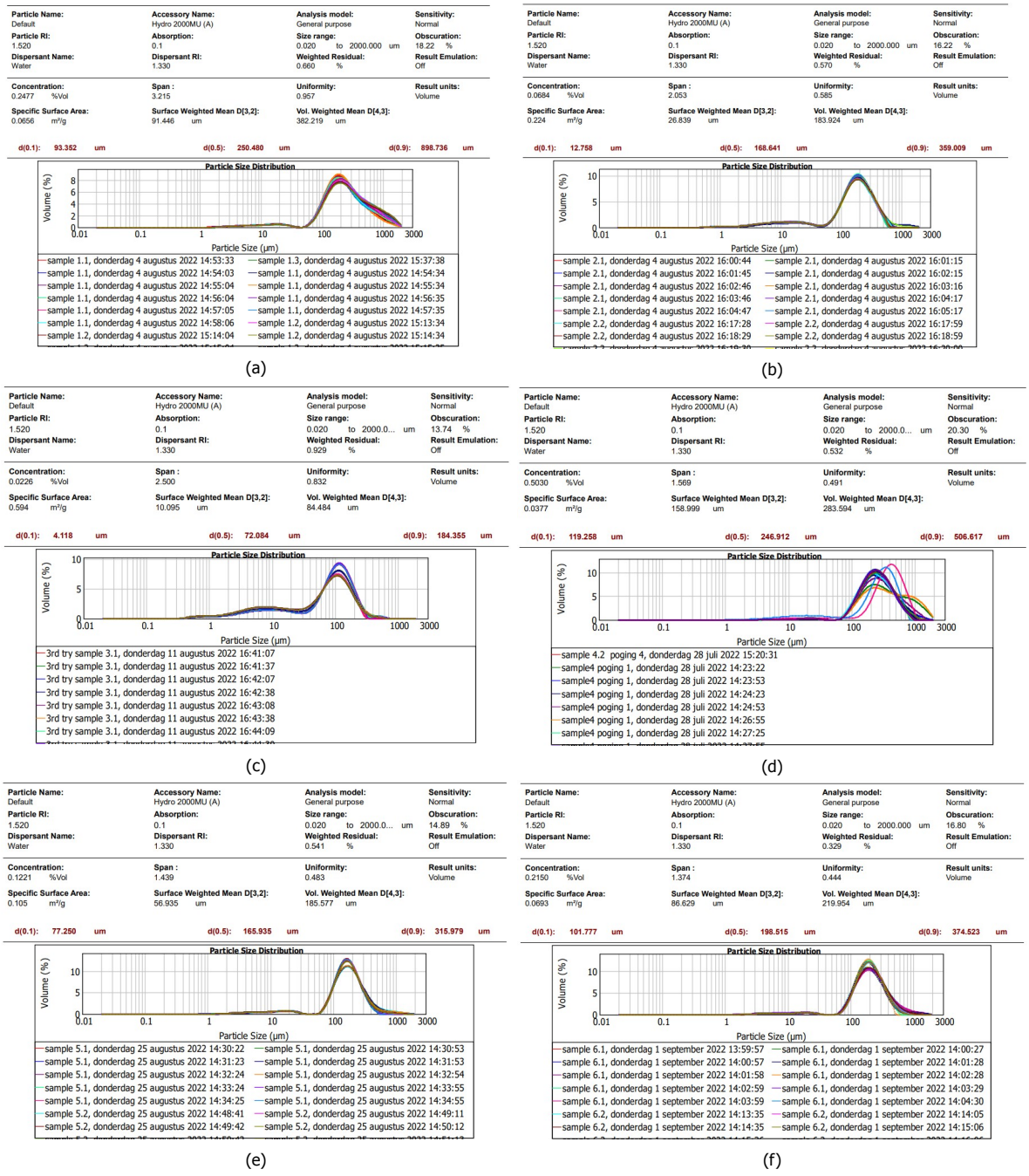

Figure A.10: The information above the graphs is from the first of the analysed samples. Sediment composition at location 1 (a), 2 (b), 3 (c), 4 (d), 5 (e) and 6 (f).

A.4. Data processing

A.4.1. ADV Coordinate systems

The original direction and coordinate systems of the ADVs can be seen in Figure A.11. On the flexible head of the ADV is the direction of the X-axis marked. During the installation this marked X-axis was pointed upwards for all the ADVs. This gives all the ADVs consistent axis.

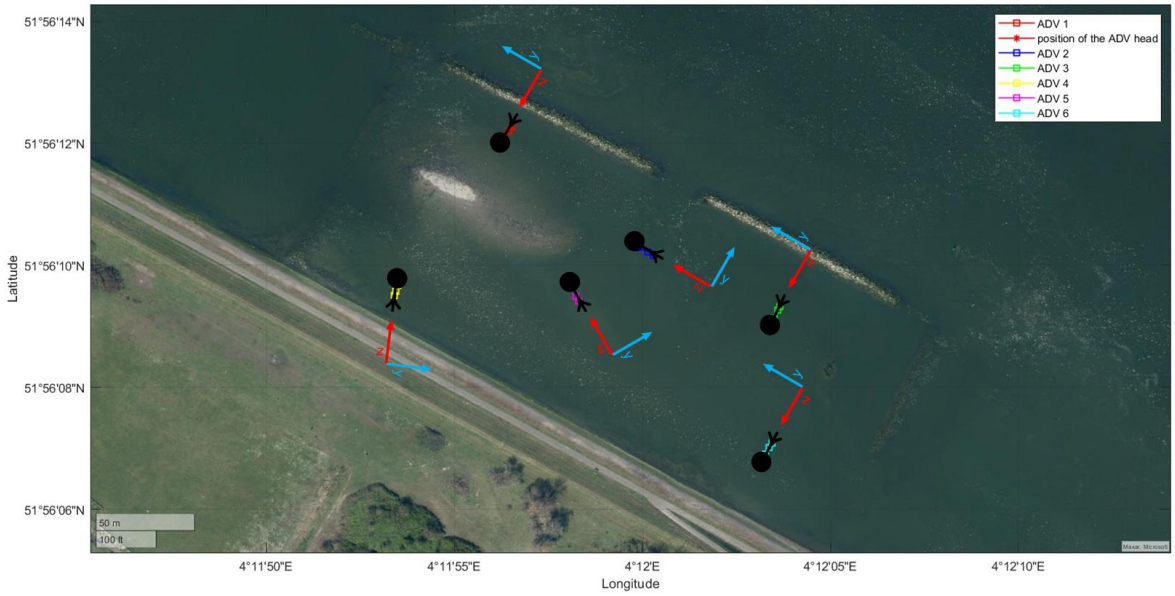

Figure A.11: Original coordinate system found with the GPS coordinates.

Because the ADV heads are typically pointed down, the Z axis is directed into the ADV head. To cause no confusion the names of the Z and the X axis have been changed in Matlab, making the Z the upward-pointing axis. Figure A.12 shows the Matlab code used to change the coordinate system from ADV 1 to the river coordinate system. The angle for the river to the North is 31 degrees and for the ADV 41 degrees. These angles have been obtained using geo.javawa.nl. The angle of the ADV has been obtained using the GPS coordinates.

What happens in the Matlab script:

1. The name and orientation of the original axis getting changed to ease the calculations.
2. The coordinate system is getting changed to a N-E coordinate system.
3. The N-E coordinate system is changed to the river coordinate system.

A.4.2. Averaging of the data

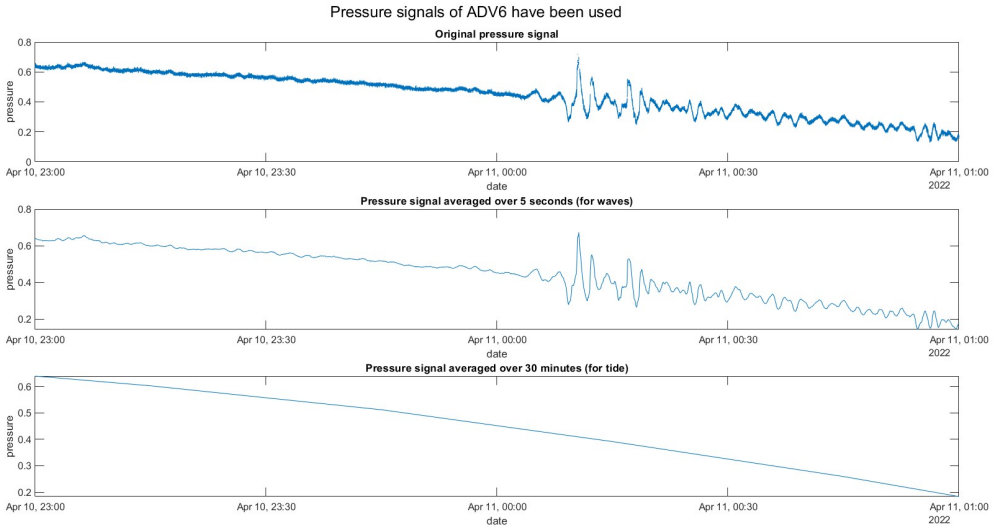

Figure A.13: The same signal averaged over different periods showing different details.

Figure A.14 shows the Matlab script used to average the velocity and pressure data from the ADV. The ADV was set to measure with a frequency of $8Hz$. The difference between the original signal, the signal averaged over 5 seconds for waves, and the signal averaged over 30 minutes for the tide, is shown in Figure A.13.

```
river_angle=31;

    if ADV==1
    % ADV1
    %changing the original coordinate system (cs) to a more practical cs. We
    %try to change al the origal cs
        vx=-Y_reshaped; % positive x direction is pointed in flood direction
        vy=-X_reshaped; % positive y direction is pointed towards the dam
    % average velocity and angle calculation
    disp 'ADV 1';
    %first we have to fix the values because the arc tangend does not reconise
    %in which quadrent the angle lies
        for i=1:length(vy);
            if vx(i)>0
                if vy(i)>0
                theta(i)=atand(vy(i)/vx(i));
                else
                theta(i)=atand(vy(i)/vx(i))+360;
                end
            else
                theta(i)=atand(vy(i)/vx(i))+180;
            end
        end

    %now we change the reference frame from the original to the the north
        for i=1:length(theta);
            if theta(i)<41;
                theta_c(i)=theta(i)-41+360;
            else
                theta_c(i)=theta(i)-41;
            end
        end

    %at least we change the north coordinate system to the one with the river
    %now we only have the magnitude and the direction of the flow
        for i=1:length(theta_c);
            if theta_c(i)>=(360-river_angle);
                theta_cc(i)=theta_c(i)+river_angle-360;
            else
                theta_cc(i)=theta_c(i)+river_angle;
            end
        end
    end
```

Figure A.12: Code from Matlab.

```
function [X,Y,p,V,time,time_num,st_n,fs_n,fulltime] = reshape_continue (meantime,start_c,finish_c,variable_X,variable_Y,variable_p)
%meantime in minutes
% start and finish as start and finish data of the whole dataset
time1_tide=(start_c:minutes(meantime):finish_c);
time_tide=datenum(time1_tide);

start_date=datetime('2022-03-22 01:00:00.000', 'InputFormat','yyyy-MM-dd HH:mm:ss.SSS');
finish_date=datetime('2022-04-12 01:00:00.000', 'InputFormat','yyyy-MM-dd HH:mm:ss.SSS');
fulltime=(start_date:minutes(meantime):finish_date);
fulltime_num=datenum(fulltime);

st_n=find(fulltime>=start_c);
st_n=st_n(1);
fs_n=find(fulltime>=finish_c);
fs_n=fs_n(1);

L=length(variable_X);
n = meantime*60*8; % average every n values
C1=variable_X(1:L);
a=C1;
C1 = arrayfun(@(i) mean(a(i:i+n-1),'omitnan'),1:n:length(a)-n+1)'; % the averaged vector
C1=reshape(C1,1,length(C1));

C2=variable_Y(1:L);
a=C2;
C2 = arrayfun(@(i) mean(a(i:i+n-1),'omitnan'),1:n:length(a)-n+1)'; % the averaged vector
C2=reshape(C2,1,length(C2));

C3=variable_p(1:L);
a=C3;
C3 = arrayfun(@(i) mean(a(i:i+n-1),'omitnan'),1:n:length(a)-n+1)'; % the averaged vector
C3=reshape(C3,1,length(C3));

X=C1;
Y=C2;
V=sqrt(Y.^2+X.^2);
p=C3;
fulltime=fulltime+0.5*minutes(meantime);
fulltime=fulltime(1:length(fulltime)-1);
time=time1_tide(1 : length(time1_tide) )+0.5*minutes(meantime);
time_num=time_tide(1 : length(time_tide) );
disp 'this function only returns time 1 from the chosen start to finish x,y,z are the whole dataset';
end
```

Figure A.14: Code from Matlab used for averaging.

B Hydrodynamic conditions

In this section an more in depth explanation will be given about the theories and methods that have been used to obtain the data in Section 4. This will consist of extra graphs and calculations that give a deeper understanding in the material presented in that section.

B.1. CTD and RBR data

B.1.1. Pressure

The data from the CTD and RBR was obtained from the same position in the groyne area. The air pressure data was obtained from a CTD which was positioned on the land several meters away from the groyne area. The ship data in the plot was found by manually selecting ships that passed the groyne area. The site that was used for this is marinetraffic.com. This data is shown in Figure B.1.

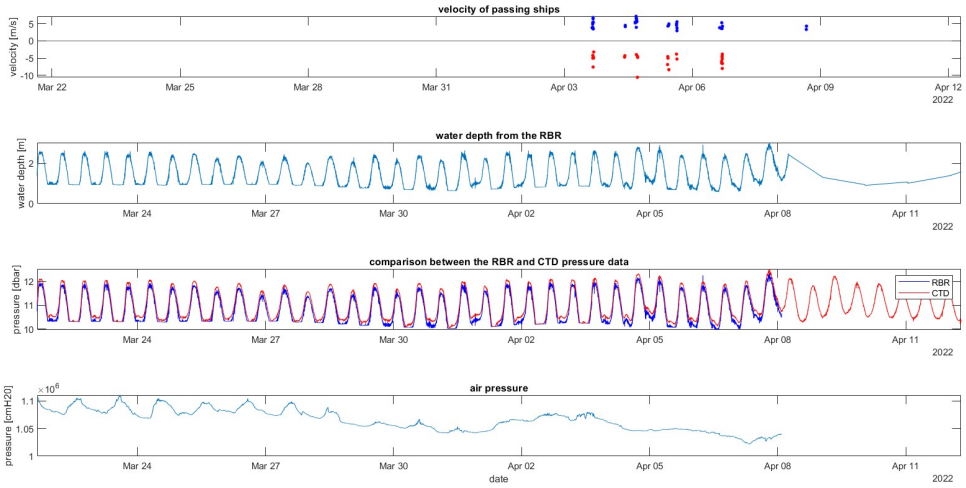

Figure B.1: Pressure data comparison between the CTD and the RBR.

B.1.2. Salinity

The salinity has been obtained from the CTD. Figure B.2 shows the measured change in conductivity during the measuring period. The conductivity can be used to obtain the salinity of the water which is shown in Bennett (1976). In this research these calculations have not been performed on the conductivity. This means that the exact amount of salinity in the water is unknown, but from the conductivity the changes in salinity can be observed. From the graph it can be observed that the salinity has a peak during the descending part of the tides. This can be caused by either the difference between the ebb and flood flow in the groyne area or the density difference between the fresh and salt water. In Section 4.2 it was seen that during flood, the water level had a threshold before the water started flowing through the groyne area, which could affect the interaction between the fresh and salt water. Baroclinic processes also play a role in the change in salinity. However these processes are outside the scope of this project.

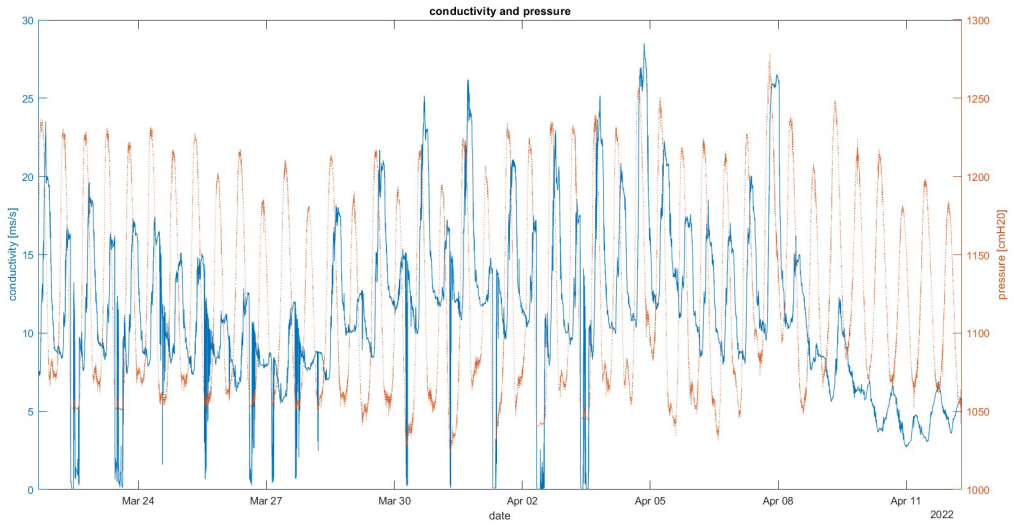

Figure B.2: Salinity and pressure obtained from the CTD data.

B.1.3. Temperature

Figure B.3 shows the temperature changes during the tides. The location of the temperature peaks differs per tide. This is caused by the changing sea and river temperatures, as well as the exchange of fresh and saline water in the groyne area.

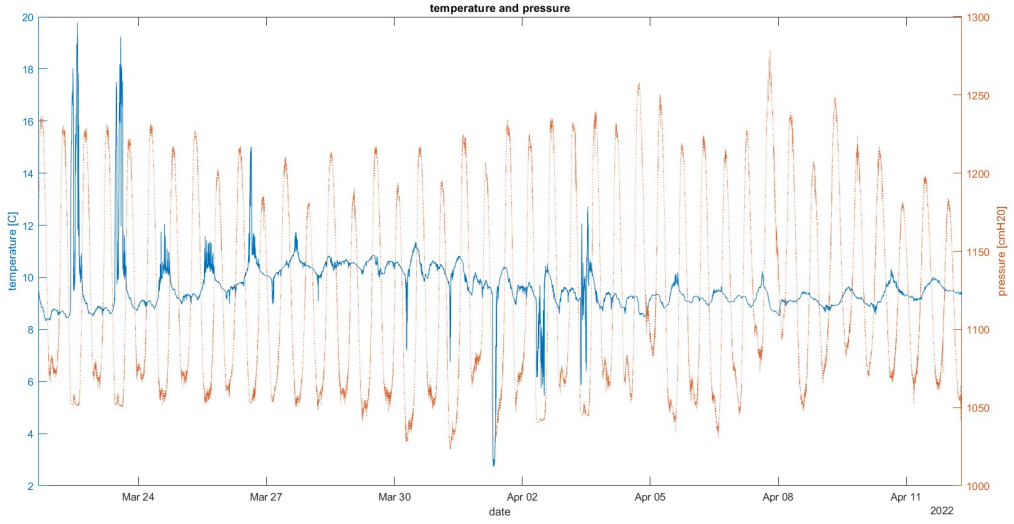

Figure B.3: Temperature of the water and pressure obtained from the CTD data.

B.2. Tide

B.2.1. Extra tidal roses

Figure B.4 shows tidal roses from other tides which have not been shown in Section 4. It can be observed that the behavior of the flow is consistent with the described flow in Section 4.2.

(a)

(b)

(c)

Figure B.4: Extra tidal roses of different tides. (a) Tide at 10-04-22/11-04-22. (b) Tide at 06-04-22. (c) Tide at 22-03-22.

B.2.2. Distribution of the velocities

Figure B.5 shows the velocity distributions in all directions. It can be observed that for location 1, 4 and 6 the velocity peaks during ebb around 180 degrees and flood around 0 degrees contain the highest velocities. For these locations it can be observed as well that between these ebb and flood peaks there are almost no velocities in other directions. Location 5 has similar ebb and flood peaks as the locations discussed above. However, it is shown that the spreading of the directions from smaller velocities is much larger at location 5 compared to these other locations. Location 3 has a similar flood direction, where its highest velocities are around 0 degrees. It can be observed from this location that there is a very large spread for the ebb velocities which are mainly directed to the North. It is shown that for location 2 the peaks are more perpendicular to the river, with a large spread in these velocities. The distribution of the directions of all locations is consistent with the analysis in Section 4.2 and with the tidal roses.

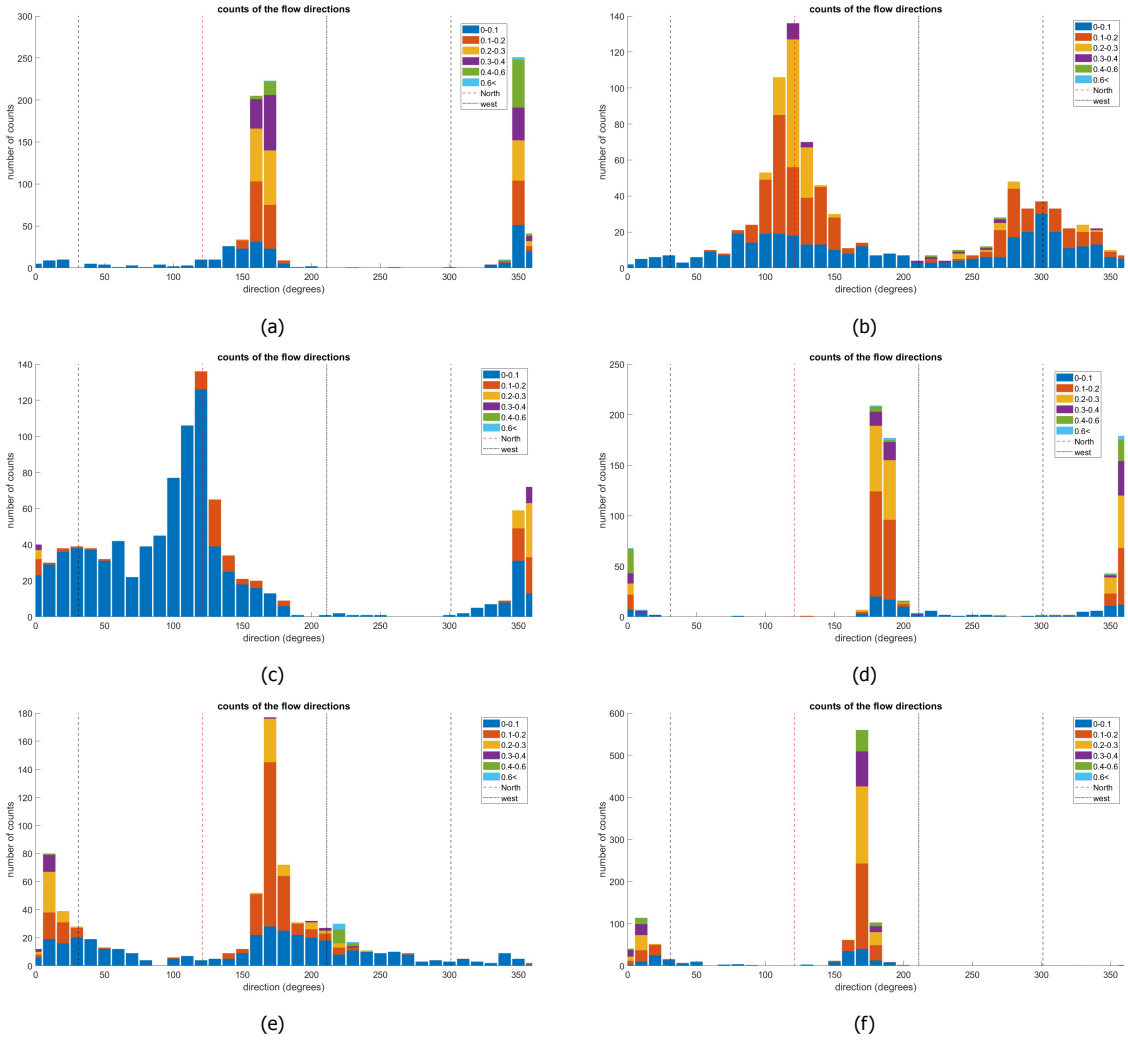

Figure B.5: The Y-axis are in counts instead of percentages. 1 count represents 1 velocity measurement averaged over 30 minutes. 0 degrees is in the direction of the river. Velocity directions at location 1 (a), 2 (b), 3 (c), 4 (d), 5 (e) and 6 (f).

B.2.3. Extra velocity peaks information

These are the velocities obtained during their peaks in the tide.

Table B.1: Peak velocities at every location.

location	average peak velocity	minimum peak velocity	maximum peak velocity
1	0.50 m/s	0.33 m/s	0.99 m/s
2	0.31 m/s	0.19 m/s	0.48 m/s
3	0.21 m/s	0.06 m/s	0.39 m/s
4	0.53 m/s	0.24 m/s	1.54 m/s
5	0.35 m/s	0.16 m/s	1.01 m/s
6	0.43 m/s	0.34 m/s	0.53 m/s

B.2.4. Velocity peaks statistics

For the statistical analysis the peaks in the velocity have been used. The velocity itself has been averaged again as has been done for all tidal velocities over 30 minutes. Because of the inequalities between the flood and ebb peaks as discussed in Section 4.2, a bimodal distribution been used. The kdensity function from Matlab has been used to obtain the full distribution and the parameters for the distributions of the different ebb and flood peaks.

All peaks are used with no constraints such as a minimum peak time or peak width. Figure B.6 shows the probability of not exceeding the threshold velocity at location 1. For this threshold velocity the upper bound of the critical velocity has been used. From the combined distribution it can be seen that 35% of the velocity peaks at location 1 exceed the threshold velocity at that location.

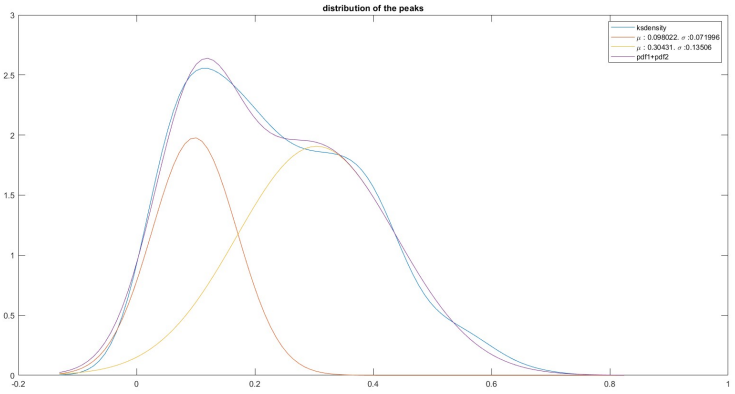

(a)

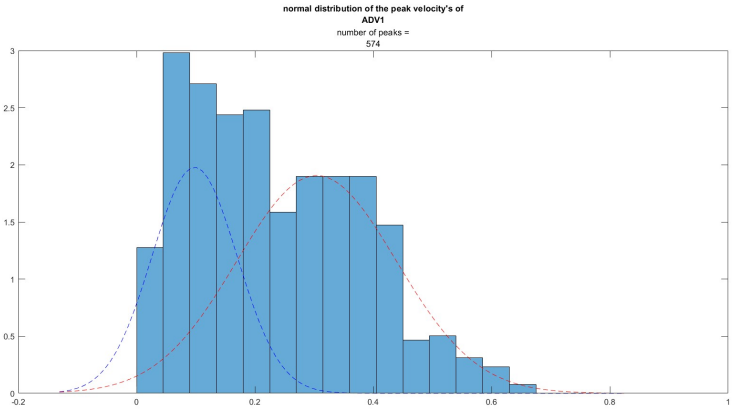

(b)

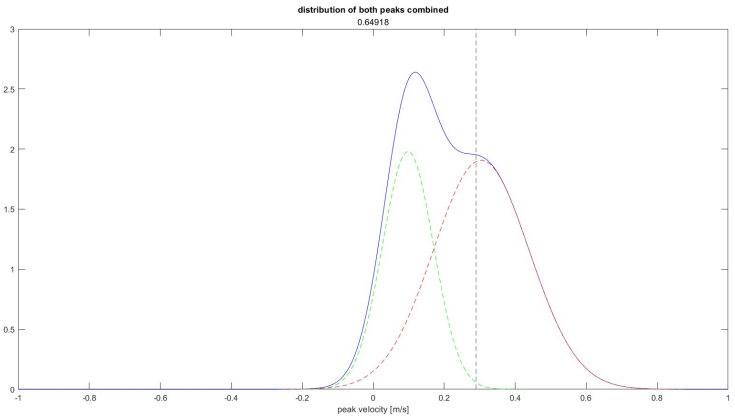

(c)

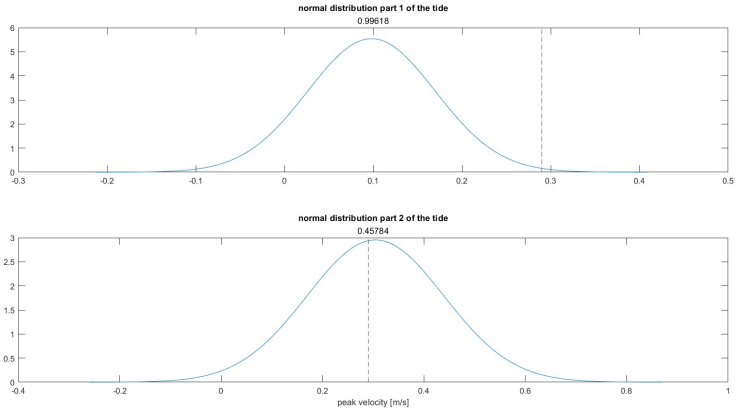

(d)

Figure B.6: The peaks have been found using the findpeaks function of matlab. (a) Obtaining the parameters for the distributions with the kdensity function. (b) Both individual density functions. (c) Probability of the peak velocity not exceeding the threshold velocity. (d) Individual probabilities of the peak velocities not exceeding the threshold velocity.

The full probabilities for the other location are shown in Figure B.7. The number of peaks for the other locations are: 630 peaks at location 2, 812 at location 3, 504 at location 4, 549 at location 5 and 677 for location 6. It can be observed that the probabilities obtained from the peaks are not consistent with Figure 5.3. This can be caused by an unequal distribution of peaks over the whole measuring period. For example, more peaks were detected at flood than at neap tide.

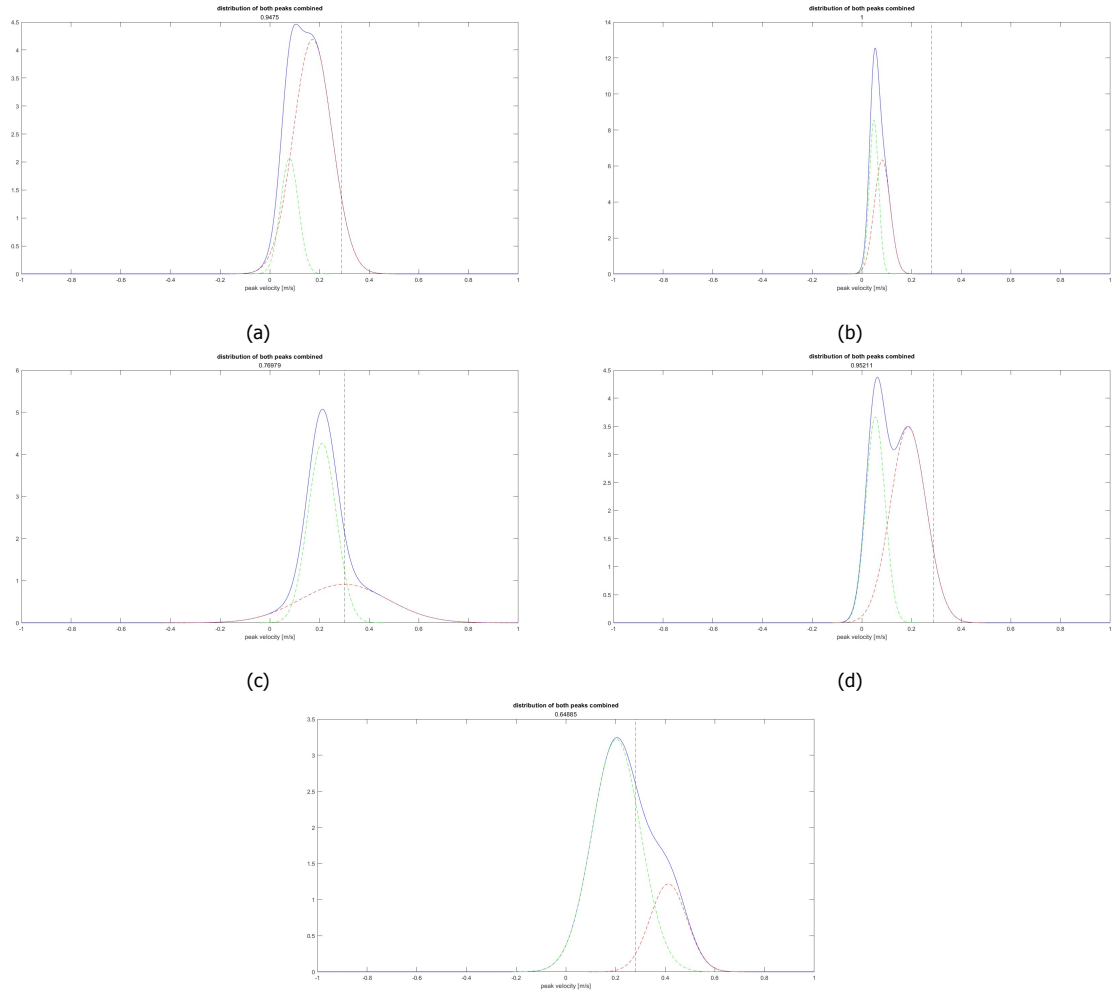

Figure B.7: The full probabilities for all locations. The individual probability function are noted with the dashed lines. Location 2 (a), 3 (b), 4 (c), 5 (d) and 6 (e).

B.2.5. ADCP data

From the ADCP the velocities over the depth have been measured along the sail paths. This data has been used to obtain the colorplots of the flow velocities in different cross sections of the groyne area. In Figure B.8 are the graphs shown of 4 different measurements done after each other in row 2. These measurements have been done during the rising stage of the tide. From these figures, the difficulty of recognizing and placing particular events can be observed. It is difficult to link recurring events to certain locations along the cross section. Using the features on the bed is one of the few tools used to recognize a location. However, due to differences in sail paths, it can be observed that even the features on the bed are different between measurements.

Figure B.9 shows a measurement that is obtained while there are waves present during measuring. The signal can be seen to be distorted.

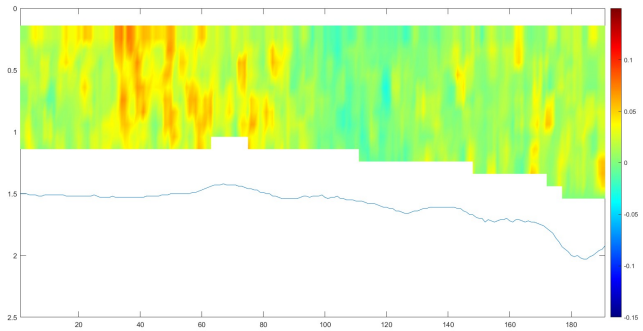

(a)

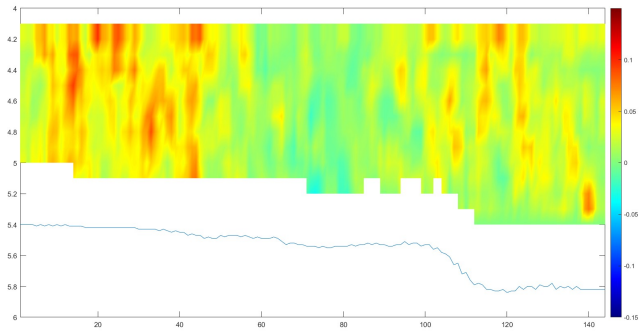

(b)

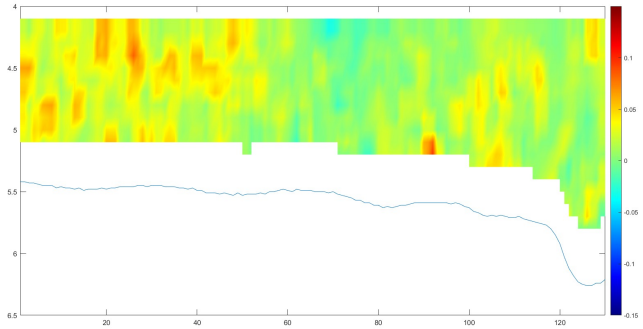

(c)

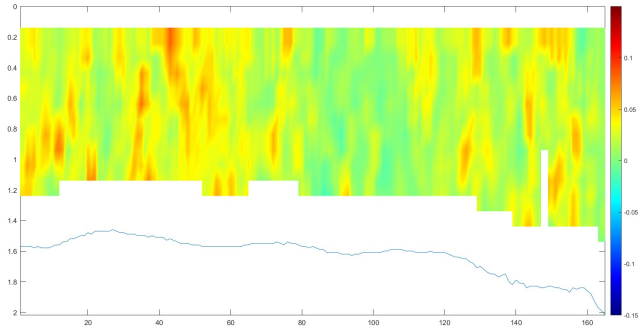

(d)

Figure B.8: The measurements have been done immediately after each other. (a) Start at 12:43:58. (b) Start at 12:47:18. (c) Start at 12:49:50. (d) Start at 12:52:14.

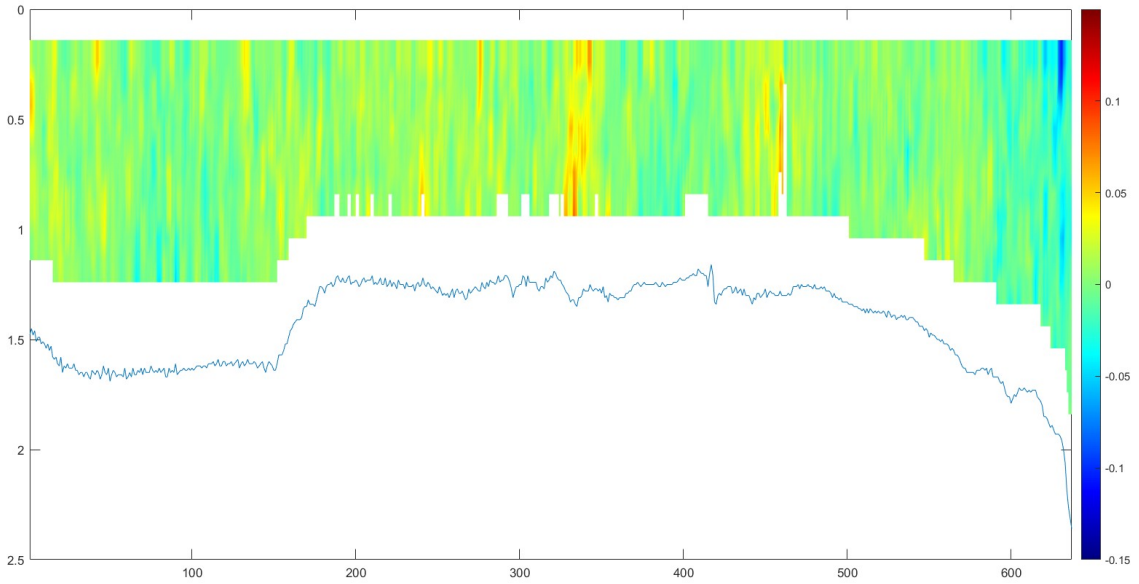

Figure B.9: Distorted ADCP measurement due to waves. This measurent was done close to the peak of the tide.

B.3. Shipping waves

B.3.1. Full characteristics of the individual waves

The wave shear has been calculated using Soulsby and Clarke (2005). The wave height, depths, starting time and period of the wave have been observed manually from the data. Other values have been calculated using linear wave theory and the method of Soulsby and Clarke (2005). Waves 5, 10 and 6 have been used in Figures 4.16, 4.17, 5.6 and 5.7. From the different wave properties it can be observed that shear stress from either the wave or the tide can be dominant. This dominance depends on the combination of parameters of the tide and the parameters of the waves such as: water depth, tidal velocity, wave height and wave period. This agrees with the found correlation in Section 4.3.2.

Table B.2: Occurrence and direction of the wave in respect to the tide.

Wave number	Time wave	Wave direction	Occurrence in the tide
13	$9-4,20:23$	ebb	Mid/peak
12	$31-3,12:22$	ebb	flood
10	$9-4,05:42$	flood	Mid flood
9	$24-3,06:41$	flood	Start peak
6	$1-4,17:09$	flood	Start ebb
5	$6-4,07:40$	flood	ebb
14	$5-4,08:33$	ebb	ebb

Table B.3: Wave 13.

Wave 13	ADV 1	ADV 2	ADV 3	ADV 4	ADV 5	ADV 6
Wave height [m]	0.1894	0.3381	0.3848	0.3001	0.3718	0.5659
Start wave	20 : 24 : 02	20 : 23 : 40	20 : 23 : 23	20 : 24 : 02	20 : 23 : 42	20 : 23 : 17
Wave period [sec]	60	90	76	68	65	74
Wave length [m]	287.7	444.7	402.4	269.3	303.2	391.8
Depth ADV	1.97	2.12	2.86	1.33	1.92	2.43
Depth bed	2.34	2.49	3.19	1.6	2.22	2.86
X-velocity difference	−0.41	−0.47	−0.67	−1.01	−0.86	−0.41
Y-velocity difference		−1.13			−0.99	
Tidal X-velocity	0.07	0.03	0.00	0.01	−0.04	0.02
Absolute tidal velocity	0.11	0.03	0.01	0.03	0.06	0.07
Shear wave	6.74E − 2	2.12E − 1	1.96E − 1	2.61E − 1	2.83E − 1	4.54E − 1
Shear current	1.70E − 2	1.19E − 3	1.09E − 4	2.38E − 3	4.98E − 3	5.5E − 3

Table B.4: Wave 12.

Wave 12	ADV 1	ADV 2	ADV 3	ADV 4	ADV 5	ADV 6
Wave height [m]	0.09	0.11	0.13	–	0.11	0.16
Start wave	12 : 23 : 08	12 : 22 : 37	12 : 22 : 14	–	12 : 22 : 43	12 : 22 : 02
Wave period [sec]	79	81	79	–	83	85
Wave length [m]	257.1	280.2	188.4	–	258.6	336.7
Depth ADV	0.71	0.85	1.59	0.31	0.69	1.17
Depth bed	1.08	1.22	1.92	0.58	0.99	1.6
X-velocity difference	−0.88	−0.46	−0.43	−1.31	−0.525	−0.92
Y-velocity difference		−0.49		–	−0.29	
Tidal X-velocity	0.08	0.03	0.03	0.15	0.04	0.01
Absolute tidal velocity	0.08	0.14	0.06	0.15	0.05	0.03
Shear wave	3.42E − 2	3.61E − 2	8.67E − 3		4.46E − 2	3.31E − 2
Shear current	1.04E − 2	2.96E − 2	4.26E − 3		4.04E − 3	1.12E − 3

Table B.5: Wave 10.

Wave 10	ADV 1	ADV 2	ADV 3	ADV 4	ADV 5	ADV 6
Wave height [m]	0.56	0.32	0.39	0.49	0.15	0.51
Start wave	5 : 41 : 47	5 : 42 : 21	5 : 42 : 27	5 : 41 : 47	5 : 42 : 07	5 : 42 : 34
Wave period [sec]	96	94	100	99	95	100
Wave length [m]	411.1	418.4	517.4	332.5	396.9	485.1
Depth ADV	1.50	1.65	2.40	0.88	1.48	1.97
Depth bed	1.87	2.02	2.73	1.15	1.78	2.40
X-velocity difference	1.5	0.40	0.63	1.96	1.07	0.36
Y-velocity difference		−1.04			−0.69	
Tidal X-velocity	0.28	−0.02	0.00	0.12	−0.01	0.15
Absolute tidal velocity	0.28	0.14	0.03	0.12	0.01	0.16
Shear wave	5.94E − 1	3.14E − 1	2.41E − 1	2.97E − 1	4.26E − 2	4.14E − 1
Shear current	1.15E − 1	2.79E − 2	1.00E − 3	2.12E − 2	1.44E − 4	2.96E − 2

Table B.6: Wave 9.

Wave 9	ADV 1	ADV 2	ADV 3	ADV 4	ADV 5	ADV 6
Wave height [m]	0.15	0.11	0.12	0.25	0.18	0.14
Start wave	6 : 40 : 53	6 : 41 : 46	6 : 41 : 39	6 : 40 : 56	6 : 41 : 11	6 : 41 : 44
Wave period [sec]	110	70	55	99	71	71
Wave length [m]	543.6	355.4	314.6	410.1	342.2	385.7
Depth ADV	2.12	2.26	3.01	1.48	2.07	2.58
Depth bed	2.49	2.63	3.34	1.75	2.37	3.01
X-velocity difference	0.32	0.18	0.40	0.49	0.54	0.57
Y-velocity difference		−0.30			−0.25	
Tidal X-velocity	0.39	−0.04	0.20	0.36	0.15	0.29
Absolute tidal velocity	0.40	0.03	0.20	0.36	0.15	0.29
Shear wave	3.31E − 2	2.20E − 2	1.50E − 2	1.68E − 1	5.25E − 2	1.87E − 2
Shear current	2.22E − 1	1.18E − 3	4.31E − 2	1.95E − 1	3.07E − 2	9.37E − 2

Table B.7: Wave 6.

Wave 6	ADV 1	ADV 2	ADV 3	ADV 4	ADV 5	ADV 6
Wave height [m]	0.23	0.22	0.33	0.47	0.3	0.34
Start wave	17 : 08 : 33	17 : 09 : 06	17 : 09 : 16	17 : 10 : 02	17 : 10 : 22	17 : 09 : 17
Wave period [sec]	94	87	94	75	70	99
Wave length [m]	453.2	432.5	528.2	298.0	327.3	527.9
Depth ADV	2.00	2.15	2.89	1.34	1.93	2.47
Depth bed	2.37	2.52	3.22	1.61	2.23	2.90
X-velocity difference	0.91	0.32	0.46	0.64	0.56	0.45
Y-velocity difference		−0.71			−0.20	
Tidal X-velocity	−0.28	−0.12	−0.09	−0.18	−0.21	−0.27
Absolute tidal velocity	0.28	0.18	0.11	0.19	0.22	0.27
Shear wave	1.16E − 1	1.04E − 1	1.62E − 1	5.29E − 1	1.98E − 1	1.84E − 1
Shear current	1.10E − 1	4.27E − 2	1.31E − 2	5.53E − 2	6.69E − 2	8.17E − 2

Table B.8: Wave 5.

Wave 5	ADV 1	ADV 2	ADV 3	ADV 4	ADV 5	ADV 6
Wave height [m]	0.16	0.2	0.21	0.30	0.21	0.31
Start wave	07 : 39 : 37	07 : 40 : 07	07 : 40 : 12	–	07 : 40 : 00	07 : 40 : 22
Wave period [sec]	75	99	118	–	95	114
Wave length [m]	337.9	461.9	631.5	–	412.2	574.6
Depth ADV	1.70	1.85	2.59	1.03	1.62	2.16
Depth bed	2.07	2.22	2.92	1.30	1.92	2.59
X-velocity difference	0.46	0.21	0.22	0.56	0.39	0.37
Y-velocity difference		−0.41			−0.10	
Tidal X-velocity	−0.29	−0.10	−0.07	−0.20	−0.18	−0.30
Absolute tidal velocity	0.30	0.15	0.09	0.20	0.18	0.31

Table B.9: Wave 14.

Wave 14	ADV 1	ADV 2	ADV 3	ADV 4	ADV 5	ADV 6
Wave height [m]	0.10	0.11	0.12	0.22	0.18	0.13
Start wave	8 : 33 : 27	8 : 33 : 07	8 : 32 : 47	8 : 33 : 37	8 : 33 : 07	8 : 33 : 57
Wave period [sec]	81	78	85	81	73	61
Wave length [m]	311.7	315.7	411.5	219.7	266.6	274.1
Depth ADV	1.14	1.30	2.06	0.48	1.06	1.63
Depth bed	1.51	1.67	2.39	0.75	1.36	2.06
X-velocity difference	−0.51	−0.32	−0.21	−0.89	−0.57	−0.47
Y-velocity difference		−0.51			−0.28	
Tidal X-velocity	−0.36	−0.10	0.02	−0.19	−0.18	−0.39
Absolute tidal velocity	0.37	0.26	0.01	0.20	0.18	0.39
Shear wave	3.08E − 2	2.92E − 2	1.53E − 2	2.82E − 1	1.28E − 1	2.40E − 2
Shear current	2.09E − 1	9.61E − 2	1.14E − 4	7.14E − 2	4.92E − 2	1.81E − 1

B.3.2. Calculation for the ship wave arrival period

The deepest point over the river's width is assumed to be 16.4 m deep ("Boskalis en Van der Kamp baggeren Nieuwe Waterweg: nu geschikt voor grootste mammoetschepen", 2018). It is assumed that between the groynes in a normal unmodified groyne field the average depth is 5 meter. The angle of the cusp locus line and the vessel is between 20 and 35 degrees (Schiereck and Verhagen, 2012). The angle at which the waves travel from the ship is perpendicular to this cusp locus line. This means that the angles of the waves are 70 to 55 degrees from the ship as can be observed in Figure B.10 indicated as situation 1 and situation 2.

For situations 1 and 2 the distances are shown in the figure. These distances have been measured using the measuring tool from geo.javawa.nl. The distance at which the ship wave travels is indicated by the black and red line. The black line represents the distance the wave travels in the deeper water and the red line in the more shallow water. It is assumed that waves travel with the velocity of shallow waves in the linear wave.

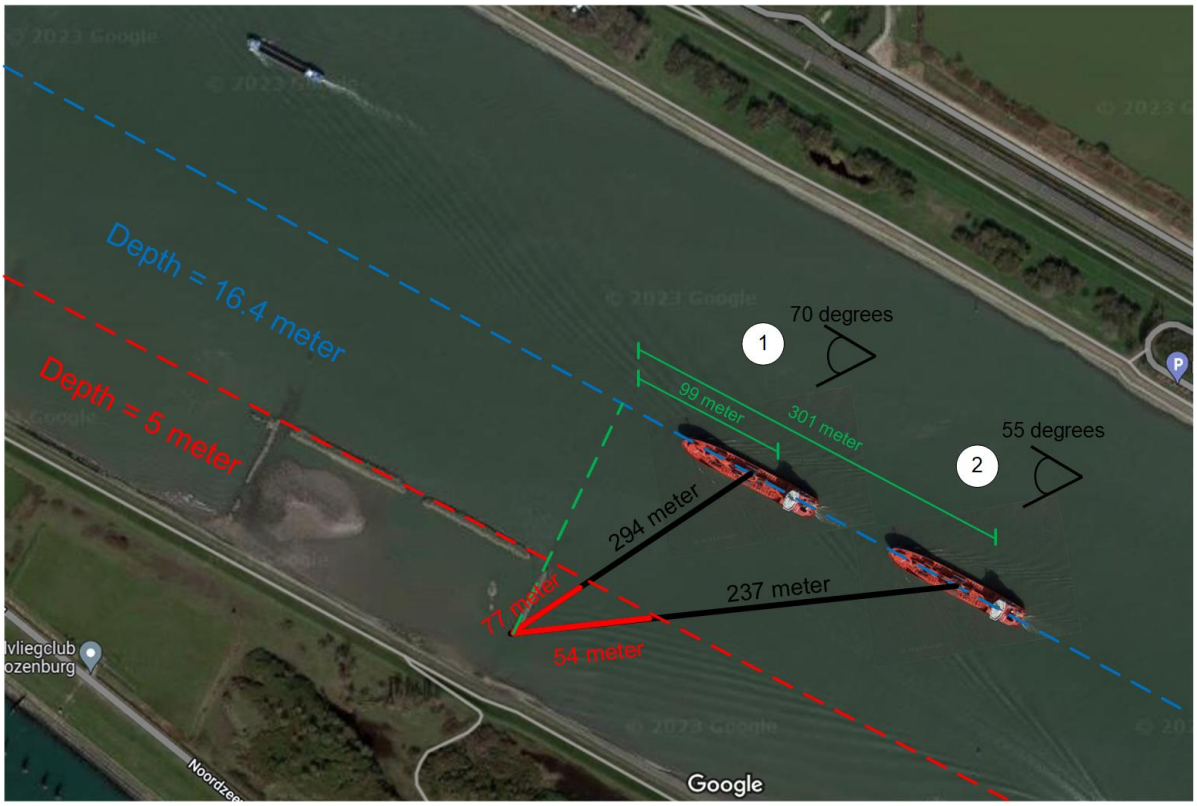

Figure B.10: Geometry and distances for two situations. Background obtained from Google Earth.

With Equation B.3.1 the velocity of the waves can be calculated for waves travelling in the deep part as well as in the shallow part. With the distances between the ship and the entrance, an assumption can be made of the time it takes for a wave to reach the groyne area. These times are shown in Table B.10.

$$wave\ velocity \rightarrow v = \sqrt{g * d} \tag{B.3.1}$$

Table B.10: Distances in the deep water are indicated with the black lines and distances in the shallower water in the red lines.

	deep water	shallow water	total time
70°	19 sec	8 sec	27 sec
55°	23 sec	11 sec	34 sec

According to AIS data the ships travel with a velocity between 6 and 20 knots, with a knot being around $0.5\,\mathrm{m\,s^{-1}}$. The green lines indicate the distance from the two situations to the beginning of groyne area. The ships have been observed at the precise time when they are leaving the groyne area. This means that the length of the groyne area has to be added to the green distances, which is $304\,\mathrm{m}$. The time for the ships that it takes to travel from the start positions at 1 and 2 to the end of the groyne can be seen in Table B.11.

Table B.11: The traveling times of the ships in the 2 situations.

	20 knots	6 knots
70°	40 sec	134 sec
55°	61 sec	202 sec

The difference between the travel time of the ship and its wave is essential for the analysis done in Section 4.3.2. The significant situations are the situations with the smallest and largest difference between the travel time of the waves and the ships. These significant situations are for situation 1, a ship traveling at 20 knots and for situation 2, a ship traveling at 6 knots. The values for these differences can be found in Table B.12. The negative numbers in this table indicate that the waves arrive earlier in the groyne area than the ships reach the end of the groyne area.

Table B.12: The differences between the time the waves reach the groyne area and when the ships reach the end of the groyne area

Time difference	20 knots	6 knots
70°	-13 sec	-107 sec
55°	-27 sec	-168 sec

The velocity for a wave in deep water is $12.7\,\mathrm{m\,s^{-1}}$ and in shallow water $7\,\mathrm{m\,s^{-1}}$. If the assumption is made that a ship wave can't travel with a higher velocity compared to the velocity of the ship, different travel times are needed for the wave. In this assumption, the wave only travels with the wave velocity if that velocity is below the ship's velocity, meaning that a wave never exceeds the velocity of the ship. For example, the wave from a ship that travels with $10\,\mathrm{m\,s^{-1}}$ has a maximum velocity of $10\,\mathrm{m\,s^{-1}}$, but when the wave reaches the more shallow part it travels at the velocity of $7\,\mathrm{m\,s^{-1}}$. This will give a different traveling time for the waves which is shown in Table.

Table B.13: The traveling times of the waves in the two situations with the assumption that a wave can't travel faster than the ship.

Wave traveling time	20 knots	6 knots
70°	37 sec	115 sec
55°	48 sec	201 sec

This assumption will give the differences which are shown in Table B.14. Because of this wide arrange of assumptions a wider range has been used in Section 4.3.2

Table B.14: The differences between the time the waves reach the groyne area and when the ships reach the end of the groyne area, with the assumption of the maximum wave velocity.

Time difference	20 knots	6 knots
70°	-3 sec	-19 sec
55°	-13 sec	-1 sec

C | Sediment behavior

This section will be used to further elaborate on the material presented in Section 5. A full explanation of the method and the criterion that was used to obtain parameters for the bed roughness and transport graphs for other locations are shown.

C.1. In depth in the calculation of the bed friction

In Section 5.2.2 was explained that it is in some cases possible to obtain values for bed friction and the roughness height from the vertical velocity profiles. An attempt was also made for this research, but the results did not pass the criteria of Collins et al. (1998). In this section, a more elaborate demonstration be given to show this calculation and analysis.

From Equations 5.2.3 and 5.2.2 the z_0 and u_* can be obtained. To obtain coefficients A and B a Natural log is fitted through a 90 degrees rotated vertical velocity profile. The sample that is used for this demonstration is the second measurement from the second row during the rising tide. The colorplot from this measurement is shown in Figure C.1.

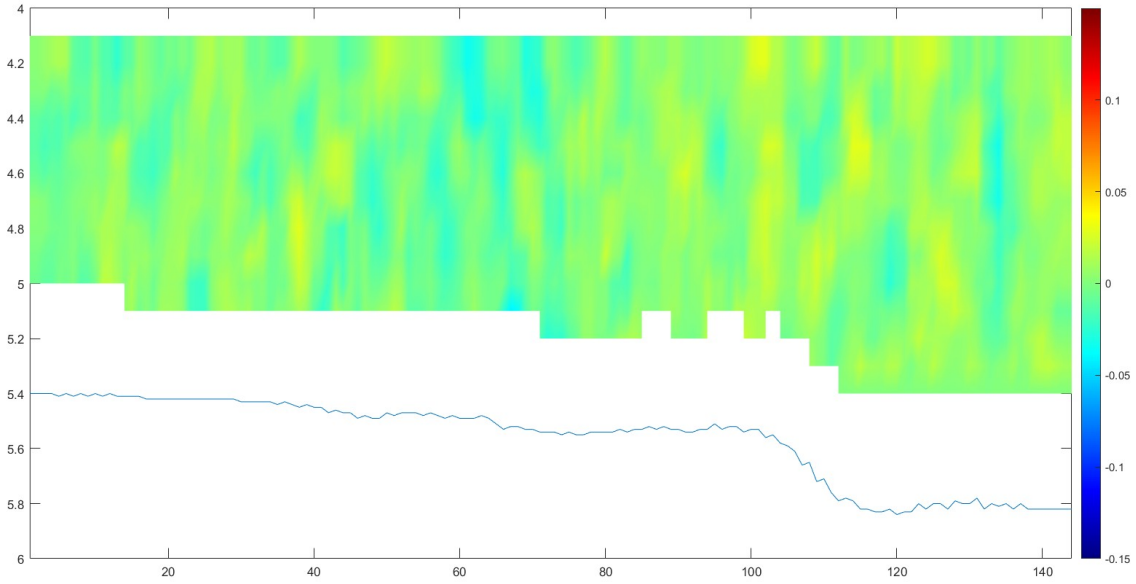

Figure C.1: The colorplot from the measurement used for the demonstration.

There are 144 vertical profiles obtained during this measurement and for this demonstration there will be looked at number 71 counted from the dam to the river bank. The fitted graph with the obtained values for coefficients A and B is shown in Figure C.2. Using these coefficients it is found that $z_0 = 0.0295$ and $u_* = 0.0046$ with $\kappa = 0.41$.

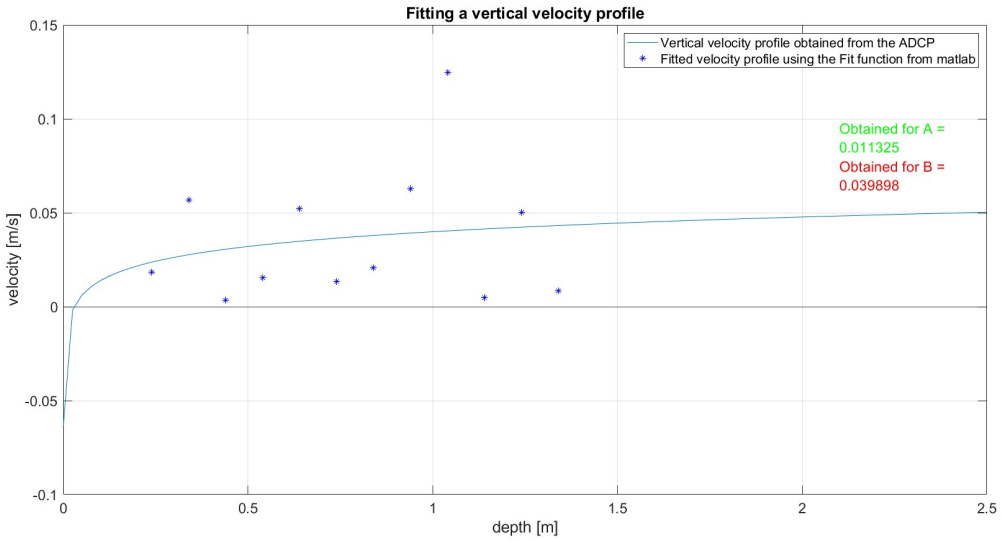

Figure C.2: Fitting a vertical velocity profile to the measurements.

For this to be valid there are 3 criteria from Collins et al. (1998): Coefficient B should be close to 0, the correlation coefficient between the fitted and original data has to be above 0.9 and z_0 has to be between $0.03\,\mathrm{mm}$ and $0.7\,\mathrm{mm}$. To obtain the Correlation coefficient, the Matlab function named Corrcoef is used and this gave a correlation coefficient of 0.17. As seen from all the numbers, this vertical profile failed on all 3 criteria and doesn't qualify. Figure C.3 shows the correlation coefficients obtained for all velocity profiles of this measurement, where none of the points pass the criterion of 0.9.

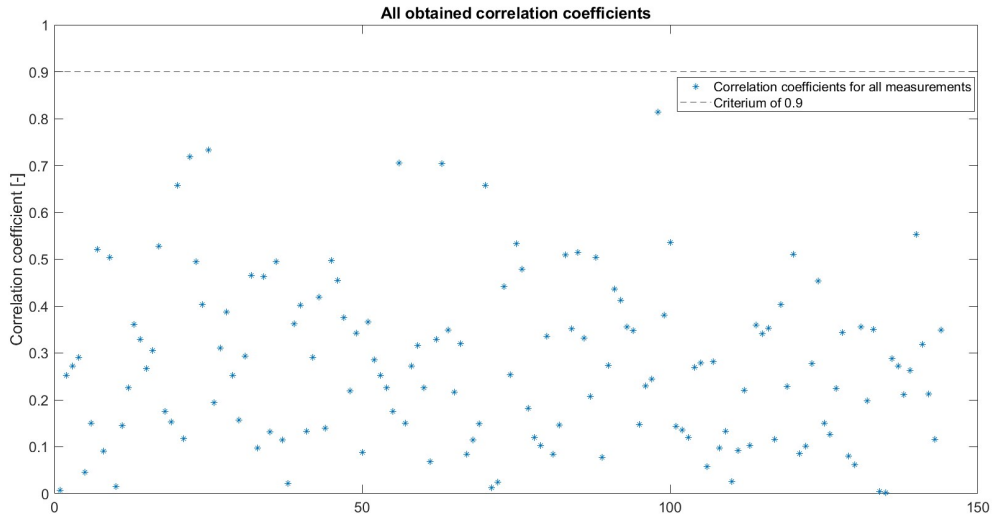

Figure C.3: Correlation coefficients for all vertical profiles.

C.2. Extra transport graphs

C.2.1. Transport during neap and spring

These graphs show the difference between the absolute transport during neap and spring tide for all the locations which haven't been shown in Section 5.

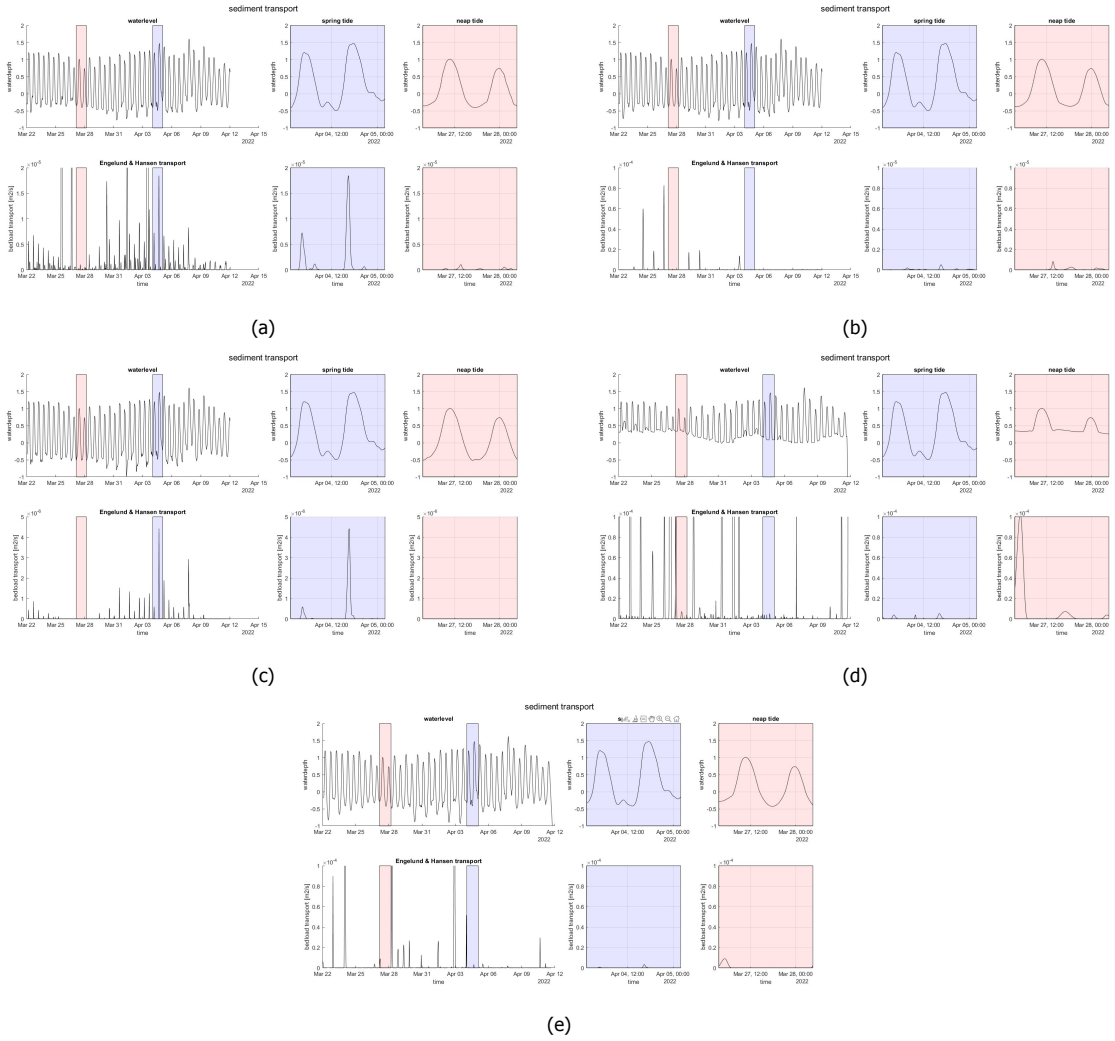

Figure C.4: The transport calculated with the Engelund and Hansen (1967) formulas. Location 1 (a), 2 (b), 3 (c), 4 (d) and 5 (e).

C.2.2. Transport during the passing of a wave

The graphs show the sediment transport during the passing of 3 different waves for all the locations which haven't been shown in Section 5.

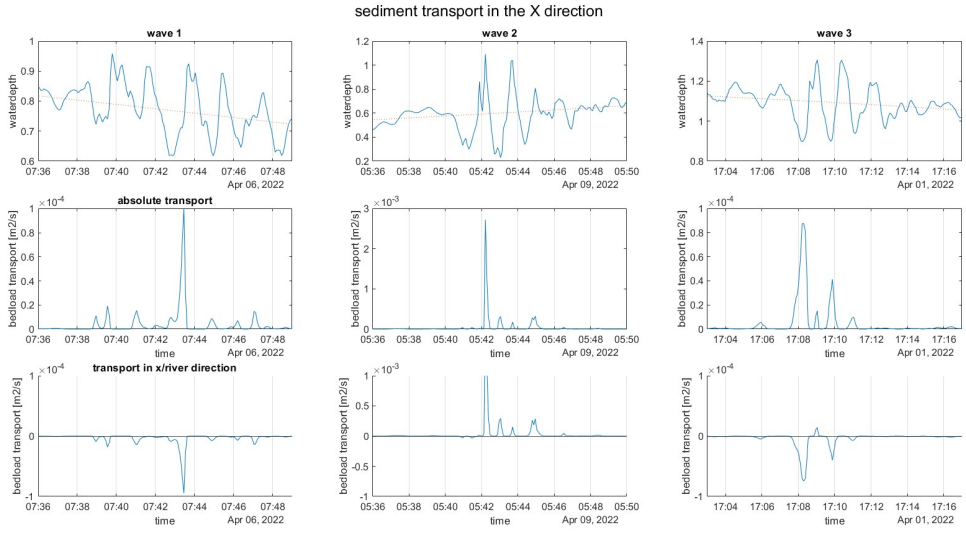

(a)

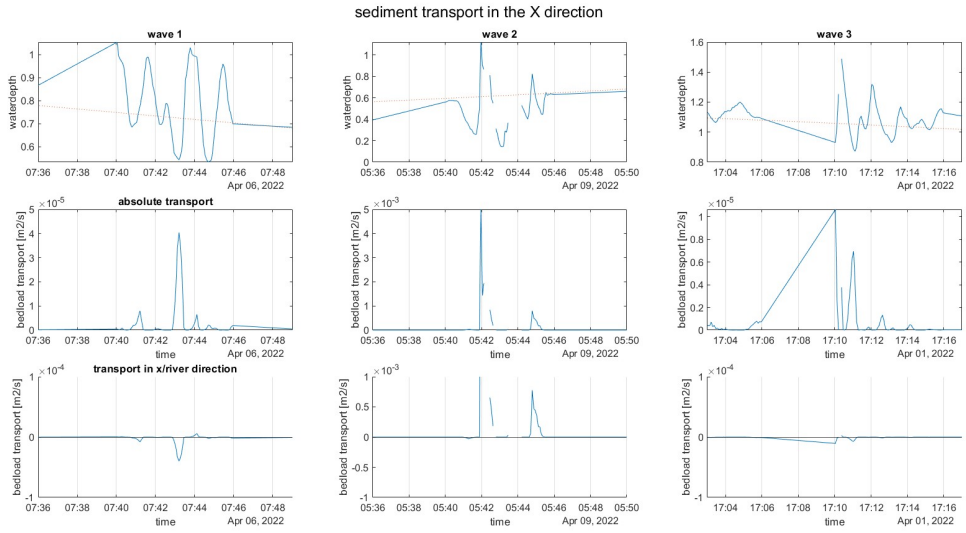

(b)

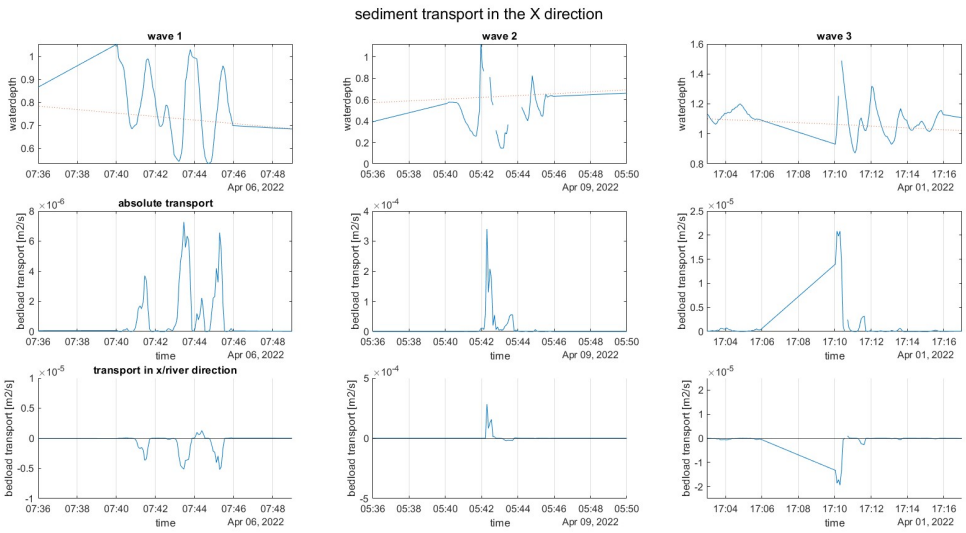

(c)

Figure C.5: The transport calculated with the Engelund and Hansen (1967) formulas. Location 1 (a), 4 (b) and 5 (c).